Nerve-Mediated Airway Hyperreactivity in Obesity-Related Asthma: The Central Role of Elevated Insulin

By

Gina Nicole Calco

A DISSERTATION

Presented to the Physiology & Pharmacology Graduate Program
and the Oregon Health & Science University
School of Medicine
in partial fulfillment of the requirements for the degree of

Doctor of Philosophy

March 2022

School of Medicine

Oregon Health & Science University

CERTIFICATE OF APPROVAL

This is to certify that the PhD dissertation of

Gina Nicole Calco

has been approved

_____
David Jacoby, MD, Mentor/Advisor

_____
Zhenying Nie, MD, PhD, Mentor/Advisor

_____
Beth Habecker, PhD, Chair

_____
Daniel Marks, MD, PhD, Member

_____
George Giraud, MD, PhD, Member

_____
Alina Maloyan, PhD, FAHA, Member

TABLE OF CONTENTS

List of Abbreviations

5-HT: 5-hydroxytryptamine a.k.a. serotonin

ACh: acetylcholine

ANOVA: analysis of variance

BAL: bronchoalveolar lavage fluid

CGRP: calcitonin-gene related peptide

COX: cyclooxygenase

CNS: central nervous system

DRG: dorsal root ganglia

EFS: electrical field stimulation

ELISA: enzyme-linked immunosorbent assay

ERK: extracellular signal-regulated kinase

HFD: high-fat diet

IgE: immunoglobulin E

IGF-1: insulin-like growth factor-1

IGF-2: insulin-like growth factor-2

IL: interleukin

i.p.: intraperitoneal

IR-A: insulin receptor isoform A

IR-B: insulin receptor isoform B

i.v.: intravascular

LABA: long-acting β2-agonist

LFD: low-fat diet

MAPK: ras/mitogen-activated protein kinase

MCh: methacholine

NANC: nonadrenergic, noncholinergic

NC: normal chow

NEBs: neuroepithelial bodies

NGF: nerve growth factor

NK1: neurokinin-1 receptor

NK2: neurokinin-2 receptor

NOS: nitric oxide synthase

NSAIDs: nonsteroidal anti-inflammatory drugs

PBS: phosphate-buffered saline

PGP9.5: protein gene product 9.5 (a.k.a. ubiquitin carboxyl-terminal hydrolase isozyme L1 or UCHL1).

PI3K: phosphoinositide-3 kinase

RAR: rapidly-adapting receptors

SABA: short-acting β2-agonist

SAR: slowly-adapting receptors

SEM: standard error of the mean

SNIRKO: sensory neuron insulin receptor knockout mice

SubP: substance P

TBS: tris buffered saline

TNF-α: tumor necrosis factor alpha

VEH: vehicle

VIP: vasoactive intestinal peptide

WT: wild-type C57Bl/6 mice

List of Tables

List of Figures

Acknowledgements

Thank you so much to my mentors, lab members, family, and friends. I would not have grown into the person I am without your unending support, guidance, and love. I thank you with my whole heart for being there through all of the ups and downs that have come throughout my PhD training.

To Dr. Zhenying (Jane) Nie, thank you so much for always being willing to guide me through difficult *in vivo* physiology experiments, staying late in the lab to help me with data collection, and spending time with me to revise my manuscripts. I have learned so much from you about how to approach a scientific question, dig through the literature, and work through experimental design. You have been an excellent mentor and friend.

To Dr. David Jacoby, thank you for teaching me how to be a physician scientist. Thank you for inviting me to join you in the ICU and for meeting with me every week, even when I did not have any data to show. I appreciate your positivity when my data was negative and your encouragement when experiments were going well. To Dr. Allison Fryer, thank you for listening to my talks and helping me improve my presentation and communication skills. Your leadership has helped me learn how to think like a scientist.

To my fellow (past and present) lab members: Matt, Becky, Brenda, Emily, Katie, Ali, Nicole, Jess, Aubrey, Lauren, Shaye, and Ubaldo. Thank you for working with me, giving me advice, lending your ear to my ideas and explanations of my data, offering help, and listening when I excitedly shared my results. Thank you for fun lab meetings, presentation practices, birthday treats, and impromptu happy hours.

To my DAC committee, thank you for taking the time to guide me through this journey. I appreciate the ideas, questions, and advice you have given me that has led me to greatly improved science. Thank you for rooting for my success and serving as wonderful mentors and examples of excellent scientists and physician scientists.

Thank you to the many people at OHSU that made my life so much easier. I especially want to thank the microscope core staff: Stefanie Kaech-Petrie, Brian Jenkins, and Hannah Bronstein for their help with learning how to optimize the microscopes and 3D rendering software. Thank you to Dr. Alina Maloyan and Yem Alharithi for being excellent collaborators.

To my friends, you mean the world to me. Thank you so much for cheering me on throughout this process and encouraging me no matter what. Thank you for being there even when the world was falling apart.

To my family, thank you for your support. I would not be the person I am today without you behind me every step of the way. To my fiancé, Jasper, thank you for literally everything. I appreciate you always listening to my stories and being on my side through it all. You have made it all worth it.

Dissertation Funding: NRSA F30 HL154526, Pulmonary T32 HL083808, MSTP T32 GM109835, Tartar Trust Fellowship

Publications

Manuscripts:

Calco GN, Proskocil BJ, Jacoby DB, Fryer AD, Nie Z. Metformin prevents airway hyperreactivity in rats with dietary obesity. Am J Physiol Lung Cell Mol Physiol. 2021 Dec 1;321(6):L1105-L1118. doi: 10.1152/ajplung.00202.2021. Epub 2021 Oct 20. PMID: 34668415; PMCID: PMC8715020.

Proskocil BJ, **Calco GN**, Nie Z. Insulin acutely increases agonist-induced airway smooth muscle contraction in humans and rats. Am J Physiol Lung Cell Mol Physiol. 2021 Apr 1;320(4):L545-L556. doi: 10.1152/ajplung.00232.2020. Epub 2021 Jan 27. PMID: 33501891; PMCID: PMC8238158.

Calco G, Erickson H, Toubat O, Spellicy S. MD/DO-PhD trainees: Flexing, adapting, and progressing during COVID-19. J Clin Transl Sci. 2020 Nov 23:1–3. doi: 10.1017/cts.2020.559. PMCID: PMC7844159.

Calco GN, Fryer AD, Nie Z. Unraveling the connection between eosinophils and obesity. J Leukoc Biol. 2020 Jul;108[3]:123-128. doi: 10.1002/JLB.5MR0120-377R. Epub 2020 Mar 14. PMID: 32170879.

Selected abstracts & presentations:

Calco GN, Fryer AD, Jacoby DB, & Nie Z. Hyperinsulinemia Increases Reflex Bronchoconstriction in Obese Mice. American Thoracic Society Conference 2022. *Accepted poster presentation.*

Calco GN, Jacoby DB, Fryer AD, & Nie Z. Sex differences in bronchoconstriction in diet-induced obese rats. American Physician Scientist 17th Annual Meeting. 2021 April 9-11. Virtual. Poster Presentation.

Calco GN, Proskocil BJ, Jacoby DB, Fryer AD, & Nie Z. Insulin acutely potentiates M3 muscarinic receptor function in rat tracheal smooth muscle. American Physician Scientist 15th Annual Meeting. 2019 April 5-7. Chicago, IL. Poster Presentation.

Calco GN, Proskocil BJ, Jacoby, DB, Fryer AD, & Nie, Z. The role of eosinophils in obesity-related asthma. International Eosinophil Society Symposium. 2019 July 9-13. Portland, OR.

Calco GN, Proskocil BJ, Jacoby, DB, Fryer AD, & Nie, Z. Sex differences in bronchoconstriction in diet-induced obese rats. European Respiratory Society International Congress. 2019 Sept 28-Oct 2. Portland, OR.

Abstract

Obesity increases both the incidence and severity of asthma, but the underlying mechanisms leading to the development of obesity-related asthma remain elusive. High insulin levels, a part of the metabolic dysfunction frequently present in obese individuals, increase the risk of asthma, indicating that increased insulin has a role in the pathophysiology of obesity-related asthma. Several models of asthma have shown that altered airway innervation and function mediate airway hyperreactivity, which is defined as increased bronchoconstriction in response to inhaled agonists. Therefore, dysfunctional airway nerves contribute to the mechanisms behind obesity-related asthma.

I hypothesized that hyperinsulinemia in obesity drives morphological changes and dysfunction in airway sensory and parasympathetic nerves leading to airway hyperreactivity. In this dissertation I investigate the mechanisms underlying obesity-related asthma. First, I demonstrate that insulin can potentiate airway smooth muscle contraction in response to muscarinic receptor stimulation, which may contribute to, but does not fully account for, parasympathetic nerve-mediated obesity-related airway hyperreactivity. Then, I show that increased circulating insulin increases airway hyperreactivity via nerve-mediated reflex bronchoconstriction. Hyperinsulinemia also induces hyperinnervation of airway sensory nerves. Finally, hyperinsulinemia also induces hyperinnervation and increases expression of the neurotransmitter substance P in offspring mice of obese mothers, which may explain increased nerve-mediated airway hyperreactivity in this model.

I am the first to show how hyperinsulinemia, a key factor in obese asthmatics but not other asthma phenotypes, modifies airway nerve innervation and function, leading to increased reflex bronchoconstriction. The findings in this dissertation add to our understanding of the underlying mechanisms linking insulin with airway nerve changes and excessive bronchoconstriction. These results emphasize the need and suggest targets for novel therapeutics specific to obesity-related asthma for preventing and treating this disease.

Chapter 1. Introduction

Introduction

A. Asthma

a. Overview

Asthma is a complex chronic airway disease defined by a reversible airflow obstruction that leads to wheezing, shortness of breath, and cough. It affects 262 million people worldwide and caused approximately 461,000 deaths in 2019[3]. Asthma is characterized by hyperreactivity, a heightened bronchoconstriction response to a variety of non-specific stimuli. Asthma is a heterogeneous disease, and optimal treatment depends on characterizing the pathophysiology of asthma subtypes, which define the therapeutic targets.

b. Asthma Subtypes

Asthma can be considered a disease made up of subtypes grouped by clinical and physiological characteristics. Distinct features of severity (lung function, symptoms and exacerbations) and inflammatory characteristics (including T_H2 immunity) divides asthma into unique phenotypes.

i. Clinical Phenotypes

Asthma may be broken into phenotypes based on clinical characteristics, based on triggers, onset, and inflammatory processes[4]. The below asthma phenotypes are not an exhaustive list of all asthma subtypes, but rather a selection of some of the many clinical presentations of asthma.

Early-onset allergic asthma: Originates in early childhood and is associated with other atopic diseases such as atopic dermatitis and allergic rhinitis. Patients have higher T_H2 cytokines, eosinophils, mast cells, and IgE levels. This subtype has a strong family history component. Early-onset allergic eosinophilic T_H2 asthma generally responds well to corticosteroid therapy.

Late-onset nonatopic asthma: Onset defined as occurring after 12 years of age. Patients with adult late-onset asthma have lesser allergic processes, lower lung function, and lack of T_H2–associated inflammation[5]. Non–T_H2-late-onset asthma is associated with gender, obesity, smoking, and aging.

Exercise-induced asthma: Refers to asthma whose symptoms are experienced primarily following exercise and may be worsened by cold, dry condition. The relationship of this form of the disease to T_H2 immunity is not clear.

Aspirin-induced asthma: Bronchoconstriction is induced by aspirin (acetylsalicylic acid) and other nonsteroidal anti-inflammatory drugs (NSAIDs) that block cyclooxygenase (COX). These drugs shift the phospholipase A2 pathway away from prostaglandins and towards cysteinyl leukotriene, leading to increased bronchoconstriction and mucus production. This phenotype is characterized by an eosinophilic rhinosinusitis, nasal polyposis, aspirin sensitivity, and asthma[6].

Cough-variant asthma: An occult form of asthma with the main symptom being cough and particularly at night[7]. Bronchodilator treatment is generally effective[8].

Smoking-related asthma: A small group of adult asthma patients with a history of smoking. Characteristics include poor lung function, high symptoms, and uncontrolled asthma despite treatment.

Obesity-related asthma: Asthma predominately associated with late-onset nonatopic asthma[9]. Obese asthmatic patients have more severe and frequent respiratory symptoms, more exacerbations, decreased response to treatment, and an overall reduced asthma-related quality of life. The obesity-related asthma phenotype will be described in detail in this thesis.

ii. Asthma Endotypes

The complexity and variability of asthma has led to a need to better define the mechanisms leading to symptomatic disease. Asthma endotypes explain defined subtypes of asthma that can be identified by an underlying pathophysiology using biomarkers, molecular causes, and distinct treatment responses[10]. In particular, two major endotypes include allergic asthma driven by high T_H2 inflammation and nonatopic asthma, which has little inflammation[11]. Obesity-related asthma falls under this nonatopic endotype. The main drivers of inflammation in nonatopic asthma are still unclear.[12, 13] Endotype-specific classifications of asthma were defined with the intention of designing highly tailored pathogenesis-directed therapies and, ultimately, better treatment outcomes for asthmatic patients. Despite the many distinctly characterized endotypes and phenotypes, however, there can still be substantial overlap between the classifications and, thus, variable responses to treatments.

c. Characteristics of Asthma

The main characteristic features of asthma include airway hyperreactivity, airway inflammation, and structural remodeling. Airway hyperreactivity is defined as an increased sensitivity of the airways to an inhaled constrictor agonist resulting in greater

bronchoconstriction[14, 15]. Common agonists used in testing airway hyperreactivity include methacholine, an M_3 muscarinic receptor agonist, and serotonin[16], which activates 5-HT receptors. Airway nerves are important mediators of airway hyperreactivity. Airway inflammation refers to the influx of immune cells into the airways. In T_H2-driven allergic asthma eosinophils are the major infiltrating immune cell. Other commonly seen immune cells are mast cells and T_H2 T-cells. Cytokines including IL-4, IL-5, and IL-13 and immunoglobulin E (IgE) are defining inflammatory mediators. Structural remodeling involves a wide array of pathophysiological changes to the airway. These changes include smooth muscle hypertrophy, angiogenesis, goblet cell and mucus gland hyperplasia, sub-basement membrane fibrosis, and narrowing of the airway lumen[17].

d. Current Asthma Treatments

Asthma cannot be cured, but can be medically managed to improve quality of life. The National Heart, Lung, and Blood Institute first released guidelines for asthma in the United States in 1991, which were most recently updated and released in 2007[18]. An expert panel met in 2018 to update the asthma guidelines, and published selected topic updates in 2020[19]. Current asthma treatments reverse bronchoconstriction (β_2 adrenergic receptor antagonists and muscarinic receptor antagonists) and reduce airway inflammation (inhaled corticosteroids). The recommendation for individuals twelve years or older with mild persistent asthma is a daily low-dose inhaled corticosteroid and an as-needed short-acting β_2-agonist [20] for quick-relief therapy or an as-needed inhaled corticosteroid and a SABA used concomitantly. For those with moderate to severe persistent asthma, inhaled corticosteroids with formoterol (a long-

acting β_2-agonist; LABA) therapy in a single inhaler is recommended for daily control and acute relief. For patients with uncontrolled persistent asthma, the panel conditionally recommends adding a Long-Acting Muscarinic Antagonists to the combination of inhaled corticosteroids and long-acting β_2-agonist.[21]

Newer biologics based on molecular biomarkers have been developed to reduce the disease burden in patients with severe or persistent asthma, and they directly address the underlying mechanisms of their unique asthma endotypes. These include drugs that target IgE (Omalizumab), IL-5 (mepolizumab, reszilumab), IL-5 receptor (benralizumab), IL-13 (lebrikizumab), and IL-4α receptor (dupulimab). Randomized control trials with glucocorticoid-dependent severe asthmatic patients have shown adjuvant mepolizumab, benralizumab, and dupliumab therapy reduces asthma exacerbation rates[22]. Importantly, however, there are currently no targeted biologic treatments available for T_H2-low severe asthma[23].

B. Airway Structure

a. Airway Anatomy

The airway, or respiratory tract, is made up of organs that allow airflow exchange. It is composed of structures that both transfer air as well as structures that allow for oxygen and carbon dioxide exchange.[24] Mammalian airways begin with a single hollow tube and go on to form a series of branches. The conducting part of the airway transfers air but does not directly participate in gas exchange and consists of the nasal and oral cavities, pharynx, larynx, trachea, bronchi, bronchioles, and terminal bronchioles (Figure 1). The respiratory portion of the airway consists of respiratory bronchioles, alveolar ducts, and alveoli. The airways are made up of 23 generations of bifurcating tubes[25]. The trachea

divides into two mainstem bronchi at the carina. Once in the lungs, the mainstem bronchi divide into smaller bronchi. These smaller bronchi divide into bronchioles, which end in tiny air sacs known as alveoli. The alveoli are made up of single epithelial cells in direct contact with capillary endothelial cells. This is the site at which the exchange of oxygen and carbon dioxide occurs.

i. Upper Airway

The upper airway serves as the entry point for air intake. It extends from the nose and mouth to the trachea and consists of the nasal and oral cavity, pharynx, and larynx. During inspiration, air enters through the nose or mouth, passes through the pharynx to the larynx, which leads to the trachea. In addition to transporting air to the lungs, the upper airway also humidifies and warms the incoming air. The upper airways are lined with pseudostratified columnar ciliated epithelium. The mucosa contains goblet cells, ciliated and non-ciliated columnar cells with microvilli, and occasional intraepithelial mast cells, eosinophils, and lymphocytes.[26] Mucus-secreting glands, goblet cells, and fine hairs are responsible for filtering out foreign particles.

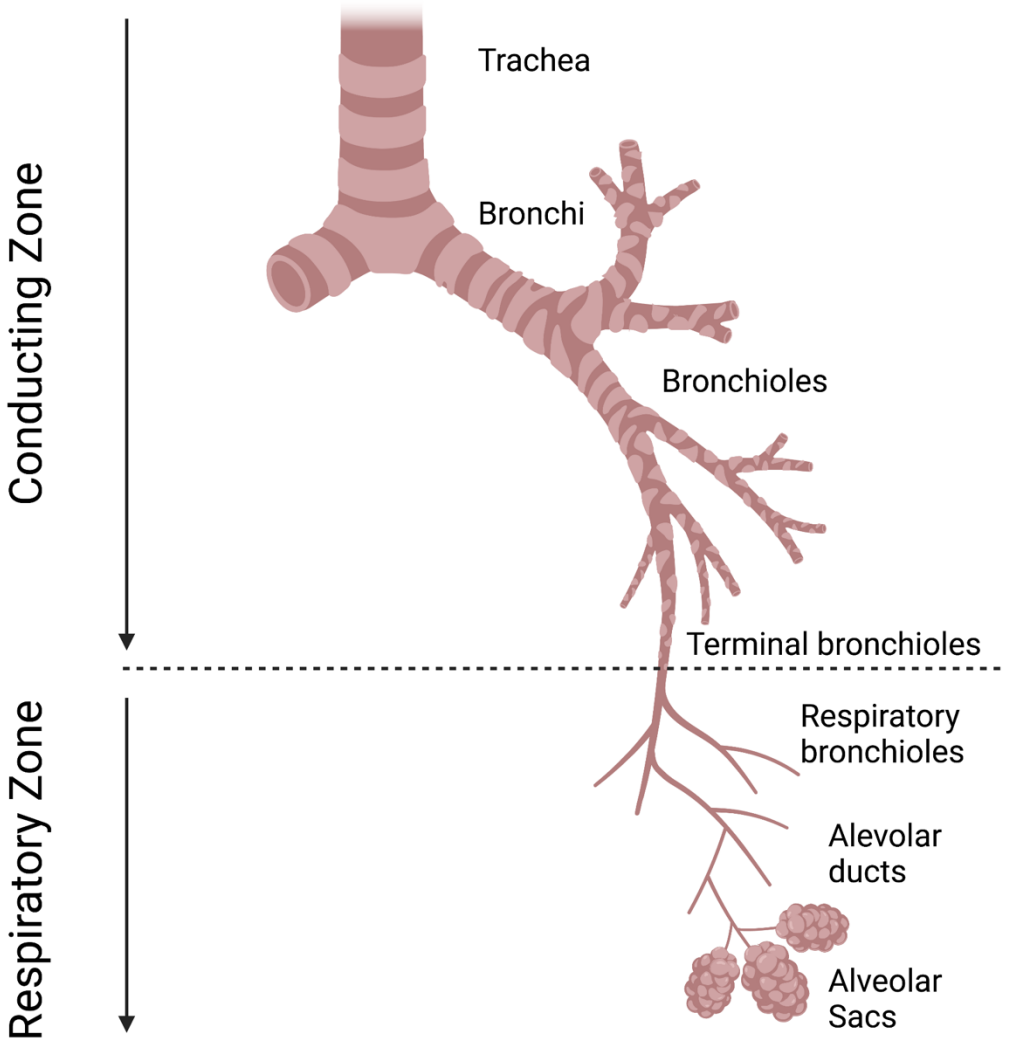

Figure 1. Airway anatomy. Air passes through the mouth and nose and down through the conducting airways, which consist of the trachea, bronchi, and bronchioles. The air continues through the respiratory zone: respiratory bronchioles, alveolar ducts, and alveolar sacs, where the site of gas exchange occurs. Image created with Biorender.com.

ii. Lower Airway

1. Trachea

The trachea is a tubular structured lined with pseudostratified columnar ciliated epithelium and supported by c-shaped rings of hyaline cartilage[24]. The rings provide structural support and prevent the trachea from collapsing. Bridging these cartilage rings on the posterior boarder is the trachealis muscle, which is smooth muscle responsible for bronchoconstriction. Postganglionic parasympathetic cell bodies arranged in various-sized ganglia are embedded outside this muscle as well as between the cartilage rings. The trachea epithelium also contains goblet cells, which are column-shaped cells. These cells produce mucin, a component of mucus, which helps to moisten and protect the airways. Mucus traps inhaled particles, which ciliated cells waft upwards for swallowing or expelling.[27] In the trachea, submucosal glands are the main source of mucus. The volume of these glands is 50 times that of the goblet cell. They decrease in size and frequency distally. Submucosal glands are regulated by both sympathetic and parasympathetic innervation.[25]

2. Bronchi and Bronchioles

The two mainstem bronchi diverge from the trachea to the left and right. They contain cartilage, smooth muscle, and a mucosal lining. The inner epithelium is made up of respiratory epithelium or ciliated pseudostratified columnar epithelium. The bronchi also contain goblet cells. Goblet cells are non-ciliated cells that synthesize and secrete mucins, which are heavily glycosylated proteins that protect and lubricate epithelial cell surfaces, and increase in number in asthma and chronic bronchitis[28]. As branching continues distally through the bronchial tree, the amount of hyaline cartilage decreases

until it is absent in the bronchioles. The epithelium also transforms from ciliated pseudostratified columnar epithelium to simple cuboidal epithelium in the bronchioles with club cells instead of goblet cells. These club cells make surfactant which help bronchioles expand during inhalation and avoid bronchial collapse during exhalation. Pulmonary neuroendocrine cells (PNECs) make up about 1% of the airway mucosa. PNECs are short pyramid cells with cytoplasmic projections to the lumen grouped in small clusters (five cells) or neuroepithelial bodies (NEBs) (>20 cells).[29] PNECs contain signaling molecules including serotonin, substance P, calcitonin gene-related peptide (CGRP), gamma-aminobutyric acid (GABA).[30] Although the precise functions of NEBs is still not known, they are thought to respond to various airway stimuli such as hypoxia, hypercarbia, acidosis, and mechanical stretch.[31]

3. Alveoli

The terminal bronchioles divide into respiratory bronchioles, which are the narrowest airways in the lungs and these lead to alveolar ducts and alveolar sacs. These small air sacs are made up of type I pneumocytes and type II pneumocytes. Type I pneumocytes are the thin, simple squamous epithelial cells that cover the majority of the surface area and are responsible for the exchange of oxygen and carbon dioxide. Type II pneumocytes secret surfactant, which keeps the alveoli from collapsing and can convert into type I cells in order to repair damage.[32] Alveoli also contain macrophages that phagocytize foreign particles, dead cells, and bacteria.

The alveoli have a large total epithelial surface area of about 80 m^2, which allows for an efficient site of gas exchange.[33] Here, blood and gas are brought within 1 micron of

each other. Capillary networks surround the alveoli, where oxygen molecules move through a single layer type I pneumocytes, then through a single capillary endothelial layer to enter the bloodstream. Carbon dioxide diffuses from the capillaries to the alveoli along its concentration gradients.[34, 35]

b. Blood Supply in the Lungs

The lungs are unique in that they have two circulatory systems. First, there are the pulmonary arteries, which are a low-pressure system of deoxygenated blood arising from the right ventricle that participate in gas exchange. These arteries form an extensive meshwork of capillaries surrounding the alveoli. Second, there are the bronchial arteries, which branch from the aorta and form a high-pressure system that is part of systemic circulation. These arteries supply oxygen to the airway tissues including the trachea, bronchi, and bronchioles. The bronchial arteries drain into the bronchial veins, which flow back into the systemic circulation.[36]

c. Anatomical Differences between Human and Mouse Airways

Although mouse lungs have similar general organization to humans, there are still significant differences in architecture, connective tissue, and cellular composition. Human lungs have two lobes on the left and three on the right while mice have only one left lobe and four right lobes [37]. Airway branching in the mouse is also more asymmetric compared to humans and gives rise to fewer generations of airway branches[38]. Mice also have a thinner respiratory epithelium and a relatively large airway lumen[39]. Furthermore, mice have a paucity of submucosal glands, but a large number of club cells, whereas humans have a large distribution of glands throughout the airway.

C. Airway Nerves

In the airways, sensory neurons send processes through airway epithelium, detect stimuli, and relay signals through the central nervous system. This relay activates parasympathetic nerves, which are the dominant autonomic nerves in the airways controlling airway smooth muscle. Vagal parasympathetic nerves release acetylcholine, which activates M_3 muscarinic receptors on airway smooth muscle, causing bronchoconstriction. Acetylcholine release is limited by inhibitory neuronal M_2 muscarinic receptors on presynaptic postganglionic parasympathetic nerves. Together, this pathway forms nerve-mediated reflex bronchoconstriction (Figure 2).[40]

a. Afferent Sensory Nerves

i. Anatomy

Airway sensory nerves are primarily responsible for communicating mechanical and chemical information from the airway epithelium to the central nervous system. Activation of these nerves elicits neuronal reflexes, some of which include cough, altered breathing pattern, and bronchial hyperreactivity. These reflexes are important in both lung homeostasis and disease[41]. Sensory nerves are pseudo-unipolar, meaning they have a cell body with an axon that extends out and branches into two segments with one part innervating the airway and the other synapsing onto neuron located in the

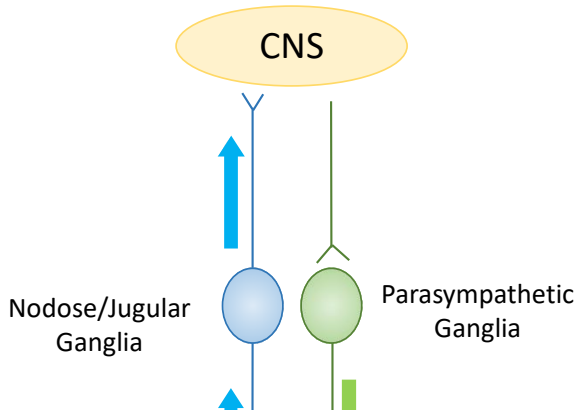

brainstem[42]. The majority of airway sensory nerve cell bodies are located within the nodose and jugular vagal ganglia. Some airway sensory nerve bodies are located in the upper thoracic dorsal root ganglia along the spinal cord (T1-T6).[43] Airway nerve processes that ascend to project in the brainstem terminate in the paratrigeminal nucleus and the nucleus of the solitary tract[41], while processes that descend to terminate in the trachea, primary bronchi, and lungs.

ii. Developmental Origin Characterization

The vagal sensory neurons innervating the respiratory tract have cell bodies located in two distinct ganglia referred to as the nodose ganglion and the jugular ganglion (also known as the inferior and superior vagal ganglion or nodose and supranodose ganglion). These two ganglia arise from separate developmental origins. Neurons within the jugular ganglion derive from neural crest cells located in the dorsal midline of the neural tube during development, while neurons in the nodose ganglia are derived from epibranchial placodes. Similar to jugular ganglia, dorsal root ganglia neurons derive from neural crest cells.[44]

iii. Subtypes of Sensory Nerves

Sensory nerves can be broadly categorized by the conduction velocities of their axons as 1) C-fibers (slowest), 2) Aδ intermediate, and 3) Aβ fibers (fastest). C-fibers are nociceptors that can be subclassified as pulmonary C-fibers or bronchial C-fibers, depending on whether they receive their blood supply from the pulmonary or bronchial circulation, respectively[45]. C-fibers can also be named after their embryonic origin, nodose or jugular. Nodose C-fibers can be stimulated by many different chemical

stimuli, while jugular fibers are more likely to express neuropeptides. C-fibers project to the airway epithelium and are responsible for activating nerve-mediated reflex bronchoconstriction[46]. C-fibers may also be involved in peripheral reflexes that activate parasympathetic ganglia[47].

Aδ fibers stimulate cough and terminate in the extrapulmonary bronchi, trachea, and larynx. These fibers are myelinated and thus, conduct faster action potentials than C-fibers. Finally, Aβ fibers are categorized based on action potential adaptation as either slowly adapting receptors (SARs) and rapidly adapting receptors (RARs).[44] These are myelinated and the largest and fastest neurons of the three. RARs terminate within or beneath the airway epithelium and are present throughout the airways, while SARs are more associated with the airway smooth muscle.[44]

b. Efferent Parasympathetic Autonomic Nerves

i. Anatomy

Preganglionic parasympathetic nerve cell bodies reside in the dorsal motor nucleus of the vagus and the nucleus ambiguus, both of which are located in the brainstem[44]. As the vagus nerves descend through the body, on the left side it loops around the aorta and on the right side it loops around the subclavicular artery merging to form the recurrent laryngeal nerve. The axons of efferent parasympathetic autonomic nerves are located within the vagus nerves, which run caudally along the trachea. The nerves then branch off to innervate the trachea, main bronchi, and lungs. These nerves synapse onto postganglionic cell bodies embedded within the trachea. Two distinct parasympathetic pathways exist: the first is the classic pathway that utilizes

acetylcholine as the neuroeffector (postganglionic) transmitter, and the second is a noncholinergic pathway dependent on nitric oxide and vasoactive intestinal peptide (VIP) for postganglionic transmission[48].

ii. Neurotransmitters

Acetylcholine (ACh) is the main neurotransmitter responsible for bronchoconstriction in the airways. It is released from preganglionic parasympathetic nerves as well as epithelial cells[49] and synapses onto postganglionic nicotinic receptors. Acetylcholine binds to muscarinic receptors located on airway smooth muscle, ultimately causing contraction and controlling airway tone. Acetylcholine is synthesized by the enzyme choline acetyltransferase, which transfers an acetyl group from coenzyme A to choline[50]. It is stored in intracellular vesicles and released from nerve terminals under normal resting conditions as well as in response to stimulation[51]. Acetylcholine binds to nicotinic and muscarinic receptors on the post-synaptic membrane and relays the neural signal. After acetylcholine is released into the synapse, it is rapidly broken down by acetylcholinesterase, located on the post-synaptic membrane, and hydrolyzed into choline and acetate. Choline is then transported back into the axon terminal and used to make more acetylcholine.[52] Acetylcholinesterase inhibitors, such as physostigmine, inhibit acetylcholinesterase from breaking acetylcholine down and increase the level and duration of acetylcholine action, enhancing stimulation of postsynaptic cholinergic receptors in the central or peripheral nervous systems[53].

Substance P is a neurotransmitter and neuropeptide expressed by airway sensory nerves that causes bronchoconstriction. Substance P is part of the tachykinin family and

originates in sensory nerve ganglia and has been localized to airway epithelial nerve endings[54, 55]. It causes bronchoconstriction by both directly binding to neurokinin-1 (NK1) receptors on airway smooth muscle[56] and also by indirectly potentiating nerve function through neurogenic inflammation. Substance P nerve fiber density expression increases in models of asthma and contributes to airway hyperresponsiveness[57]. Other neuropeptides in the airways include nitric oxide synthase (NOS), calcitonin gene-related peptide (CGRP), and vasoactive intestinal peptide (VIP)[58-60]. These neuropeptides are important in mediating asthma physiology and can be dysregulated in asthma pathology[61, 62].

iii. Reflex Bronchoconstriction

Reflex bronchoconstriction is initiated by activation of airway epithelial nerves signaling to the central nervous system. The signal then propagates through preganglionic parasympathetic nerves to synapse in the vagal (nodose/jugular) ganglia. Postganglionic parasympathetic nerves transmit the signal onto airway smooth muscle, releasing acetylcholine and causing bronchoconstriction.

c. Efferent Sympathetic Autonomic Nerves

Sympathetic nerves in the airway may control tracheobronchial blood vessels, but do not directly innervate airway smooth muscle[63]. Sympathetic preganglioinic neurons reside in the intermediolateral cell column of the spinal grey matter[44]. Sympathetic nerves do not significantly contribute to airway tone in humans[64].

d. Efferent Bronchodilatory Autonomic Nerves

Non-adrenergic non-cholinergic (NANC) nerves are involved in the relaxation of airway smooth muscle[65]. Vasoactive intestinal peptide (VIP) and nitric oxide synthase (NOS) are associated with NANC nerves. These nerves arise from the myenteric plexus of the esophagus and project axons to the trachealis muscle.[66] It is not clear what role NANC nerves may play in asthma pathology.

e. Central Nervous System Nerves

The central nervous system connects the afferent sensory and the efferent parasympathetic nerve communication. Studies using retrograde neuronal tracers to label preganglionic nerves projecting to the airways have found airway neurons located in the nucleus ambiguous, dorsal motor nucleus of the vagus, and the reticular formation located between those two structures[67, 68]. Central terminations of the afferent airway fibers are located in the nucleus of the solitary tract (nTS)[69, 70]. Different afferent nerve subtypes (for example those from bronchospasm, bradycardia, gastric relaxations) coming from the airways end in adjacent or overlapping regions of the nTS.[71] Plasticity in the nTS through substance P-mediated mechanisms in airway sensory nerves may contribute to central sensitization and modulate output to efferent nerves of the airways leading to airway hyperreactivity.[72]

f. Receptors in the Lungs and Heart

Contraction of the airways is mediated mainly by M_3 muscarinic receptors located on airway smooth muscle, while relaxation is mediated by $ß_2$ adrenergic receptors. $5HT_{2A}$ serotonin receptors are also located on airway smooth muscle and contribute to muscle

contraction. M_2 muscarinic receptors are present on airway smooth muscle; however, they only indirectly promote smooth muscle contraction by antagonizing relaxation[73] and only make up 20% of the muscarinic receptor population (compared to 80% M_3 receptors) [74]. M_2 muscarinic receptors are also found on postganglionic parasympathetic airway nerves. They serve to inhibit the release of acetylcholine from nerve terminals. In addition, $5HT_3$ and $5HT_4$ serotonin receptors are located on airway nerves[75].

Both the sympathetic and parasympathetic branches of the autonomic nervous system control the heart. Short preganglionic sympathetic nerves arising from the sympathetic chain release acetylcholine onto nicotinic receptors of postganglionic cell bodies in the stellate ganglia. Norepinephrine acts on $ß_1$ adrenergic receptors in the SA node increase heart rate, in the AV node to increase conduction velocity, and in the cardiomyocytes to increase contractility. Preganglionic parasympathetic nerves release acetylcholine onto postganglionic cell bodies in the cardiac ganglion. Acetylcholine arising from postganglionic nerves and binding to M_2 receptors slow the heart rate and reduces the contractility of atrial cardiomyocytes.[76]

D. Obesity-Related Asthma

a. Overview

Obesity-related asthma is a significant comorbidity exacerbated by the accelerating global obesity public health crisis. There are over 250,000 new obesity-related asthma cases per year in the United States[4, 77-81]. Over 60% of adults with severe asthma are obese[82,83], and respond poorly to typical asthma medications, such as corticosteroids, leading to higher healthcare costs[84] and a substantially reduced quality of life[4,85]. The

molecular mechanisms of obesity-related asthma and associated increased bronchoconstriction remain unclear, however, limiting our ability to develop new therapeutic strategies.

b. Early vs. Late-onset

Asthma may develop in either obese children or obese adults, but the pathophysiology is distinctly different. Children more frequently develop early-onset, allergic T_H2-driven asthma as described previously, whereas obese adults tend to develop asthma in the absence of T_H2-driven inflammation in the lungs[86]. Obesity in children exacerbates an eosinophilic, allergic asthma. In adults, obesity is likely a consequence of obesity-induced metabolic changes. The former may be described as having early onset asthma complicated by obesity, while the latter develop asthma due to obesity.

c. Obesity-Related Asthma and Airway Inflammation

Although obesity and metabolic syndrome are associated with general systemic inflammation, four large clinical studies found no relationship between obesity-associated asthma and the cellular airway inflammation normally associated with allergic asthma[87-90]. In alignment with this conclusion, studies in diet-induced obese C57BL/6 mice show that increased bronchoconstriction in these mice does not correspond to airway inflammatory cell infiltration[91]. Lack of airway inflammation in obesity-related asthma may explain why corticosteroids are less effective in the treatment of asthma in these patients[92,93]. This evidence suggests an alternate mechanism of increased bronchoconstriction underlying asthma in obese patients.

d. Mouse Models of Obesity-Related Asthma

Animal models are useful for investigating aspects of disease that would be challenging to fully examine in humans. Nonspecific innate airway hyperreactivity to both methacholine and serotonin is increased in multiple mouse obesity models, including ob/ob mice[94], db/db mice[95], Cpe^{fat} mice[96], and diet-induced obese mice.[91] Therefore, these individual gene mutations are not response responsible for the relationship between obesity and airway hyperreactivity, rather something more complex is at play.

i. Ob/Ob Mice

Ob/ob mice have a deficiency in the leptin gene. Leptin is a satiety hormone synthesized by adipocytes that suppresses appetite and increases metabolism by binding to its receptor in the hypothalamus.[97] Ob/ob mice have a low resting metabolic rate, hypoactivity, hyperinsulinemia, hyperglycemia, increased serum[98] corticosterone, and increased fasting triglycerides and cholesterol[98]. Studies using ob/ob mice indicate that these mice have increased innate airway hyperreactivity[94], ozone-induced airway hyperreactivity, and ozone-induced increased pro-inflammatory airway cytokine production including macrophage inflammatory protein-2 and IL-6[99].

ii. Db/Db Mice

Db/db mice have a mutation in the leptin receptor, leading to obesity, insulin resistance, and type 2 diabetes[100]. Similar to ob/ob mice, db/db mice have hyperphagia, weight gain, and hypoactivity. They are also hyperinsulinemic, hyperglycemic, hyperlipidemic, and hypercholesteremic. Db/db mice have innate, nonspecific airway hyperreactivity to

both serotonin and methacholine.[81] Ozone exposure also causes increases in airway responsiveness and increases in bronchoalveolar lavage IL-1β levels, tumor necrosis factor alpha (TNF-α) mRNA expression, and neutrophils in db/db mice compared to wild type mice[95].

iii. Cpe^{fat} Mice

Cpe^{fat} mice have a deficiency in carboxypeptidase (Cpe), which is required for processing insulin, enkephalins, neurotensin, and other neuropeptides.[101] Cpe^{fat} mice develop a more moderate obesity compared to ob/ob and db/db mice. Studies with Cpe^{fat} mice have shown innate airway hyperreactivity to methacholine and increased airway cytokines, including monocyte chemotactic protein-1 and soluble TNF receptors[96].

iv. Diet-Induced Obesity

The diet-induced obesity model more closely mimics the weight gain in response to high-fat/high-calorie foods that is seen in humans. C57BL/6 mice fed a diet of 45-60% fat become obese[102] and can be used to study ensuing metabolic dysfunction. Diets high in sugar in rodents do not seem to initiate the development of metabolic changes that characterize obesity[103]. Diet-induced obese mice are hyperinsulinemic and hyperglycemic. An advantage of the diet-induced obesity model is that it more closely resembles the comorbidities of human obesity and does not produce as extreme obesity and hyperphagia as the genetic mutation models. Because it does not rely on genetic manipulation, it can also be used to induce obesity in multiple animal species. Similar to the genetically modified animals discussed, diet-induced obese mice have innate airway

hyperreactivity as well as enhanced ozone-induced pulmonary cytokine inflammation[91]. Airway hyperreactivity, however, occurs in diet-induced mice on 60% fat only when substantial weight gain has occurred, which takes longer to achieve than genetic obesity mouse models[81].

e. Obesity-Related Asthma Treatment

Obese patients tend to have poor asthma control. One study showed obese individuals have a five-fold increased risk of hospitalization due to asthma exacerbations compared with lean asthmatics[79]. Obese individuals do not respond well to standard asthma treatments. In obese asthmatic patients, inhaled corticosteroids and the combination of inhaled corticosteroid and long-acting β agonists work better than Montelukast, a selective D4 leukotriene receptor antagonist[93, 104]. None of these treatments, however, are as effective in obese individuals as they are in lean individuals. A higher BMI also strongly correlated with lingering asthma symptoms despite 3 months of intensive treatment with high doses of inhaled corticosteroids[88]. Unfortunately, all of the currently approved asthma medications were developed in lean animal models of asthma and tested in lean patient population. Because the phenotype and development of asthma in obesity differs from that of lean asthmatics, the response to treatment is also altered in these individuals. This has led to a gap in the treatment of obese asthmatic patients.

Weight reduction surgeries result in significant improvements in airway hyperresponsiveness, severity, medication use, and hospitalization[105-107]. Bariatric surgery, however, is expensive and comes with risk of complications. Changes in diet and exercise that result in weight loss can also show asthma improvements[108].

However, in a study that randomized obese asthmatics to dietary intervention, exercise, or exercise plus dietary intervention for the treatment of asthma, only patients in the dietary intervention and exercise plus dietary intervention experienced significant improvements in asthma control[108]. Both of these groups had significant weight loss, indicating that exercise alone may not be sufficient for asthma improvements in obese individuals. Despite the potential for decreasing obesity-related asthma with lifestyle interventions, this is a particularly difficult outcome to achieve and the majority of patients will require additional medical interventions to control their asthma.

E. Insulin

a. Overview

Insulin is an anabolic pleiotropic hormone that regulates glucose and lipid metabolism as well as growth and differentiation of cells (Figure 3). Insulin is synthesized initially as single-chain precursor polypeptide, preproinsulin, and then processed to proinsulin by cleavage of its N-terminal signal peptide. Proinsulin is converted to insulin and C-peptide and stored in secretary granules of pancreatic β-cells awaiting release[109]. Insulin content in β-cells is dynamic. It accumulates in the presence of nutrients and decreases in response to nutrient deprivation. It plays a major role in metabolism regulation. Glucose stimulates the fusion of insulin granules with the plasma membrane and initiates exocytosis of insulin granules. In the bloodstream, insulin stimulates muscle, liver, and adipose tissue to uptake glucose via translocation of the insulin-sensitive glucose transporter (GLUT-4) from intracellular vesicles to the cell membrane[110]. GLUT4 is one of thirteen glucose transporters that catalyze hexose transport across cell membranes via ATP-independent, facilitative diffusion.

b. Insulin Receptor and Signaling

In many insulin-sensitive peripheral tissues, including the liver, adipose tissue, and skeletal muscle, the main function of the insulin receptor is to mediate glucose transport into cells. The insulin receptor belongs to the tyrosine kinase receptor family.[111] The insulin receptor subfamily consists of the insulin receptor, insulin-like growth factor I (IGF-1) and II (IGF-2) receptors, and the insulin receptor-related receptor (IRRR). In

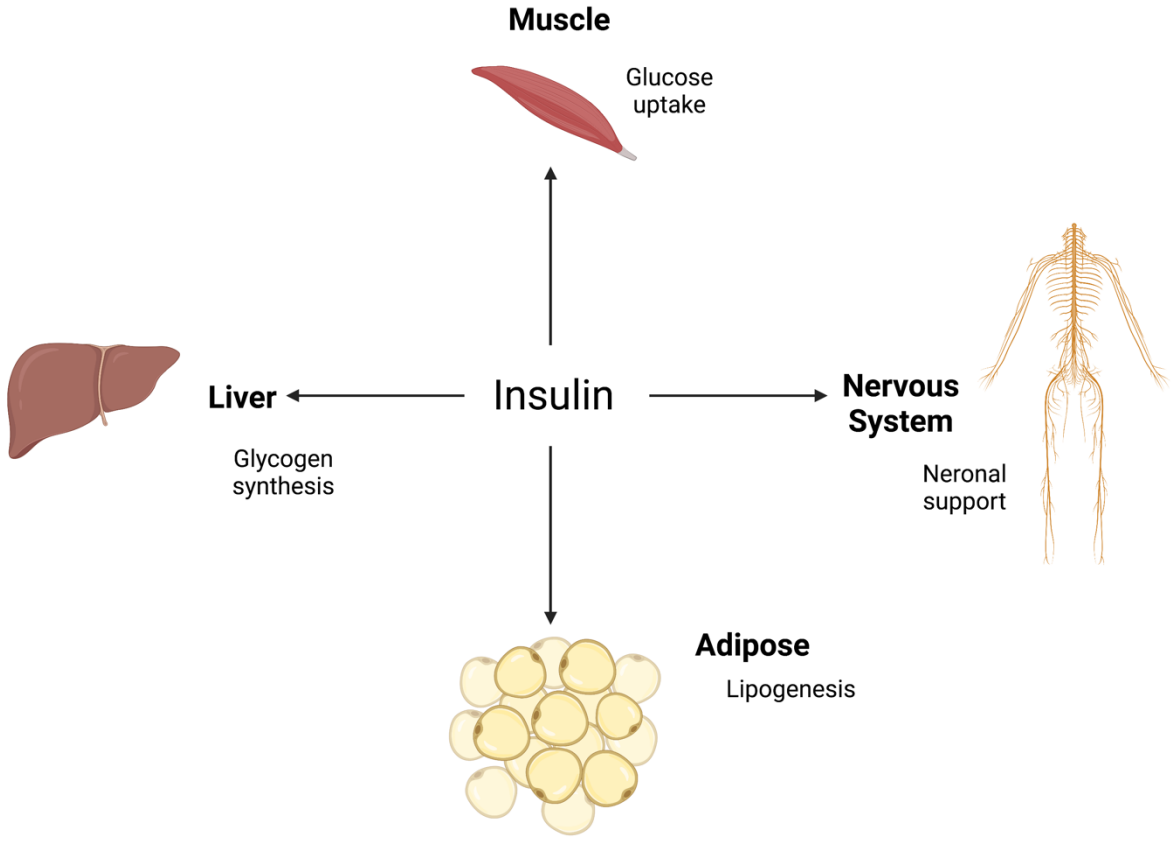

Figure 3. Effects of insulin on body tissues. Insulin is a pleiotropic hormone that regulates glucose and lipid metabolism as well as the growth and differentiation of cells. Insulin has unique functions on each tissue including the liver, adipose, muscle and nervous system. Image modified from *Bunner et al*. and created with Biorender.com.

cells expressing both insulin and IGF-1 receptors, hybrid receptors form consisting of one half of each.

i. Structure

1. mRNA Isoforms

The insulin receptor is encoded by a gene with 22 exons and 21 introns. It has two isoforms (IR-A and IR-B) that result from exon 11 alternate splicing. Exon 11 encodes 12 amino acids that are present in the α-subunit[112]. Insulin has higher binding affinity for IR-A than IR-B, while IR-B has a more efficient signaling activity[112, 113]. IR-A has more mitogenic actions, whereas IR-B is predominantly involved in metabolism, glucose regulation, and lipid storage[114]. Relative distribution of IR-A and IR-B expression vary depending on the tissue. IR-A is the main isoform expressed in the nervous system, fetal tissue, and various cancers including breast, hepatocellular, lung, colon, and thyroid cancer[115]. IR-B, however, is the dominant isoform in adipose, liver, and skeletal muscle[116]. IR-B is also involved in adipocyte, hepatocyte, and hematopoietic cell differentiation[117]. Alternative insulin receptor splicing may explain functional differences in insulin action between tissues.

2. Receptor Subunits

The insulin receptor is composed of two subunits, α (135 kDa) and β (95 kDa), which form a disulfide-linked heterotetramer[69] (Figure 4). The α -subunits contain a cysteine-rich region, which is critical to ligand-binding[118]. Cysteine residues in the COOH-terminal region of the α-subunits form disulfide bonds with β-subunit cysteine residues, which links the α and β-subunits together. The β-subunit is composed of three regions:

the extracellular, transmembrane, and cytosolic domains. The cytosolic tyrosine kinase domain has an ATP binding sequence and tyrosine residues that are phosphorylated in response to insulin ligand binding.[119]

ii. Signaling Pathway

Insulin receptor signaling is initiated by insulin or IGF-1 binding causing a conformational change in the β subunits and bringing them closer together. This activates β subunit tyrosine autophosphorylation. This activates insulin receptor substrate (IRS) and Shc. Activation of signaling happens via phosphorylation of specific serine/threonine sites and stimulates two major canonical downstream pathways, one of which is the phosphoinositide-3 kinase (PI3K)/Akt and the other Ras/mitogen-activated protein kinase (MAPK) also known as the extracellular signal regulated kinase (ERK) pathway. Insulin binding to isoform A initiates the mitogenic signaling cascade, while binding to isoform B activates the metabolic pathway[117, 121]. This results in a diverse series of cellular processes in peripheral tissues. The metabolic arm contributes to glucose metabolism, while the mitogenic arm leads to gene expression, cell growth, and differentiation[122, 123]. Insulin (and pro-insulin), insulin-like growth factor 1 (IGF-1), and insulin-like growth factor 2 (IGF-2) can all bind and activate the insulin receptor; however, they have different binding affinities and potencies[124].

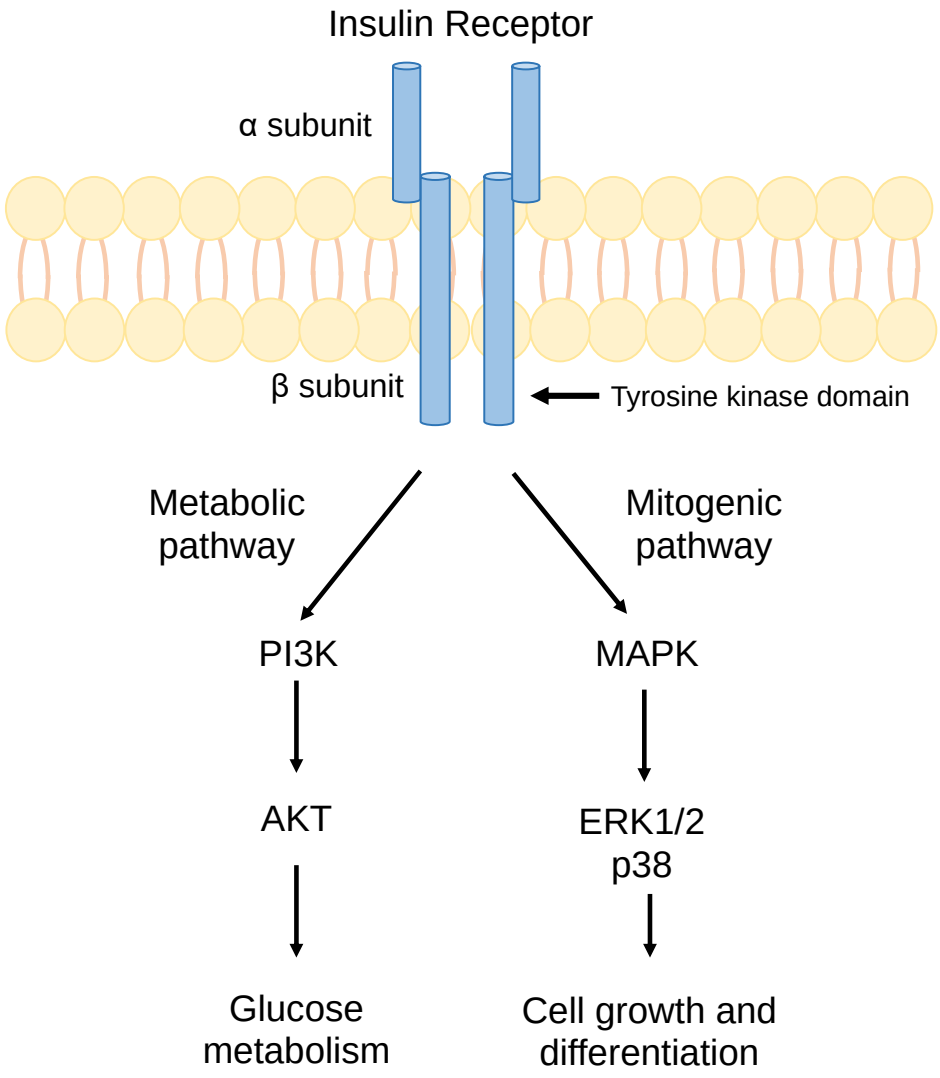

Figure 4. Insulin signaling pathway. Insulin binding to and activating its receptor leads to both metabolic effects such as glucose metabolism as well as mitogenic outcomes including cell growth and proliferation.

1. Insulin Receptors in Neurons

The insulin receptor is widely expressed in neurons in the peripheral and central nervous systems[125]. Neurons in the brain and periphery respond to insulin by promoting satiety, hormonal regulation, and metabolic homeostasis through PI3K/Akt signaling[126]. Administrating insulin to the brain reduces food intake and body weight[127]. Importantly, however, glucose uptake by the majority of neurons is considered either insulin-independent or indirectly regulated by insulin. The Ras/MAPK pathway facilitates neuronal cell growth, maintenance, and survival. ERK activation in particular is an important signaling molecule for many neuronal functions including survival[128], memory[129], and synaptic plasticity[130].

c. Insulin Dysfunction in Obesity

During obesity, excess caloric and nutrient intake, or metabolic overload, leads to adipose tissue expansion and visceral adiposity. In obesity, adipocytes have maximally expanded leading to adipose tissue dysfunction and infiltration of immune cells, which is associated with insulin resistance of the adipose tissue itself.[131] Insulin resistance is defined as a state of reduced responsiveness of target tissues to normal circulating levels of insulin and is the central feature of type 2 diabetes and metabolic syndrome. Resistance to insulin in hepatocytes increases plasma glucose levels due to reduced glycogen synthesis as well as the inability of skeletal muscle and adipocytes to take up glucose[132]. In addition reduced insulin receptor responsiveness leads to compensatory insulin hypersecretion in order to regulate blood glucose levels. High insulin concentrations in cell models show that insulin acts as a mitogen. There is mounting evidence supporting an important role of hyperinsulinemia in type 2 diabetes activating

the mitogenic pathway and leading to increased rates of certain cancers such as pancreas, liver, prostate, endometrial, and breast[133]. And while peripheral tissue insulin receptors are downregulated in response to insulin excess, insulin receptors expressed in the central nervous system do not show that same downregulation[134].

d. Insulin and Obesity-Related Asthma

Insulin resistance and compensatory hyperinsulinemia are common in obese individuals and increase the risk of asthma, independent of other variables[86]. Insulin resistance is associated with the development of asthma symptoms in obese adults[77, 135] and asthma-like symptoms including incident wheezing independent of obesity[136]. These effects appear to rely on metabolic dysfunction and not on increasing body weight or adiposity alone. In a recent study of two unique cohorts, the risk of having asthma and reduced lung function in adulthood was higher in those with high blood insulin levels in early childhood, independent of body mass index[137].

In animal studies, insulin has been implicated as a mediator in models of obesity-related asthma. Hyperinsulinemia in obese rats leads to potentiated parasympathetic nerve-mediated bronchoconstriction and loss of inhibitory M_2 muscarinic receptor function without affecting smooth muscle contractility to acetylcholine[138]. Insulin also enhances extracellular matrix laminin expression and induces hypercontractility and hyperproliferation of airway smooth muscle[139]. Furthermore, insulin resistance induced by obesity can amplify TGF-β1 expression, lung fibrosis, and airway hyperresponsiveness in mice without significant cellular infiltration into the

airways[140]. These findings point to insulin as playing a key role in obesity-related asthma.

e. Insulin Knockout Mouse Models

Mouse models with insulin signaling disruption have been instrumental in understanding metabolism, insulin resistance, diabetes, and growth restriction. Mice have two insulin genes Ins1 and Ins2. The two genes code for preproinsulin 2 (Ins2), which is an ortholog to the insulin genes in other mammals, and preproinsulin 1 (Ins1), a rodent-specific retrogene. These two insulin genes are located on different chromosomes, chromosome 7 (Ins1) and chromosome 19 (Ins2)[141]. Ins2 has three exons and two introns, while Ins1 has only one intron homologous to the first intron of Ins2[142]. Glucose homeostasis is normal after ablation of either gene alone[143]. Interrupting both Ins2 alleles and one allele of Ins1 reduces circulating insulin by over 50% without greatly affecting glucose homeostasis[144]. Deleting both Ins1 and Ins2 leads to growth retardation and death within 48 hours of birth[145].

Mice lacking the insulin receptor gene Insr are born with slight growth retardation but no metabolic abnormalities[146]. After birth, however, these mice quickly deteriorate. Glucose and insulin levels rise, β-cell failure occurs, and the animals die shortly thereafter from diabetic ketoacidosis[147]. Because this phenotype is lethal, it does not allow for the opportunity to study insulin receptor function in adult mice. Cre promoter-specific tissue knockouts have been developed in order to gain insights into tissue-specific insulin receptor function. In the Cre-loxP system, Cre recombinase recognizes two directly repeated loxP sites and excises the DNA flanking the loxP sites (floxed genes), which

inactivates the gene of interest.[148] Multiple tissue-specific Insr conditional knockout mice have been created including muscle[149], adipose tissue[150], liver[151], β-cells[152], and sensory nerves[153].

F. Maternal and Prenatal Influences on Asthma

Maternal health and in utero exposures have many effects on offspring. Maternal asthma has been shown to increase childhood asthma risk more than paternal asthma[154]. Furthermore, better maternal asthma control during pregnancy reduces the risk of asthma in her child[155]. In pregnant IL-5-overexpressing transgenic mice with eosinophilia and airway hyperreactivity, maternal IL-5 crosses the placenta and causes eosinophilia in the fetus. This exposure to high IL-5 levels in utero leads to increased airway sensory innervation and reflex bronchoconstriction into adulthood, even after normalization of IL-5 and eosinophil levels after birth.[156] These findings suggest that intrauterine exposure to adverse maternal factors is an important factor that contributes to a child's asthma risk.

a. Developmental Origins of Health and Disease Hypothesis

The developmental origins of health and disease (DOHaD) hypothesis proposes that in utero exposure to maternal health factors, such as obesity, affects offspring's body composition and metabolic function thereby predisposing offspring to obesity and metabolic disease later in life[157]. Importantly, the offspring of overweight and obese mothers are at an increased risk of developing respiratory complications such as wheezing and asthma[158-161]. A high saturated fat maternal diet throughout pregnancy and lactation also plays a key role in adult offspring airway hyperreactivity[162]. Maternal

health, therefore, appears to be important in the development of asthma in offspring and targeting therapies toward pregnant mothers may be a useful strategy for preventing offspring asthma.

G. Neural Mechanisms of Airway Hyperresponsiveness (Hyperreactivity)

Airway responsiveness describes the ability of the airways to narrow in response to constrictor agonists. Airway hyperresponsiveness, also known as airway hyperreactivity, therefore, is defined as increased sensitivity in response to an inhaled agonist that results in constriction of airways known as bronchoconstriction[163]. Airway hyperresponsiveness is a defining characteristic of asthma and the severity correlates with severity of asthma and treatment needed to control symptoms[164]. Airway responsiveness can be measured using constricting agonists such as histamine or methacholine. Loss of M_2 receptor function has been associated with increased acetylcholine release and increased airway hyperreactivity in multiple animal models of human diseases including obesity[138], antigen challenge [165], virus infection[166], exposure to ozone[167], and exposure to organophosphorus pesticides[168]. The mechanisms responsible for the airway hyperreactivity in individual asthma subtypes are still currently under investigation, but may involve changes throughout the reflex bronchoconstriction mechanism: in afferent (sensory) nerves, the central nervous system, or efferent (parasympathetic) nerves.

a. Afferent Sensory Nerves in Hyperreactivity

Sensory nerve endings are found throughout the trachea and primary bronchi epithelium. The distribution of these epithelial nerves fluctuates with denser patches located in airway bifurcations and areas with fewer nerves in the distal airways[169].

Because of the plasticity of airway nerves, increases in nerve length and branching of nerves in the airway epithelium can result from asthma pathology (Figure 5). Abnormal nerve remodeling in asthmatic patients and mouse models suggests that sensory nerves may be responsible for increased airway hyperresponsiveness in asthma[170].

i. Substance P Expression

Increase in expression of sensory neuron neuropeptides, such as substance P, also likely contributes to airway hyperreactivity in asthma. In biopsies from asthmatic humans, airway epithelial nerves were found to have increased an increase in the percentage of nerves expressing substance P[170]. Substance P is a neuropeptide that induces vasodilation, microvascular leakage, and mucus secretion. In asthma patients, substance P induced hyperresponsiveness to methacholine by increasing maximal airway narrowing to methacholine twenty four hours after inhalation[171]. Substance P has also been found to be increased in the epithelium[172] and bronchoalveolar lavage[173] of asthmatic patients. Despite these findings, drugs targeting substance P or its receptor neurokinin 1 (NK1) have not been clinically successful[174-176].

Decreased substance P metabolism may also lead to airway hyperreactivity. Neutral peptidase is a cell surface metalloprotease and the main proteolytic enzyme responsible for substance P degradation.[177] Decreased neutral endopeptidase activity could result in enhanced neurogenic airway inflammation, and airway hyperreactivity in this context has been shown in antigen challenge[178], viral infection[179, 180], and cigarette smoke[181]. Neutral endopeptidase is also significantly increased in the airway epithelium of patients

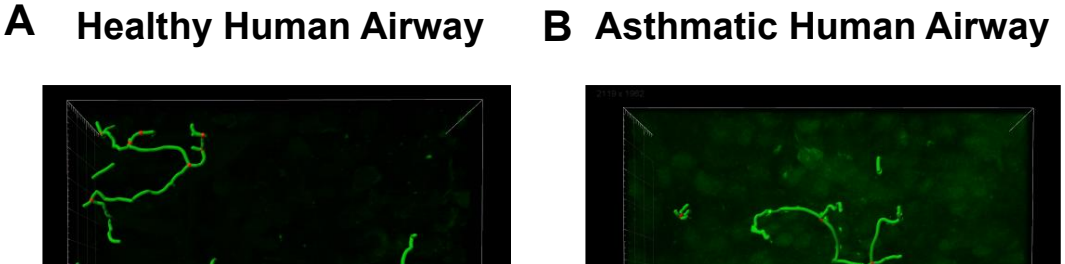

using inhaled steroids, which may play a role in the beneficial effects of corticosteroids in asthma treatment[182].

Substance P has been also identified as an neuropeptide involved in appetite stimulation in obesity[183]. Blocking the NK1 receptor in diet-induced obese and *ob/ob* mice resulted in decreased weight and food intake and improvement in glucose levels[183]. Another study demonstrated that diet-induced obese Balb/c mice had higher levels of serum substance P than lean mice[184]. Therefore, substance P may be involved in obesity-related asthma pathogenesis. The supporting evidence for this, however, is limited.

b. Central Nervous System in Hyperreactivity

Neuroplasticity can occur in the nucleus of the solitary tract (NTS), nucleus ambiguous, and other regions of the brain. Changes in these areas may contribute to airway hyperreactivity through central sensitization[72]. Neuroplasticity at these synapses in the brain can exaggerate, prolong, or suppress the reflex bronchoconstriction output. Neurons in the NTS have shown increased firing activity after antigen exposure in rats[20]. Furthermore, extended exposure to allergen increases the intrinsic excitability of NTS neurons in rhesus monkeys[185]. These studies point to a role for the central nervous system in airway hyperreactivity.

c. Parasympathetic Nerves in Hyperreactivity

Parasympathetic nerves regulate airway tone and mediate airway hyperreactivity via release of acetylcholine onto M_3 muscarinic receptors[186]. Release of acetylcholine is

limited through an inhibitory feedback mechanism controlled by M_2 muscarinic receptors on presynaptic postganglionic parasympathetic nerves[187]. Importantly, airway hyperreactivity in asthma can be caused by M_2 muscarinic receptor dysfunction on parasympathetic nerves.

i. M_2 Muscarinic Receptors

Loss of M_2 muscarinic receptor function on parasympathetic airway nerves leads to increased acetylcholine release and a subsequent increase in vagally-mediated bronchoconstriction. M_2 receptors are dysfunctional in human asthmatic patients[188, 189]. Animal models of asthma and airway hyperreactivity also demonstrate M_2 receptor dysfunction in antigen challenge[165], viral infection[166], ozone exposure[167], and organophosphorus pesticides exposure[168]. Decreased neuronal M_2 receptor function and airway hyperreactivity are also present in diet-induced obese rats and are associated with increased insulin blood levels[190]. Despite the disparate causes of these asthma models, decreased M_2 function was a contributing mechanism to airway hyperreactivity behind each. This data underscores the importance of these receptors in the development of asthma.

H. Methods of Airway Nerve Activation

The responsiveness of airway nerves can be assessed through three main methods. While pharmacological activation of nerves produces a reflex bronchoconstriction response, vagal nerve simulation and electrical field stimulation more directly assess the parasympathetic nervous system control.

a. Serotonin-Induced Nerve Stimulation

Serotonin (5-HT) is a neurotransmitter and vasoactive amine that has diverse physiological activities. Platelets are the main source of serotonin in human lungs[191], but it is also synthesized by PNECs and mast cells[192]. In mice, serotonin strongly activates vagal c-fibers in the respiratory tract via 5-HT_{3AB}, 5-HT_1, and 5-HT_4 receptors to initiate a neuronal-mediated reflex bronchoconstriction response[193]. Increasing doses of serotonin can be used to assess airway nerve responsiveness. Serotonin induces bronchoconstriction through activating airway sensory nerves and causing a reflex response. Although $5HT_{2A}$ serotonin receptors are also located on airway smooth muscle, vagotomy eliminates the bronchoconstriction response to serotonin in mice. This indicates that serotonin acts mainly on airway nerves rather than directly on airway smooth muscle to cause contraction[16].

b. Vagal Nerve Stimulation

Direct vagal nerve electrical stimulation *in vivo* in vagotomized animals stimulates the vagus nerves to fire and causes airway bronchoconstriction. It simultaneously causes a drop in heart rate. Varying electrical pulse voltage and frequency can be used to test lung function and vagal nerve composition[194-196]. Pharmacological drugs, stimulation frequency, and intensity can be used to isolate and test parasympathetic and sympathetic nerve function within the vagus nerve. Vagotomy can be used to isolate parasympathetic control of airway tone in animal models of asthma[138, 197]. This method is difficult to successfully use in smaller animal models like mice, but works well in larger rodents such as rats, and in guinea pigs.

c. Electrical Field Stimulation

Another way of assessing airway nerves is by testing function *ex vivo* in an organ bath setup. The trachea is removed from the animal and sectioned rings are suspended in a warmed and oxygenated physiological salt solution (Krebs buffer) solution. Loops of suture are tied around the tissue and a force transducer at one end measures the force of smooth muscle contraction in response to a generated electrical field stimulation. Electrical field simulation predominantly activates presynaptic nerves[198]. Voltage and frequency of the electrical pulses determine nerve activation[199, 200]. Electrical field simulation can lead to either contraction or relaxation depending on the nerves that are stimulated (cholinergic, capsacin-sensitive, adrenergic, or non-adrenergic non-cholinergic) and the mediator released such as acetylcholine, catecholamines, or tachykinins [201].

I. Methods of Imaging nerves

a. Imaging Airway Nerves

Innervation of the airway is structurally complex and historically has been difficult to fully characterize using conventional histological techniques. Analysis of images from thin tissue section were limited in their ability to capture the complexities of 3D neural structure, which led to incongruent conclusions with regard to neural changes in airway disease. Other methods, such as design-based stereology[202] and optical sectioning[203], are limited by their inability to capture rare or infrequent events (such as sensory nerve branching in the epithelium), under-sampling, and variability in background intensity.

A newer method of visualizing nerves in three dimensions expands the possibilities for understanding and quantifying nerve morphology in whole-mount tissues (Figure 6).

This method uses immunostaining, tissue optical clearing, laser-scanning confocal microscopy, and digital reconstruction of airway nerves.[169, 204] Tissue clearing is the process of making tissues transparent by removing lipids or equilibrating tissue in a solution that has a refractive index which matches that of the tissue proteins. This minimizes the refractive index differences and photon scattering of light when it travels between tissue layers of varying densities and, ultimately, improves image resolution.[205] Optical section involves using a microscope to capture images of thin slices of a much thicker specimen by illuminating images in-focus and removing the contribution of out-of-focus light in each plane[206]. Using tissue clearing and confocal optical sectioning allows for accurate quantification of histological features like nerve length, branching, and density, as well as neurotransmitter and receptor expression, along all nerves in three dimensions (Figure 7).[169, 204]

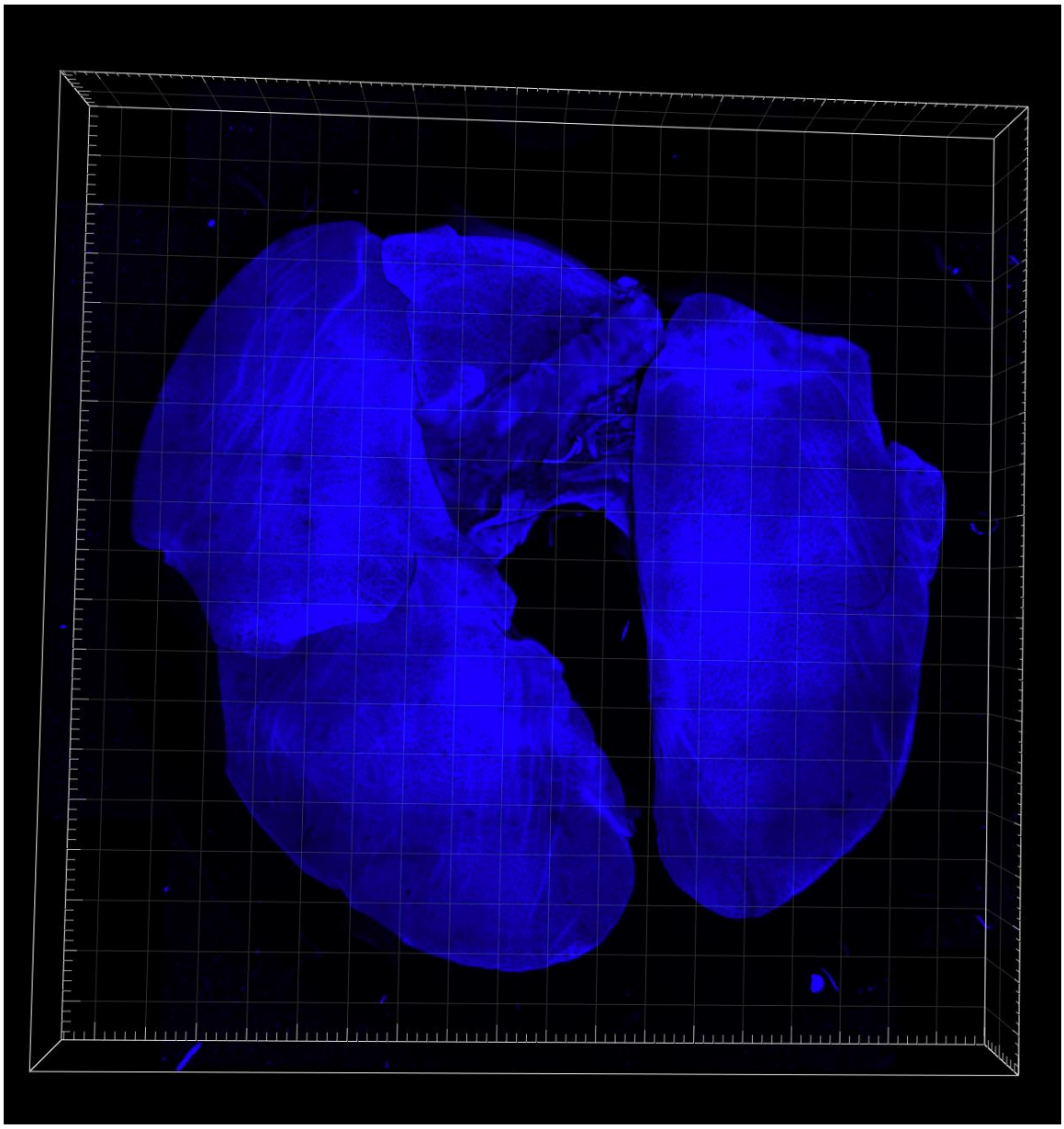

Figure 6. Three-dimensional confocal image of whole mouse airway. Whole-mount mouse lungs and trachea stained with nuclear stain 4′6-diamidino-2-phenylindole, dilactate (DAPI), optically cleared with Ce3D, and imaged on a laser-scanning confocal microscopy. Using tissue clearing and confocal optical sectioning allows for accurate quantification of histological features in three-dimensions.

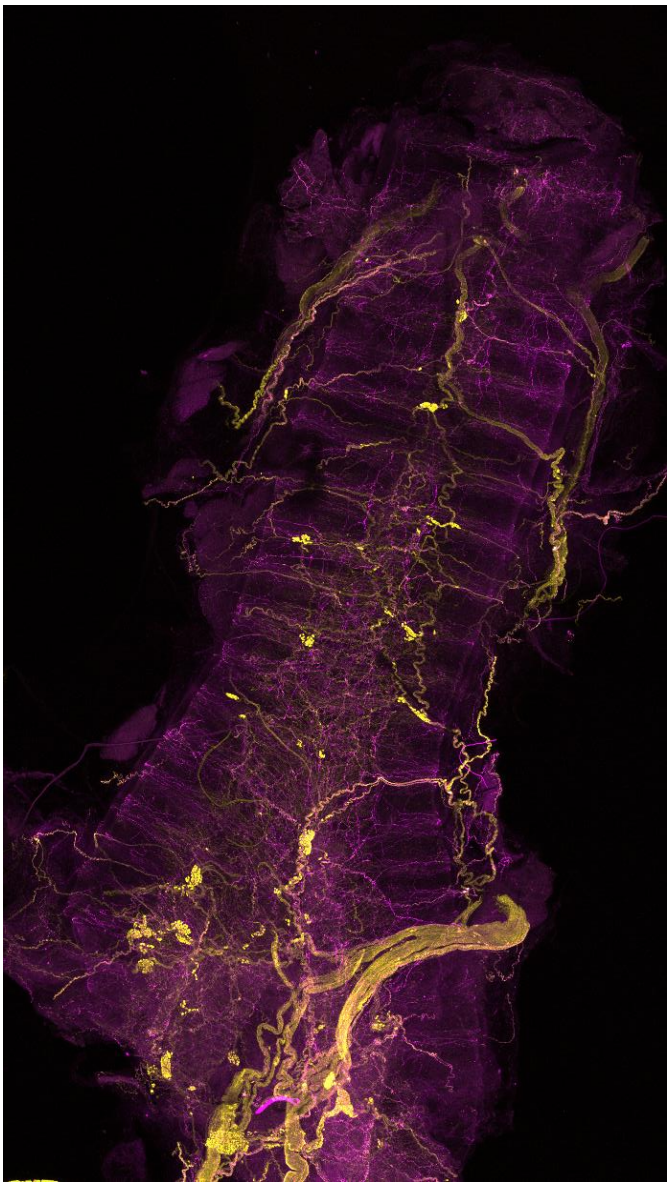

Figure 7. Maximum projection confocal image of mouse trachea. Whole-mount mouse trachea and airway nerves shown immunostained with panneuronal marker anti-PGP9.5 (yellow) and anti-substance P (magenta), optically cleared with Ce3D, and imaged on a laser-scanning confocal microscopy. Nerve length, branching, density, and neurotransmitter and receptor expression along all nerves in three dimensions can be measured.

J. Summary and Hypothesis

Obesity is a significant asthma comorbidity exacerbated by the growing global obesity public health crisis. Although obesity is known to increase the incidence and severity of asthma, the mechanisms driving obesity-related asthma are still not fully defined. Insulin resistance and hyperinsulinemia are common in obese individuals and increase the risk of uncontrolled and treatment-resistant asthma. There have been a limited number of investigations into mechanisms involving insulin and excessive nerve-mediated bronchoconstriction of the airways, a defining feature of asthma, in obesity-related asthma. Understanding the role of insulin and its effect on the development of obesity-related asthma is critical to targeting preventative interventions and treatments. It is my hypothesis that hyperinsulinemia in obesity drives hyperinnervation and dysfunction in airway nerves leading to nerve-mediated hyperreactivity. Here I establish that hyperinsulinemia in obesity potentiates parasympathetic nerve-mediated airway hyperreactivity and acts on airway smooth muscle (Chapter 3). This thesis is the first to demonstrate the importance of airway sensory nerves in obesity-related airway hyperreactivity. I show that hyperinsulinemia increases airway hyperreactivity via nerve-mediated reflex bronchoconstriction (Chapter 4). Furthermore, hyperinsulinemia induces hyperinnervation of airway sensory nerves, not only in diet-induced obesity, but also in hyperinsulinemic adult offspring born to obese mothers (Chapter 5).

Chapter 2. General Methods

A. Model Rationale

a. Rationale for Using Rats and Mice as Animal Models of Obesity-Related Asthma

The use of animals models is essential to my experiments. Animal models are necessary for testing and fully understanding the complex pathophysiological mechanisms of asthma *in vivo* that involve the interactions of many cells and signaling in the body. There are many animal species that have been used to model the pathogenesis of asthma including guinea pigs, rats, mice, rabbit, equines, cats, dogs, and primates[2]. Rats were chosen as a model to study obesity-related asthma in these experiments because Sprague-Dawley rats have a heterogenetic genetic background, similar to humans, that causes the development of obesity with a high-fat diet feeding in some (obese-prone), but not all (obese-resistant), rats[207]. It is also possible to isolate and electrically stimulate the vagus nerve in these rats to directly test parasympathetic airway nerve function, which is far more difficult to do in smaller rodents, such as mice. Using rats also minimizes cost and resource burden compared to that of larger mammals. The ability to genetically manipulate Sprague-Dawley rats, however, is limited compared with mice.

Mice were subsequently chosen as a model to study obesity-related asthma in other experiments due to: 1) availability of transgenic animals (e.g. sensory neuron insulin receptor knockout), 2) availability of protocols, reagents, and equipment (e.g. mouse ventilator, antibodies), and 3) minimizing cost and resource burden as compared to larger mammals. C57BL/6 and 129S4/SvJae mice were used over other strains because the transgenic animals necessary for the insulin sensory receptor knockout experiments (Advillin-iCre #032027 and IR-floxed #006955) were available on these backgrounds. Furthermore, C57BL/6 mice become obese when fed a high-fat diet[208], making an ideal model for testing obesity-related asthma. The mouse models used in these studies may only capture certain aspects and symptoms of human asthma, specifically airway hyperreactivity. Sensory hyperinnervation has been previously reported to occur in both human and mouse airways in the context of airway hyperreactivity, but whether these changes occur in obesity-related asthma is unknown.

B. Animal Models

a. Mice

All animals were handled in accordance with standards established by the US Animal Welfare Acts set forth in NIH guidelines and approved by the Institutional Animal Care and Use Committee at Oregon Health & Science University. Male and female mice were housed in temperature controlled pathogen-free facilities with ad libitum access to food and water on a 12-hour light/dark cycle. All mice cages were changed regularly (biweekly).

Table 1. Summary of mouse lines

Mouse	Citation/Stock no.	Description
Advillin-iCre	Lau et al., 2011 #032027	Expression of Cre protein driven by advillin promoter and dependent on tamoxifen activation. Expresses flox-stopped genes in sensory nerves.
Insulin Receptor floxed	Brunning et al., 1998 #006955	Express loxp sites flanking exon 4 of the insulin receptor gene
WT	#000664	C57BL/6 mice purchased from Jackson Laboratory and bred in-house

b. Rats

Rats were housed in pairs in temperature controlled pathogen-free facilities housed on a 12-hour light/dark cycle with weekly cage changes. They were given ad libitum access to food and water. All animals were handled in accordance with standards established by the US Animal Welfare Acts set forth in NIH guidelines and approved by the Institutional Animal Care and Use Committee at Oregon Health & Science University.

Obese-prone Sprague Dawley male and female rats were developed by Charles River Labs and bred in-house. Obese-prone rats were developed by selectively breeding the highest weighing rat pairs with each other. Offspring became obese when fed a high-fat diet.

Table 2. Animal diet composition

Diet	Carbohydrates (% calories)	Protein (% calories)	Fat (% calories)	Fiber (% composition)
High-Fat Diet	20.3	18.1	61.6	6.5
Low-Fat Diet	71.8	18.0	10.2	4.7
Normal Chow Diet	58.0	28.5	13.5	5.1

C. Genotyping from Mouse Ear Samples

Equipment:

- Isoflurane chamber
- Forceps
- Scissors
- 96 well Veriti Thermal Cycler (Applied Biosystems)
- Gel electrophoresis chamber

Reagents:

- Alkaline lysis buffer, pH 12
    - 50mL ddH_2O
    - 125µL 10N NaOH
    - 20µL 0.5M EDTA
- Neutralization solution, pH 5
    - 50mL ddH_2O
    - 325 mg Tris-HCl
- Econotaq
- Agarose
- DNA ladder
- QIAquick gel extraction kit

a. Retrieving Mouse DNA

1. Anesthetize mice in isofluorane chamber with 2L/min O_2
2. Using forceps and scissors, clip small ear sample - about the size of a sesame seed
3. Add 75µL lysis buffer to sample
4. Put tube with ear and lysis buffer in Thermal Cycler - Hotshot program
    a. Step 1 - 95ºC - 30 min - Alkaline lysis boil
    b. Step 2 - 4ºC - hold - cooling
5. Add 75µL neutralization solution
6. Store at -20ºC until ready to genotype

b. PCR Amplification

1. Calculate amounts needed for Reaction mix: # samples + 3 controls + 10%
   Ex. 24 samples + 3 controls + 3 extra = 30 reactions total to prepare

Ex. Solution	Amount per sample	# reactions	Total
EconoTaq	12.5 µL	30	375 µL
Primer 1	1 µL	30	30 µL
Primer 2	1 µL	30	30 µL
Primer 3	1 µL	30	30 µL
Primer 4 (or sub H_2O)	1 µL	30	30 µL
RNAse free H_2O	7.5 µL	30	225 µL
Total Reaction mix	24 µL	30	720 µL

2. Add 24µL of Reaction mix and 1µL of extracted DNA to each tube
3. Prepare 1 positive control (DNA from mouse with gene), 1 negative control (DNA from mouse without gene), and 1 H_2O (no DNA) control
4. Place tubes in Thermal Cycler. Select appropriate program and run.
    a. Reaction temperatures and duration for annealing vary for each gene, so separate programs have been saved into the machine. Each program cycles 35 times. PCR denaturation occurs at 95ºC (Advillin) or 94ºC (IR FLOX) for 30 seconds, and extension at 72ºC for 1 minute. Annealing temperature/duration is 60ºC for 15 seconds.

Table 3. Genotyping primers

Mouse	Forward	Reverse
Advillin	CTT TGT GAT GTT TCA GTT CCA G	AGG ATC TGC ACA CAG ACA GGA
IR Flox	GGG GCA GTG AGT ATT TTG GA	TGG CCG TGA AAG TTA AGA GG

c. Gel Electrophoresis

1. Plan gel layout: one well per sample, plus one well (at least) for DNA ladder on each row. Determine whether you'll use a large or small gel, depending on number of samples.
2. Large gel: Make 2% agarose using 4 grams of agarose plus 200mL TAE. Small gel: 1.2 grams of agarose plus 60mL TAE.
    a. Heat to dissolve using microwave. Let cool in chemical hood. Once it's cool enough to hold, add 20 µL SybrSafe DNA stain, 6 for small gel (or 2/0.6 µL ethidium bromide). Swirl to mix.

b. Pour agarose into gel container. Make sure it isn't leaking. Add comb for wells.
    i. If something happens, like the gel is leaking or breaks or you get a lot of bubbles, you wait for it to harden and re-melt the agarose in the beaker. Any impurities in the agarose (say from dropping the gel on the floor before re-melting it) result in images with lots of little dots and squiggles in them, which is not ideal.
c. Add 10 µL of sample and 2.5 µL loading dye to each sample well. Add 4 µL of DNA ladder to central well (ex. TrackIt 100bp ladder - up to 2000 bp, or Ultra low bp ladder - up to 300bp).
d. Run sample at ~100 volts until the color line is ~2/3rds of the way down.
e. Image gel on UV light table.
   Expected band sizes:
   Advillin* – WT = 324 bps; mut = 194 bps
   IRKO FLOX – WT = 105 bp; Het 105 bps + 145 bps; mut 145 bps

   *Note: Must do qPCR to differentiate Advillin homozygote vs. heterozygote

D. Drugs

Drug information is summarized in Table 4 below and includes indication, dose and route of administration, and source.

Table 4. Drugs used for *in vivo* studies.

Drug	Indication	Dose & Route	Source
Ketamine Xylazine	Sedation & analgesia	100 mg/kg i.p. 10 mg/kg i.p. (mice)	Hospira Vet One
Urethane	Sedation & analgesia	1.6 g/kg i.p. (male rats) 1.4 g/kg i.p. (female rats)	Sigma
Pentobarbital	Euthanasia	300 mg/kg i.p.	Vortech
Succinylcholine	Paralysis	10 mg/kg i.p.	Sigma
Serotonin	5-HT receptor agonist; Reflex Bronchoconstriction	10-300 mM; 10 µL nebulized (mice)	Sigma
Methacholine	Muscarinic receptor agonist	1-1000 mM; 10 (mice) or 20 [209] µL nebulized	Sigma
Atropine	Muscarinic receptor antagonist	3 mg/kg i.p. (mice) or 1 mg/kg i.v. [209]	Sigma
Pilocarpine	M_2-receptor antagonist	1 mg/ml; 1-100 ug/ml [209]	Sigma
Guanethidine	Chemical sympathectomizer	5 mg/kg [209]	Bosche Scientific
Heparin	Prevent blood clotting	100 µL in 30 mL PBS	Fresenius Kabi

All drugs dissolved in sterile phosphate buffered saline (pH 7.4) unless otherwise noted. Used for both rats and mice unless otherwise specified in dose/route.

E. Tamoxifen Treatment

Overview: Tamoxifen treat Sensory Neuron Insulin Receptor Knockout (SNIRKO) mice to induce Cre-recombinase expression and knock out floxed insulin receptors on sensory nerves

Equipment:

- Isoflurane chamber
- Weight scale
- 1 mL syringe
- BD PrecisionGlide 25 gauge needle (blue)
- EtOH wipes

Reagents:

- Tamoxifen (Sigma #T5648)
- Corn oil

1. Make tamoxifen solution at a concentration of 20 mg/mL in corn oil. Measure out tamoxifen into light-proof container (brown glass bottle). Add corn oil. Shake O/N at 37ºC.
2. The following day, bring all equipment plus tamoxifen solution to mouse room. Anesthetize mice using isoflurane chamber and weigh on scale. Administer tamoxifen solution by i.p. injection 75 mg/kg (calculate weight (g) x 5 = # µL, for 100 mg/kg)
3. Administer same dose of tamoxifen to each anesthetized mice for 5 consecutive days of treatment total. Store tamoxifen at 4ºC in the dark so it does not degrade.
4. Wait at least 7 days before harvest/experiment final following tamoxifen injection to insure full sensory neuron insulin receptor knockout in SNIRKO mice.

F. Measuring Airway Inflammation

a. Bronchoalveolar Lavage and Blood Collection

Overview: Collect mouse blood and bronchoalveolar lavage (BAL) fluid. (Often performed in conjunction with Harvesting Mouse Tissues.) Count total white blood cells (WBCs) and assess proportion of lymphocytes, macrophages, eosinophils, and neutrophils in BAL fluid.

Equipment:

- Scissors
- Graefe Forceps
- 1mL syringe
- 1.5mL Eppendorf tubes
- Ice
- Razor blade
- Modified cannula for mouse trachea

Reagents:

- Sterile PBS

Bronchoalveolar lavage (BAL)

1. In an anesthetized mouse: use scissors and forceps to expose trachea, using scissors to open the skin and forceps to pull away glands and muscles.
2. Using the razor blade, make a small hole near the cricohyoid membrane. Insert the cannula into the trachea.
3. Using a 1mL syringe to draw up 0.5mL of PBS, insert syringe into cannula, and gently push PBS into mouse lungs. Once syringe has been emptied, draw back slowly. A frothy solution will enter the syringe. Draw back to about 0.5 mL and deposit fluid in 1.5mL Eppendorf tube on ice. (Very little fluid is recovered from the first 0.5mL)
4. Repeat twice, each time pushing 0.5 mL into lungs and then drawing slowly back out and depositing fluid in the same Eppendorf tube. More liquid should be recovered each time.

b. Bronchoalveolar Lavage WBC Counts and Differentials

Equipment:

- Centrifuge (for Eppendorf tubes)
- Cytospin centrifuge
- Cytospin slide holders
- Funnel Filters
- Coplin jars
- Slide holder for coplin jars
- Two beakers (500mL)
- Drying rack for slides

Reagents:

- Wright stain

Counting Total White Blood Cells in Bronchoalveolar lavage (BAL)

1. When all samples are ready, take ice bucket with tubes to microscope. Load 10 µL of sample (may dilute 1:10) into Hemocytometer. Average number of cells in big squares = x * 10^4 cells/mL
    1. There may be red blood cells (smaller, donut-shaped) and epithelial cells (big and fluffy) in the sample. Don't count these! Only count white blood cells.
2. Multiple # cells x 1.5 ml to get total cell amount
3. Centrifuge BAL at 300 x g for 10 min, then take off supernatant and resuspend the pellet in PBS (should be # cells/ml divided by 35 cells to get volume for about 35 x 10^4 cells in hemocytometer)
4. Cytospin:
    a. Label BAL slides
    b. Prepare slides in cytospin slide holder with disposable filter
    c. Pipette 50-100 µL into funnel and spin (make sure to use same volume for all slides)
    d. Let slides air dry vertically in a slide rack

Wright Stain for BAL

1. Fill Coplin jar with -20ºC methanol. Fix slides in methanol for 10 min. (This can be done ahead of time)
2. Fill a Coplin jar with Wright stain. Insert slides into slide holder. Fill two beakers with diH_2O. Lay out holder for drying slides.
3. Insert slides into Wright stain for 14 seconds
4. Remove from Wright stain and dunk in 1st beaker. Wait 30 seconds. Do not move.
5. Remove from 1st beaker and dunk in second. Quickly dip up and down.
6. Wipe back of slides with Kimwipe and set in drying rack

Counting Differential

2. Count 200 cells in the BAL
3. Record the number of each white blood cell type
4. Calculate percentage of each cell type to get differential

G. *Ex vivo* Measurement of Airway Smooth Muscle Contraction

a. Organ Bath Experiments

Krebs Buffer Preparation

1. 10 X Solution Prep (can be done day before)
    a. Add all the component of 10X buffer into a 1L glass bottle; add dH_2O to the marker of 1L. Stir for as long as 15 min until mixed.

10x Krebs

dH20 (L) (Total Volume)		1	2
NaCl		68.667	137.334
KCl		4.175	8.351
MgSO4 (sigma: M7506)		1.421	2.842
NaH2Po4 (sod phos monobasic anhydr S-5011)		1.766	3.532
NaHCO3 (Sod Bicarb S233 Fischer)		21.003	42.006
D-glucose (Sigma G8270)		10.000	20.000

Make 1x Krebs

2. Add 2L dH_2O into a 4L beaker, add $CaCl_2$ and put on heater and mix 5min
3. Start bubbling in carbogen (O2/5% CO2) in the beaker for 5min.
4. Pour 1/3 of needed 10x Krebs into the beaker. Bubble 5min.
5. Add in the rest of the 10X Krebs and bubble 5min.
6. Transfer 1X Krebs into the small plastic 1L measuring cup and use funnel to add to reservoir, add bubbler, tighten and start experiment.

Final Volume (Liters)	4.000
1. add x Liters dH20 to beaker, stir & heat (5-6 setting) 10min	3.6000
2. add x grams CaCl dihydrate Sigma 3881). Mix 5min	1.4700
3. add x ml 10x Krebs. Mix 3-5min	133.3333
4. take off heater/stirrer (leave heat on)	
5. Bubble 95% O2/5% CO2 10min	
6. put back on heater/stirrer	
7. stir in x mls 10x Krebs. Mix 5min	266.6667
8. Take of heater/stirrer (turn off heat). Bubble O2/CO2 5min	
9. Fill Resevoir and Begin	

Organ Bath Set-up

1. Ensure Krebs is running into all 8 organ bath wells (Figure 8)
2. Turn on vacuum to reverse

3. Adjust O2:CO2 at each well to allow gas bubbles are present in every well
4. Turn off gas and Krebs flow while calibrating
5. Calibrate Organ Bath
    a. Turn on water bath
    b. Turn on amplifier
    c. Open LabChart software
    d. Open 4 or 8 channel template
    e. Calibrate each channel (well)
        i. Click on “channel x” on R side
        ii. Open “bridge amplifier” and select 10 mV threshold for both upper and lower boxes
        iii. Click “invert”
        iv. Open “Units”
        v. Turn “off”
        vi. Re-zero program (mV should be near 0)
        vii. Click pause and record mV
        viii. Attach 1 gram weight to transducer, pause and record new mV
        ix. Open “Units” and enter mV values for 0 and 1 gram respectively
        x. Click apply and ok.
        xi. Repeat for each channel

Animal Prep

1. Pentobarb lethal dose (stock 30 mg/mL = 150ug pentobarb + 5ml PBS)
    a. Rats will require 1ml per 100g body weight injection of 30mg/ml stock solution
    b. Mice receive 450ul i.p. of Ketamine/Xylazine cocktail (8.9ml PBS, 1ms ketamine, 100ul xylazine)
2. Remove trachea from carina to larynx
3. Place trachea in 1X buffer in petri dish and remove extra tissue
4. Cut to appropriate size and tie floating knot with long string (will attach to transducer)
    a. For human- 3.0 suture, for rats - 4.0 suture
    b. For rats, one trachea can usually be cut into 4 equal segments
5. Place second floating knot on opposite side (will attach to glass hook anchor)
6. Diameter of loop should be approximately 1cm)
7. Orient smooth muscle to back of bath and attach to hook and transducer
8. Ensure whole tissue is submerged in Krebs

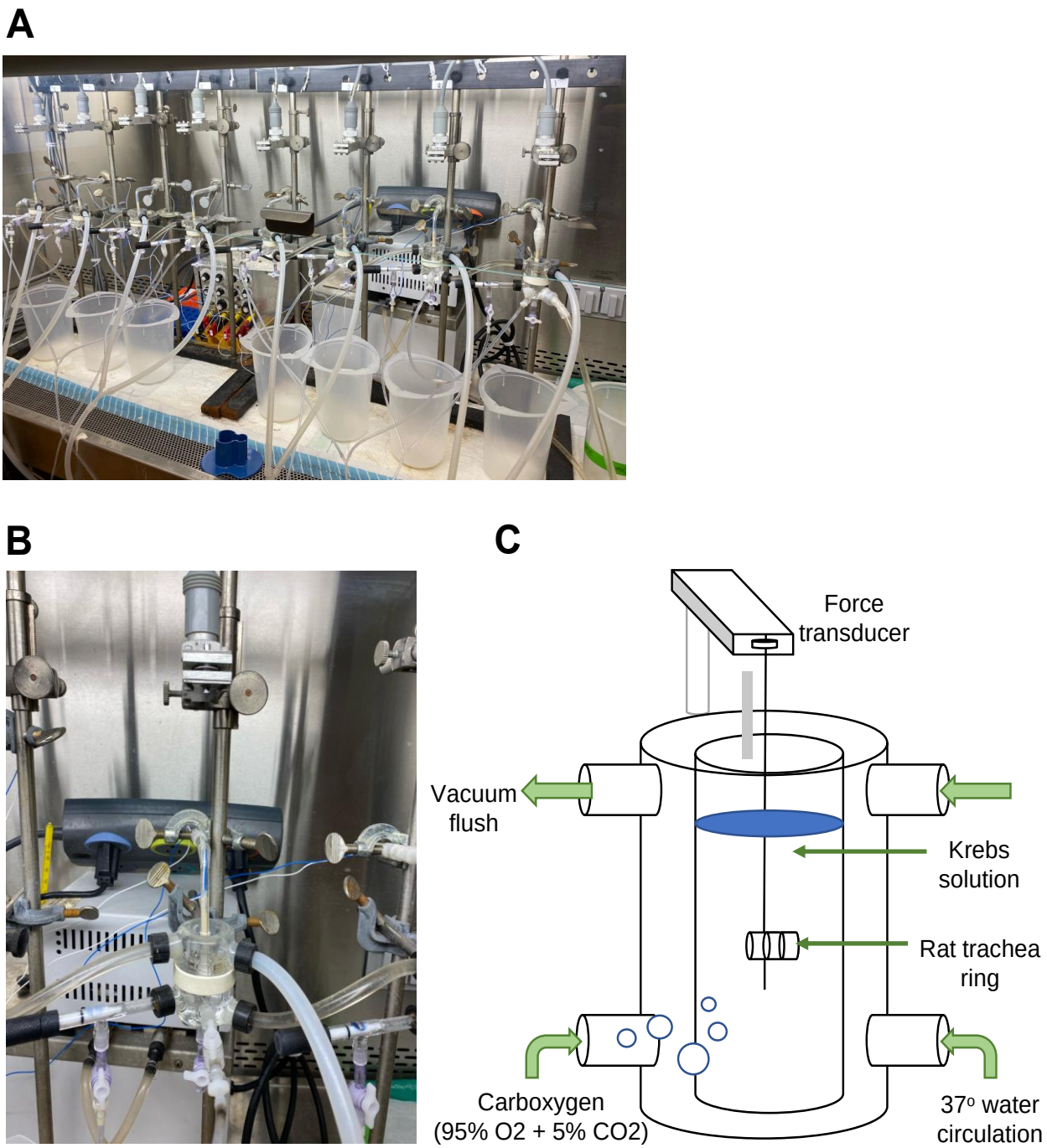

Figure 8. Organ bath setup for *ex vivo* experiments. (A) Image of setup of eight organ baths for ex vivo testing (B). Magnified image of individual organ bath with rat tracheal ring inside. (C) Schematic drawing of organ bath components

Experimental Protocol (Figure 9)

1. Click “play” on LabChart software
2. Raise transducer to achieve desired tension
    a. Rats: 1 gram; Mouse: 0.5 grams
3. Tighten locking bolt
4. Ensure strings are not touching electrodes or bath walls
5. Open stopcock to allow Krebs to wash tissues x1 minute
6. Allow 1 hour for equilibrium with 1 minute washes every 15 minutes, each time followed by tightening of transducer to desired tension
    a. For rat, 30 minutes for equilibration, with 1 minute wash every 10 minutes
7. Add baseline contraction agent to each well
    a. 1 mM KCl (500 µL per bath)

For electric field stimulation:

- Rat: 100V 0.2msec duration, 5sec on 55sec off 1-50Hz

For methacholine (MCh) dose-response curve :

- Add 5 µL MCh to 5 ml bath
  Concentrations: 0.33uM, 1uM, 3.3uM, 10uM, 33.3uM, 100uM

At the end give 1 mM KCl to ensure viable smooth muscle

1. Wash after 5 minutes

Weigh tissue at end

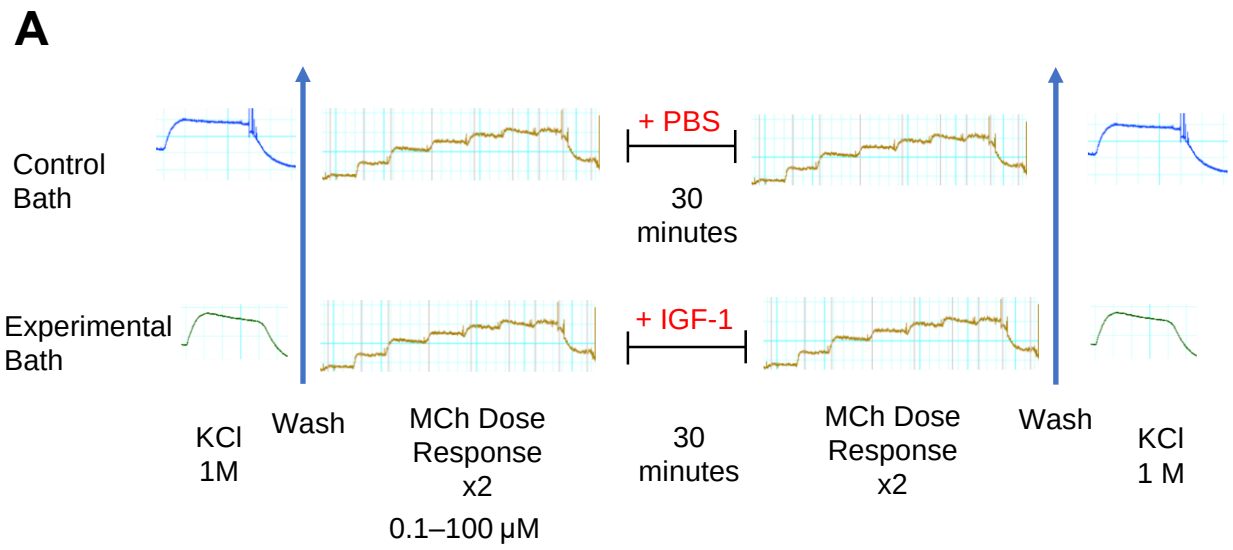

* Results are normalized by KCl curve

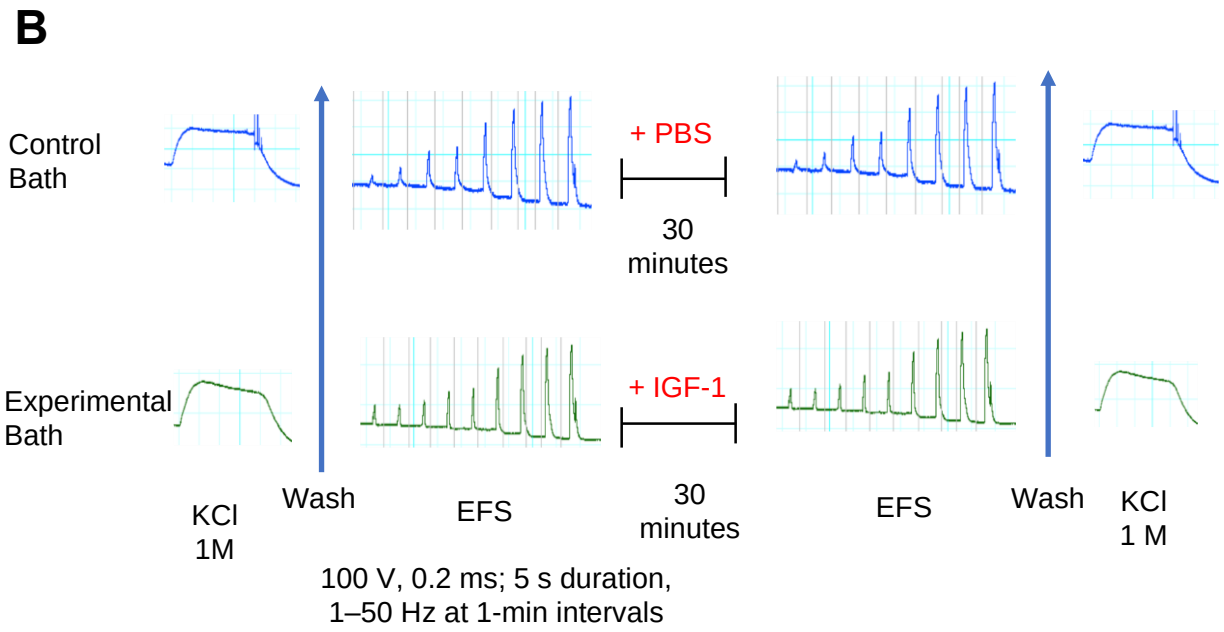

* Results are normalized by KCl curve

Figure 9. Schematic of *ex vivo* organ bath protocol for (A) methacholine dose-response curve and (B) electric field stimulation (EFS).

H. *In vivo* Measurements of Airway Physiology

a. Rat *in vivo* Airway Physiology

Equipment:

- Ventilator
- Pneumonitor attached to tubing with syringe and separate tubing with plug (for attachment to female joint of three-way stopcock)
- Heating pad
- Mercury sphygmomanometer
- Glucometer
- Syringe autopump for succinylcholine

Surgery Setup Protocol (Figure 10):

5. Make drugs for rat *in vivo* (Table 4)
6. Calibrate the machine
    a. Turn on the power strip (to allow blanket to warm)
    b. Turn on computer and lab chart
    c. Open a LabChart template -> “save as” a new file and delete any data remaining
    d. Zero Bridge Amp for blood pressure and airway pressure
    e. Calibrate Airway pressure amp
        i. Turn on vent (make sure it is set to 100 breaths/min and tidal volume = 250 mL)
        ii. Attach vent syringe to airway pressure transducer and pneumonitor
        iii. Make pressure 0 mmH_20 for a few seconds (press start on LabChart)
        iv. Stop and make pressure 300 mmH_20 and hold (press stop)
        v. Turn off units -> Look the chart for 0 -> write number on white board

            300 -> write number on white board
        vi. Record unit conversion in LabChart
    f. Calibrate blood pressure amp
        i. Pull out blood pressure mercury sphygmomanometer and flip switch to on
        ii. Attach syringe to blood pressure amp
        iii. Hold at 0 mmHg (start LabChart) and 200 mmHg (stop LabChart)
        iv. Turn off units and record on board
        v. Enter unit conversion into LabChart
7. Give Urethane i.p. (1.6 mg/kg x BW/150) for males vs. (1.4 mg/kg x BW/150) for females

a. Document time given
b. Add 0.2 mL i.v. urethane, if needed, for a top-off dose

8. Make oval cut in neck/trachea area
    a. Dissect sides to uncover jugular veins
    b. Leave blood in veins to make it easier to cannulate
    c. Prime cannula with heparinized saline to get rid of bubble
    d. Slide thread under and cut ½ to get 2 pieces
    e. Tie top tightly with suture and loosely tie bottom (do not tighten)
    f. Slide cannula in and tie bottom tightly with suture
9. Give guanethidine (take ½ hour to take full effect)
10. Mark nerves gently with suture
11. Cannulate carotid
    a. Use heparinized PBS to clear tubing/syringe
    b. Withdraw 1 mL blood and flush with heparinized PBS (1 mL)
    c. Measure glucose using glucometer
12. Administer succinylcholine
    a. Fill syringe with 30 mL succinylcholine; clear any bubbles in line
    b. Connect syringe to autopump and attach to left jugular vein cannual
    c. Set loading dose to 1.055 ml/sec then decrease to 0.155 ml/sec for maintenance

Experimental Parameters:

1. **Vagus Nerve Induced bronchoconstriction**
   20V, 0.4msec duration, 6sec on/40sec off
   Hz 2, 4, 8, 10, 15, 20, 30, 40 and 60 Hz
2. **Methacholine-induced bronchoconstriction**
   Nebulized 20 µL with vagi CUT
   1,3,10, 30, 100, 300, 1000 mM
3. **Acetylchoine-induced bronchoconstriction**
   i.v. with vagi CUT
   1,5,10, 20, 30,40, 50,60,70ug/kg
4. **M_2 Function**
   5V, 10Hz, 0.4msec duration, 6sec on/40sec off
   Pilocarpine dose: 0.001,0.01,0.1,1,10,100ug/kg

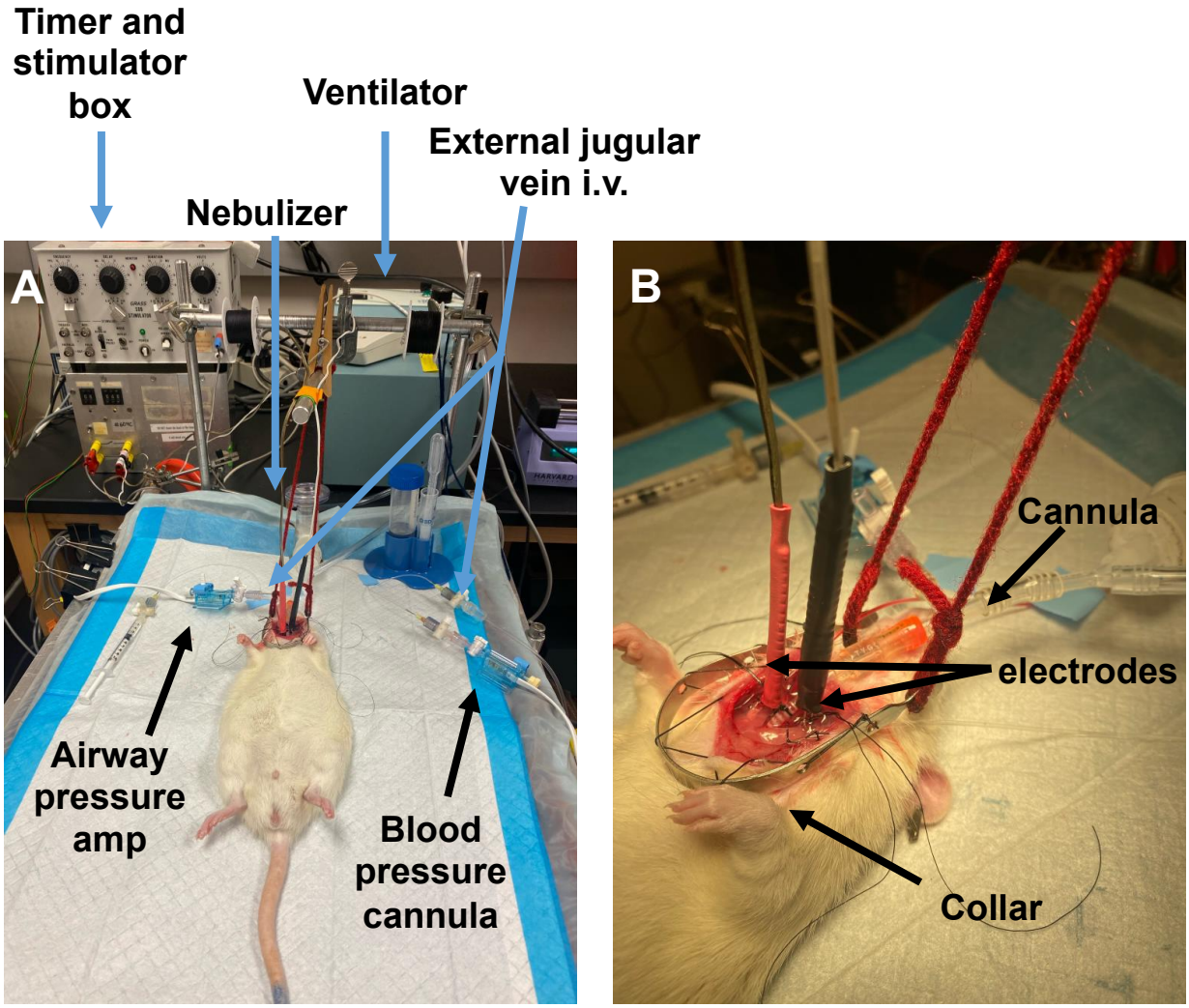

Figure 10. Rat *in vivo* airway physiology setup. (A) Labeled images of cannulated rat on ventilator showing ventilator box and timer setup. (B) Enlarged image of electrodes hooked to vagal nerves, collar, and trachea cannula.

b. Mice *in vivo* Airway Physiology

i. Ventilator Calibration

Equipment:

- Ventilator (Figure 11)
- Pneumonitor attached to tubing with syringe and separate tubing with plug (for attachment to female joint of three-way stopcock)
- 30 mL syringe attached to tubing with plug
- Heating pad
- Heat lamp

Protocol:

1. Turn on oxygen tank, ventilator, ADInstruments power supply, heating pad (set at 42ºC - press START), computer, and heat lamp (Figure 10).
2. Log into computer and pull up template for ventilator. Save as a new file with name of mouse (i.e. M2021-001).
3. Calibrate airway pressure:
    a. Turn stopcock to shut off any flow from ventilator to pressure transducer
    b. In LabChart, set airway pressure to zero:
        i. Airway Pressure -> BP Amp -> Zero -> OK
    c. Now calibrate using pneumonitor. Attach plug side to open end of stopcock by pressure transducer. In Lab Chart: Airway Pressure -> Unit Conversion -> “Off” -> OK
    d. Press “Start” in LabChart. Push/pull syringe attached to pneumonitor to 0 cm H_2O. Look at voltage reading of Airway Pressure in LabChart and write down (i.e. 0cm = ? mV)
    e. Push syringe to 18 cm H_2O; record corresponding recorded Airway Pressure value in mV from LabChart and write down (i.e. 18 cm = ? mV)
    f. In LabChart click “Stop.” Go to Airway Pressure -> Unit Conversion -> in Calibrate section type in the values for 0 cm and 18 cm from above -> OK
    g. Click “Start.” Push syringe to 14cm H_2O. Verify that LabChart Airway Pressure reads 14 cm.
    h. Repeat as needed until pressure is accurately calibrated. Remove pneumonitor and turn stockcock to resume airflow from ventilator to pressure transducer.
4. Calibrate airway flow:
    a. Turn stopcock to shut off any flow from ventilator to flow monitor.
    b. In LabChart, set airway flow to zero:
        i. AirwayFlow -> Spirometer -> Zero -> OK
    c. Now calibrate using 30mL syringe. Make sure syringe is pulled back to 25mL. Attach plug to open end of stopcock by flow monitor.

d. Press “Start” in LabChart. Slowly push 5 mL of air through syringe, watching readout on LabChart to make sure there are no spikes. (If air is pushed too fast, it will exceed the measurement ability of the flow monitor and will show up as a spike that phases out.) Push “Stop” in LabChart.
    i. Try to keep even pressure on the syringe as you push to ensure a constant velocity/flow rate
e. In LabChart, place cursor at time point of airway flow where you started to push air through the syringe, then drag until time point where you stopped to highlight the area that indicates 5mL of flow. Go to Airway Flow -> Spirometry Flow -> Calibrate -> type in 0.005L injected volume -> OK
f. Repeat as needed until flow is accurately calibrated. Remove syringe and turn stopcock to resume airflow from ventilator to flow monitor.

5. Place PEEP tube in water cylinder about 0.5cm below surface to achieve PEEP of 2 mmH_2O.
6. Press “Start” in LabChart. Make sure airway pressure reading is zero. Attach “Frank the mouse” (a fake mouse - actually a 30 mL syringe sealed tight and attached to a plug) to the ventilator. PEEP cylinder should begin bubbling and pressure reading in LabChart should oscillate at a mean of 2cm. (Adjust PEEP tube up and down to achieve 2 cm if necessary.) Flip left switch on ventilator to ON. Let run for a few seconds, then switch on right switch to perform a few inspiratory pauses. Look at all LabChart readouts to make sure everything is working properly.
    a. Leaks in the expiratory tube will show up as a lack of plateau during inspiratory pauses
    b. Leaks in the inspiratory tubing may make airway pressure peaks jagged
7. If tidal volume readout is dipping below 0mL: Airway Flow Corrected -> Arithmetic -> change equation to get baseline of 0mL (usually +/- 0.0001)
8. Verify that Tidal Volume is 200 µL. It is very rare that this gets thrown off, but sometimes accidents happen. If it isn’t at 200 µL, make slight adjustments to the silver knob where the oxygen enters the ventilator until 200 µL is achieved.
9. Verify that the deep inhalation cylinder (on the ground, 25mL cylinder filled with water) is full and tubing is close to the bottom.
10. For delivering nebulized drugs to the animal, clean out the nebulizer by pipetting 10 µL of PBS onto the silver screen and dabbing with a kimwipe. Then pipette 100 µL of dH_2O onto the silver screen, turn on the nebulizer, and run it through.

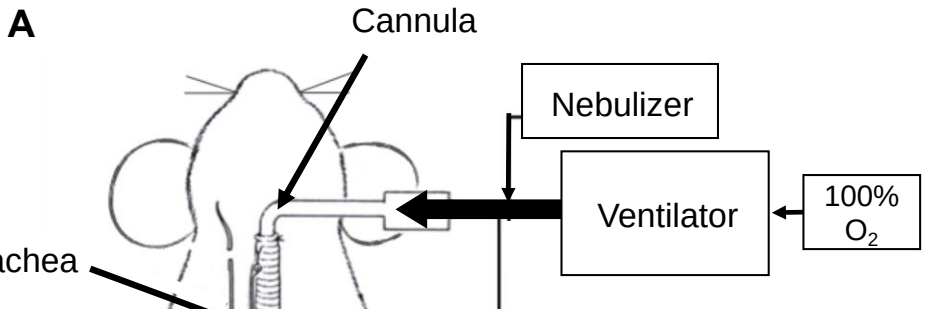

ii. Anesthesia and Surgical Preparation

Equipment:

- Mouse ventilator
- Heating pad
- Heat lamp
- Scissors
- Graefe forceps
- Gauze dampened with PBS
- EKG needle electrodes
- Rectal thermometer

Reagents:

- Ketamine/xylazine (1 mL ketamine, 100 µL xylazine into 8.9 mL PBS)
- Succinylcholine (10mg/mL, 10 mg in 1 mL)
- PBS

To ventilate mouse for dose-response experiments:

1. Anesthetize mouse with 100 mg/kg i.p. ketamine and 10 mg/kg i.p. Xylazine
2. Once mouse stops moving, place on heating pad and under heat lamp. Wait for breathing to slow, and for mouse to not reaction to soft hindpaw pinch.
3. Make a midline neck incision with scissors, extending 1 cm caudally from the base of the neck over the thorax
4. Carefully separate the submandibular glands
5. Inset a 20-gauge catheter into the cricothyroid membrane to the level of the second cartilage ring and retract the needle. Connect the end of catheter into the mouse ventilator and flip the switch on to initiate ventilation. Press start in LabChart program.
6. Place gauze dampened with PBS over exposed trachea. Gauze should be left on at all times when not performing surgery or light exposure, in order to reduce desiccation of trachea over time.
7. Inject the paralytic succinylcholine (10 mg/kg i.m.) to eliminate respiratory effort.
8. Insert EKG needle electrodes and rectal thermometer

iii. Measurements of Pulmonary Inflation Pressure and Serotonin Response

(start after performing “Anesthesia and surgical preparation” as described above)

Equipment:

- Mouse ventilator
- Digital clock with seconds visible

Reagents:

- PBS
- Serotonin (5HT) at doses of 10mM, 30mM, 100mM, and 300mM

Note: for some experiments you may need additional reagents, such as methacholine and atropine. The timing and dosage of these drugs, when used, is described in Table 4.

1. Double check that airway pressure and EKG readouts appear normal. Airway pressure should be between 7-10cm H_2O at baseline (lower for a lean wild type mouse, higher for obese mice). Heart rate should be between 200 and 400 beats per minute for a lean mouse.
2. Perform a repeated sequence of maneuvers with the mouse ventilator, first with no nebulized solution, then with PBS, then repeat with 10, 30, and 100mM doses of 5HT in sequence. When the seconds hand of the digital clock reads:
    a. 40 seconds - 2 deep inhalations to open any collapsed airways
    b. 50 seconds - 6 inspiratory pauses
    c. 58 seconds - pipette solution onto nebulizer
    d. 0 seconds - turn on nebulizer. Type dosage (i.e “neb on,” “PBS,” “10”) into LabChart and hit enter. Wait 60 seconds.
    e. 0 seconds (again) - 6 inspiratory pauses
3. Repeat after 40 seconds

I. Imaging Nerves

a. Harvesting Mouse Tissues

Purpose: to collect mouse blood, trachea, lungs, dorsal root ganglia (DRGs), and nodose/jugular ganglia for later use in immunohistochemistry, Western blot, and insulin ELISAS

Equipment:

- 1 ml syringe with needle
- 1 ml heparinized syringe with 26G needle
- 10 ml syringe with 25G needle
- Disposable blue chuck
- Microscissors
- Scissors
- Forceps
- 10 ml glass jar filled halfway with Zamboni's fixative
- Eppendorf tubes
- 1 ml pipette and pipette tips
- Petri dish
- Dissecting scope
- Micro-forceps

Reagents:

- Ketamine/Xylazine: add 0.1ml of 100mg/ml Xylazine and 1ml of 100mg/ml Ketamine into 8.9ml PBS
- EtOH spritzer
- Ice

i. Perfusion

2. Assemble equipment and mice. Scruff mouse: pick up tail near bum with left hand. Place mouse on top of cage horizontal to bars such that it has something to grab with its hands. Take right hand, using thumb on one side and curled fingers on the other, and moving somewhat from tail to head squish mouse against cage bars and grab. When you're done you should have the neck and back firmly scruffed in right hand. Still holding tail with left, lift mouse up and turn hand over so mouse belly is visible. Tuck tail into pinky of right hand so left is free to grab syringe.
3. Anesthetize mouse with using ketamine/xylazine solution
    a. BW(ul) of the working solution.
    b. Depth of anesthesia can best be judged by toe pinching.

4. Weigh mouse: Place on gram scale to obtain weight and write down.
5. Spritz belly and neck of anesthetized mouse with EtOH to damp down fur and help prevent fur from getting in all the tissues you're collecting.
6. Using forceps in left hand, pinch midline skin of abdomen about two-thirds of the way between diaphragm and urinary meatus. Using scissors in right hand, cut hole through skin and muscle until viscera are visible, then extend midline excision anteriorly to diaphragm.
7. Cut horizontally from midline incision to the mouse's left to expose descending colon. Use forceps to move descending colon and other intestines to the mouse's right so that the inferior vena cava (IVC) is visible.
    a. Collect Blood from IVC with heparinized syringe, place on ice.
    b. Blood glucose: Take glucose test strip, place into glucose meter, added a drop of blood and record glucose readout.
8. Cut the IVC.
9. Move quickly now because the mouse is bleeding out. Hold the white nub of sternum just below the diaphragm with forceps and lift so the whole diaphragm becomes visible, moving liver out of the way with closed scissors if necessary. Cut into ribcage and diaphragm, first nicking each side to collapse (but not cut!) the lungs, then moving around rib cage to cut diaphragm away, going from each side to meet in the middle.
10. Cut anteriorly along ribcage on each side, cutting towards mouse's armpits. Keep hold of sternum nub with forceps and lift as you go. Stop when you have a clear shot of the right ventricle of the heart.
11. Use 25 ml PBS syringe with a 25G needle to pierce the right ventricle - aim just above the right coronary artery, and don't push in too far or you'll puncture all the way through. Slowly start to push PBS through heart. You should see blood emptying from abdomen. Eventually this liquid should turn clear and the hands/feet/liver should noticeably pale. In a perfect perfusion on a mouse that was not previously ventilated the lungs should be white. (Ventilation damages the lungs, so they never clear completely and will still look pink and speckled).
12. Cut off the heart to prevent re-perfusion

ii. Collecting Trachea, Lungs, Head and Spine

1. Once perfusion is done, expose the trachea. Neck area should be spritzed with EtOH if it wasn't already. Cut through skin of neck (one vertical and two horizontal incisions), pull apart submandibular glands (horizontally), grab and rip apart (vertically) each of the two muscle bellies on the ventral side of the trachea, then cut through clavicles to remove ribcage fully so entirety of trachea and lungs are exposed.
2. Cut trachea above thyroid cartilage, then (pulling upward with forceps) make cut behind trachea to remove adhesions, trying not to damage carotid sheath/vagus

nerve along the way (if collecting nodose/jugular ganglia). Continue to pull upwards on trachea with forceps so that lung is pulled as well, blind cutting adhesions with scissors, and finally cutting through esophagus to remove lungs and trachea from chest cavity. Place in Zamboni's on ice.

3. Next remove head: using large scissors, cut through head at level of shoulders and posterior to ears. Either:
    a. Place in petri dish on ice for immediate nodose/jugular collection, or
    b. Remove skin from head and place in jar of Zamboni's with lungs/trachea
4. Next remove spine: cut through ribs on either side of thoracic spine, leaving about 2mm of ribs intact on either side. Airway nerves are mostly T2-T6. Use scissors and forceps to remove spine from dorsal skin and to cut posteriorly at beginning of lumbar region. Either:
    a. Place in petri dish with PBS (to keep moist) on ice for immediate DRG collection, or
    b. Place in small jar of Zamboni's with head (if staining – if not skip immediately to harvesting nodose/jugular ganglia)

iii. Harvesting Dorsal Root Ganglia (DRGs)

1. Move spine to dissecting scope. Bring very fine forceps, blunt forceps, and scissors.
2. Cut ribs off close and parallel to the spine
3. Using scissors, cut along the ventral and doral side of the central canal then cut along dorsal side of central canal to cut the spine in half.
4. Using fine forceps, pull on each white shimmery nerve root, gently pulling each ganglion out of its hole.
5. Place DRG into Eppendorf tube with ~200 µl TBS.
6. Remove liquid from tube and snap freeze DRG in liquid nitrogen (for Western/PCR) or put DRGs in TBS O/N at 4ºC (for culturing) or in Zamboni's (for staining).

iv. Harvesting Nodose/Jugular Ganglia

1. Bring mouse head to dissecting scope. Bring very fine forceps, blunt forceps, and scissors
2. Lay mouse head on side, with ear facing up and slightly back so the throat is towards you.
3. Use the ear canal as your first landmark. Clear away any remnants of hair.
4. Surgically dissect away tissue to expose the tympanic bullae (the bone dome covering the cochlea) and the carotid sheath.
5. Carefully dissect out vagus to make it easier to follow

6. Remove the tympanic bullae: poke through with sharp forceps and then break it off
7. Follow vagus to where it dives between the cochlea and the bone spur. The is where the nodose/jugular ganglion is located. Break off bones around the nodose/jugular, and carefully separate its adhesions to the cochlea before removing the cochlea completely.
8. You will now see the vagus with the nodose/jugular bulb diving into the brainstem. Cut as close to the brainstem as possible, then carefully lift out the N/J with posterior vagus nerve attached (Figure 12).

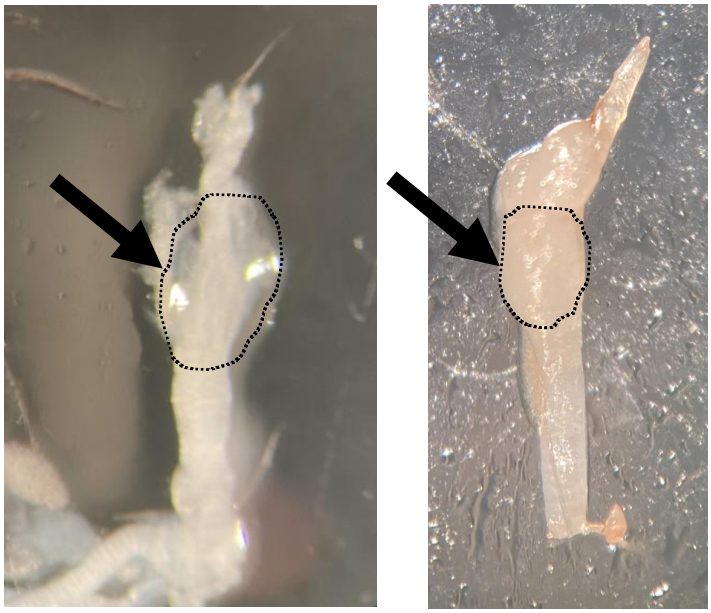

Figure 12. Harvested mouse nodose and jugular ganglia. Arrows point to nodose and jugular ganglia, which are anatomically fused in mice.

b. Immunohistochemistry and Clearing of Whole Mount Tissues

Overview: Antibody staining of airway nerves and other markers and clearing of tissue for immediate imaging

Equipment:

- 1.5mL Eppendorf tubes (2 per sample)
- Tube holder
- Shaker
- Aluminum foil

Reagents:

- Tris buffered saline (TBS), adjust to pH 7.6 using HCl
    - Tris Base: 61 grams
    - NaCl: 90 grams
    - H_2O to 1 liter
- Blocking solution: 4% normal goat serum, 1% TritonX 100, 5% powdered milk in TBS

		10mL	**25mL**	**30mL**
Triton X-100	Sigma #X100	100 µL	250 µL	300 µL
Powdered Milk	Carnation instant nonfat dry milk	50 mg	125 mg	150 mL
Normal Goat Serum	Vector #S-1000	400 µL	1 mL	1.2 mL
TBS	See above	9.5 mL	23.75 mL	28.5 mL

- Ce3D clearing solution: Gently melt N-methylacetamide in 37ºC water bath until the necessary volume can be obtained. Add to PBS on Heat/Stir pad in chemical fume hood. While stirring and gently heating, add in histodenz slowly. Note: the histodenz takes a long time to fully melt - be patient and don't add too much or the stir bar becomes stuck. Once melted, add Triton X-100 and 1-thioglycerol. Store under fume hoods indefinitely.

		5mL	**10mL**	**30mL**
N-Methylacetamide (40% v/v)	Aldrich #M26305	2 mL	4 mL	12 mL
PBS	Gibco PBS, pH 7.4	3 mL	6 mL	18 mL
Histodenz (86% w/v)	Sigma #D2158	7.275g	14.55 g	43.65g
Triton X-100 (0.1% v/v)	Sigma #X100	5 µL	10 µL	30 µL

1-Thioglycerol (0.5% v/v)	Sigma #M1753	25 µL	50 µL	150 µL

- Primary Antibodies:
    - Rabbit IgG anti-human PGP9.5 — Amsbio E3344 — 1:200
    - Rat IgG_{2a} anti-Substance P — BD Pharmigen 556312 — 1:500

- Secondary Antibodies:
    - Goat anti-rat Alexa555 IgG (H+L) — Invitrogen #A21428 — 1:1000
    - Goat anti-rabbit Alexa647 IgG — Invitrogen #A21244 — 1:1000
    - Goat anti-chicken Alexa488 — Invitrogen #A11039 — 1:1000
    - Goat anti-mouse Alexa488 F(ab')2 — Invitrogen #A11017 — 1:1000

Day 1
- Wash tissue in TBS. 2 x 2 min at RT, then 5 x 1hr at 4ºC until clear.
- Transfer to blocking solution in 1st Eppendorf tube. 4ºC for 1 day

Day 2
- Pipette off blocking solution
- Add 0.5mL of blocking solution with primary antibodies. 4ºC O/N.

Day 3
- Wash tissue in TBS. 2 x 2 min at RT, then 5 x 1hr at 4ºC.
- Pipette off TBS. Add 1.0 mL of blocking solution with secondary antibodies. 4ºC O/N.
  (ALL steps after this performed in DARKNESS)

Day 4
- Wash tissue in TBS. 2x2 min at RT, then 5 x 1hr at 4ºC.
- Take out tissue, wick away extra TBS with kimwipe, and place in fresh Eppendorf tube with Ce3D. O/N (12-72 hours) at RT in chemical fume hood.

  NOTE: if doing two antibodies from the same animal (i.e. 2 primary rabbit antibodies) then there are additional steps. Instead of clearing tissue, after washing pour off TBS and add blocking solution with special blocking antibody (i.e. Goat anti-rabbit IgG, 1:100). 4ºC on shaker O/N.
  Day 5: Wash tissue in TBS. 2x2 min at RT, then 5x1hr at 4ºC on shaker. Pour off TBS. Add 0.5mL of blocking solution with secondary antibodies. 4ºC on shaker O/N.

Day 6: Wash tissue in TBS. 2x2 min at RT, then 5x1hr at 4ºC on shaker. Place in Ce3D O/N.

c. Confocal Imaging of Airway Nerves

Overview: Confocal imaging of airway nerves and other markers

Equipment:
- ZEISS LSM900 confocal microscope (OHSU Advanced Light Microscope Core)
- ZEISS ZEN Blue software

Image Acquisition
(Detailed instructions can be found in ZEN 2 (blue edition) Software Guide)
1. Flip switches to turn on microscope & open ZEN blue software
2. Configure channels using Smart Setup
    a. To add a channel, click on the “Add” button in the “Configure your Experiment” section
    b. Select desired dye (ie DAPI, Alexa 555, or Alexa 647)
    c. Add channel to experiment; repeat for rest of dyes
    d. Use “Best Compromise”
3. Configure channels
    a. 401 nm, 553 nm, and 653 nm light excitation
4. Save above channel configuration as template
5. Look at overview of mouse trachea at 10x
    a. Use eyepieces to center sample
    b. Switch to “acquisition” to image fluorescence
    c. See Figure 13 for example image dimensions and acquisition information
    d. “Info” tab stores all image acquisition information
6. Image using 63×/1.4 oil PlanApo DIC M27 objective (0.19 mm working distance)
    a. Acquire z-stacks of full epithelial layer (typically ~20-50 µm)
    b. Take 2-3 images of each trachea area

Image Dimensions

Z-Stack	176 Slices (43.75 µm)
Channels	3
Scaling (per Pixel)	0.099 µm x 0.099 µm x 0.250 µm (Edit)
Image Size (Pixels)	1024 x 1024
Image Size (Scaled)	101.41 µm x 101.41 µm
Bit Depth	16 Bit
Image Center Position	X: 62.56 mm, Y: 27.40 mm
Stage Position	X: 62.56 mm, Y: 27.40 mm
ROI Center Offset	X: 0.00 µm, Y: 0.00 µm

Acquisition Information

Acquisition Start	10/21/2021 5:15:04 PM
Microscope	Axio Observer.Z1 / 7
Objective	Plan-Apochromat 63x/1.40 Oil DIC M27

	Track 1	Track 2
Reflector	none	none
Contrast Method	Fluorescence	Fluorescence
Pinhole	0.71 AU / 38 µm	1.00 AU / 38 µm
Laser Wavelength	561 nm: 2.00 %	405 nm: 2.00 % 640 nm: 5.00 %
Laser Blanking	Enabled	Enabled
Scan Mode	Frame	Frame
Scan Zoom	1.0	1.0
Rotation	0°	0°
Pixel Time	1.03 µs	1.03 µs
Frame Time	5.06 s	5.06 s
LSM Scan Speed	7	7
Scan Direction	Bidirectional	Bidirectional
Line Step	1	1
Averaging	2	2

	Channel 1	Channel 2	Channel 3
Channel Name	AF555-T1	AF405-T3	AF647-T3
Channel Description			
Dye Name	AF555	AF405	AF647
Channel Color			
Excitation Wavelength	553	401	653
Emission Wavelength	568	422	668
Effective NA	1.4	1.4	1.4
Detection Wavelength	550-700,657-715	410-490	550-700,657-715
Imaging Device	MA-Pmt2	MA-Pmt1	MA-Pmt2
Detector Type	Multialkali-PMT	Multialkali-PMT	Multialkali-PMT
Detector Gain	650 V	650 V	650 V
Detector Offset	0	0	0
Detector Digital Gain	1.0	1.0	1.0

Figure 13. Image dimensions and acquisition parameters. ZEISS ZEN blue information for imaging mouse trachea positions using 63x objective.

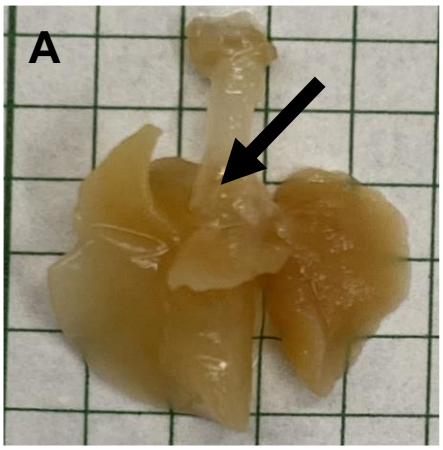

Fixed Airway

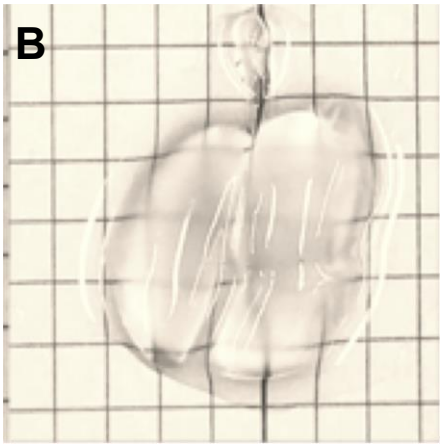

Cleared Airway

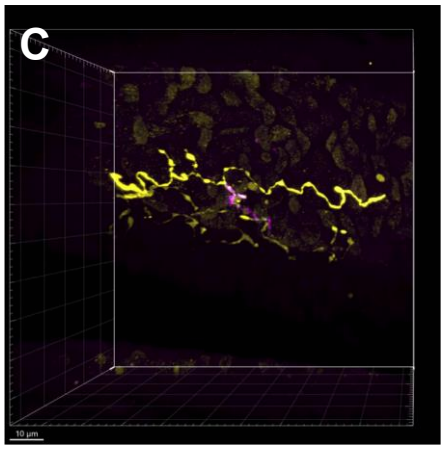

Immunostained tracheal epithelial nerves

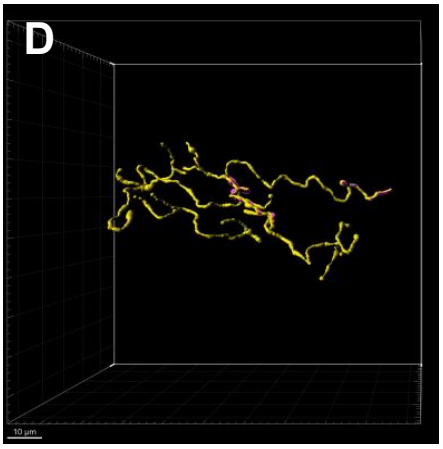

Tracheal epithelial nerve 3D model

c. This creates a mask of the PGP nerve model

5. Colocalize Substance P
    a. Create “Surface”
    b. Surface detail = 0.36
    c. Background subtraction = absolute
    d. Adjust threshold value until red Substance P is just disappearing (will likely still have some uncovered red staining)
    e. Filter above 28 voxels (to remove background)
    f. Add filter -> Intensity max channel (PGP mask – channel 4)
    g. “Duplicate to new surface” to create a surface with only those colocalized volumes
6. Collect statistics from Imaris
    a. Surface volume
    b. Filament length, no dendrite branch points, & volume

J. Measuring Animal Body Composition

Day before NMR measurement:

1. Sign up on the “MRI” calendar
2. All animals to be measured must fast overnight.
    a. Weight rats in grams and write down on weight sheet. Measure mice day of.
    b. Remove food from feeder (into trashcan).
    c. Fill out and place the fasting card outside the cage.

Day of measurement:

3. Grab special diet food (if needed), extra gloves, jump drive, and a pen.
4. Transfer the rats/mice, on a covered cart, to NMR machine
5. Create a new file folder:
    a. Open My Documents, NMR Data, Nie Lab, right click to establish a new folder, then type in date.
6. Double click on EchoMRI on the computer screen to start NMR measurements.
    a. Select rats OR mouse – on a drop down menu on the right hand side
    b. Keep water accumulation at -1
7. Select Output Directory:
    a. Open My Documents, NMR Data, Nie Lab, select created folder, select OK.
8. Run a system test:
    a. First push the rat calibration tube [209] or mouse calibration tube [210] in, all the way, into the machine.
        i. Rats: Located to the right of the computer screen.
        ii. Mouse: Located in a lower right-hand drawer (pick the large size). Tube placement top of machine.
        iii. Calibration tubes are clear with liquid inside.
        iv. If doing both rats/mice, make sure to do all one type of animal first, then recalibrate before proceeding with the next.
    b. Hit System test on the EcoMRI program.
9. After the test is finished, pull out the rat calibration tube and place it on the top of the machine. Make sure it is stable on the surface. DO NOT drop it. You may return the mouse calibration tube back to the drawer.
10. FOR MICE: measure body weight on scale before placing in tube.
11. Placing animals in the measurement tubes:
    a. Select correct tube size for animals:
        i. Rats: small for OR, medium for OP, large for very old/big rats
            1. All measurement tubes located on the shelf to the left.
        ii. Mice: tubes are placed on the drying rack next to sink. Use clear one.
    b. Remove the inner portion of the tube.

c. Encourage the animal to crawl into the tube.
d. Push the inner tube inside until you meet resistance of the animal.
e. Secure with Velcro.
f. Slide the tube into the machine until is stops at the big, outer ring.

12. Scan animals:
    a. Push F2 to label the animal.
        i. Type animal number
        ii. Record the weight from the day before
        iii. Type “OP HFD 5 week M” (genotype, diet, diet length, gender)
    b. Select Start Scan.
    c. When the scan is done the data will compile at the bottom of the screen.
13. Repeat step 14 for all the individual animals
    a. **NOTE:** Place tubes parallel to the wall as the inner tube can freely roll off the table if placed perpendicular. If tube falls it can break! So, be careful.
    b. Copy the data typed on F2 by control+c for easier data entry
14. Tube clean up:
    a. Clean out the outer and inner tube with the bleach by the sink.
    b. Then use the metal pole with a paper towel to wipe around, down in the bottom of the tube. Repeat several times until dry.
    c. Return to the shelf to dry.
15. Export data:
    a. Select all the rows of data that are need to export
    b. Push F8 to export
    c. Select the directory folder to export all data in “txt” file.
    d. Close the software – the data is automatically saved into the output directory folder.
16. Collect Data:
    a. Insert the jump drive in a slot, down by the key.
    b. Transfer the folder from new folder you created earlier to your jump drive.
17. Shut down the computer.
    a. That should also shut down the machine, but if it doesn’t, then turn off the power switch that you used earlier to turn on the computer.
18. Return the calibration tubes.
19. Return the animals.
    a. Give animals fresh special diet if needed.

K. Quantification of Insulin

a. Insulin Enzyme-Linked Immunosorbent Assay

Overview: Measure fasting plasma insulin by Mercodia Mouse or Rat Insulin ELISA kit

Equipment:

10. Mercodia Insulin Elisa Mouse (10-1247-01) or Rat (10-1250-01) kit
11. Pipettes
12. Redistilled water and 1L Corning Pyrex bottle
13. Magnetic stirrer
14. Vortex mixer
15. Microplate reader with 450 nm filter
16. Microplate shaker (700–900 cycles per minute, orbital movement)

Procedure (modified from Mercodia manufacturer instructions):
All reagents and samples must be brought to room temperature before use. Prepare a calibrator curve for each assay run. The product has been optimized and validated without plate sealer.

1. Prepare enzyme conjugate 1X solution, wash buffer 1X, and samples.
    a. For 1x enzyme conjugate solution for 1 plate: mix 1 vial 11x enzyme conjugate (provided) with 1 vial enzyme conjugate buffer (provided)
    b. For 1x wash buffer: mix 35 mL 21x wash buffer with 700 mL redistilled water
2. Prepare sufficient microplate wells to accommodate Calibrators (provided), controls and samples in duplicate.
3. Pipette 10 µL each of Calibrators, controls and samples into appropriate wells.
4. Add 100 µL of enzyme conjugate 1X solution into each well.
5. Incubate on a plate shaker (700-900 rpm) for 2 hours at room temperature (18-25°C).
6. Discard the reaction volume by inverting the microplate over a sink. Add 350µL wash buffer 1X solution to each well. Discard the wash solution, tap firmly several times against absorbent paper to remove excess liquid. Repeat 5 times. Avoid prolonged soaking during washing procedure.
7. Add 200 µL Substrate TMB into each well.
8. Incubate 15 minutes on the bench at room temperature (18-25°C).
9. Add 50 µL Stop Solution to each well. Place the plate on the shaker for approximately 5 seconds to ensure mixing.
10. Read optical density at 450 nm within 30 minutes.
11. Calculate insulin concentration by entering data into Prism (XY format) and selecting “Nonlinear fit, Sigmoidal 4PL, X is log(concentration)”
12. Solve the equation: [conc]=LogEC50-((1/hill slope)*(log((Top-Y)/(Y-Bottom)))) by filling in the variables (Top, Bottom, LogIC50, Hillslope) from Prism.

L. Molecular Biology

a. Quantification of Insulin Receptor RNA

Brief summary: Carefully separate a small sample of frozen tissue, homogenize, then extract RNA using a Qiagen RNeasy kit. Make cDNA, then run 96 well plate with desired primers and 18S as a control in the Applied Biosystems 5500 Fast Thermocycler. Quantify RNA and DNA with NanoDrop.

i. RNA Isolation from Tissue

Equipment:

- For preparing frozen tissue:
    - Dry ice in large styrofoam container
    - Sterile forceps (clean in between samples with 70% EtOH)
    - 30mg wad of damp paper towel (to help with approximating sample size)
    - For each sample:
        - 1 Sterile petri dish (small)
        - 1 Razor blade
        - 1 Falcon Tube (5mL round bottom polypropylene - should fit homogenizer)
- Homogenizer
- Ice
- For each sample:
    - 1 50mL conical tube with 35mL Ultra Pure H_2O
    - 1 50mL conical tube with 35mL Ultra Pure EtOH (plus one extra)
    - Sterile 1.5mL Eppendorf tube (labeled) on ice
    - 600 µL RLT buffer with 6 µL beta-mercaptoethanol (10 µL per 1mL RLT)
- Box of kimwipes

Preparing Frozen Tissue (skip to B for pre-prepared 30mg of tissue in Falcon tube)

1. Take samples from -80ºC freezer and put on dry ice
2. Label petri dishes and falcon tubes. Put on dry ice.
3. For each sample:
    a. Clean forceps with 70% EtOH
    b. Lay out new razor blade on clean paper towel
    c. Use forceps and gentle warming (with hands through gloves) to remove frozen sample from current container and place in petri dish)
    d. Move petri dish to bench. Quickly cut off 30mg or less with razor blade. (Refer to pre-weighed wad of damp paper towel for size approximation)
    e. Place the <30mg piece of sample in the Falcon tube. Return remainder to original container. Put both back on dry ice.

f. Throw out petri dish and razor blade. Clean forceps.

Homogenization

1. Clean bench space by homogenizer and homogenizer itself with EtOH.
2. Take styrofoam container with dry ice and samples over to homogenizer.
3. For each sample:
    a. Add 600 µL RLT with 6 µL beta-mercaptoethanol to frozen sample
    b. Run homogenizer until sample is fully puréed (time depends on tissue. ~30sec for lung, 1 minute for submandibular gland). Transfer 600 µL to Eppendorf on ice.
    c. Clean homogenizer by running it in a conical tube with 70% UltraPure EtOH. If this is not the first sample, use the second EtOH from the previous sample as the first wash in this sample.
    d. Run homogenizer in a second, clean conical tube of 70% UltraPure EtOH
    e. Run homogenizer in a conical tube of UltaPure H_2O.
    f. Dab clean with kimwipes.
    g. Spin down final product (in Eppendorfs). Transfer supernatant to another Eppendorf. Continue to RNA purification. (Or store at -80^o C)

ii. RNA purification with Qiagen kit

Protocol from: RNeasy Mini Kit (Qiagen, no. 74104)

Equipment:

- Centrifuge that holds 1.5 mL Eppendorf tubes

Reagents:

- RNA in RLT with beta-mercaptoethanol
- RNeasy Mini Kit (Qiagen, no. 74104)

1. Take Eppendorfs with supernatant from RNA isolation protocol
2. Add 1 volume (600 µL) of 70% ethanol to the lysate, and mix well by pipetting. Do not centrifuge. Proceed immediately to step 3.
3. Transfer up to 700 µL of the sample, including any precipitate, to an RNeasy Mini spin column placed in a 2 mL collection tube (supplied). Centrifuge for 15 s at ≥8000 x g. Discard the flow through. Transfer any remaining sample to the spin column and centrifuge again.
4. (DNase digestion steps) Add 350 µL Buffer RW1 to the RNeasy spin column. Centrifuge for 15 s at ≥8000 x g. Discard the flow through. Make stock solution of DNase: 10 µL DNase + 70 µL RDD buffer per sample, and mix. Add 80 µL of final solution to each spin column and let sit for 10 min. Then add 350 µL Buffer RW1 to the RNeasy spin column. Centrifuge for 15 s at ≥8000 x g. Discard the flow through.

5. Add 500 µL Buffer RPE to the RNeasy spin volume (note: in preparing the kit, add 4 volumes of ethanol (96-100%) to Buffer RPE for a working solution). Centrifuge for 15 s at ≥8000 x g. Discard the flow through.
6. Add 500 µL Buffer RPE to the RNeasy spin volume. Centrifuge for 2 min at ≥8000 x g. Place spin column in a new 2 mL collection tube (supplied). Centrifuge at full speed for 1 min to dry the membrane.
7. Place the RNeasy spin column in a new 1.5 mL collection tube (supplied). Add 30-50 µL RNase-free water directly to the spin column membrane. Wait 5 minutes. Centrifuge for 1 min at ≥8000 x g to elute the RNA.

iii. NanoDrop RNA/DNA

Equipment:
- NanoDrop 2000
- 2 µL pipette
- Kim wipes
- Paper and pen

Reagents:
- DNA/RNA to evaluate
- Solution in which DNA/RNA was eluted (exact bottle, if possible)

1. Open NanoDrop and select Nucleic Acids to measure
2. Select either DNA or RNA from drop down menu under sample name
3. Clean NanoDrop pedestal with Kim wipe. Pipette 1 µL elution solution onto pedestal and lower arm
4. Hit “Blank”
5. Wipe off pedestal with clean section of kim wipe. Pipette 1 µL of your first sample onto the pedestal, being sure to completely cover the central hole and not to create bubbles. Type in sample name and hit “Measure.”
6. Write down concentration (in ng/µL), 260 value, 260/280 and 260/230 ratios
7. Repeat steps 5-6 for all samples
8. Clean pedestal with dH_2O and dry kim wipe when finished.

iv. Making cDNA from RNA

Equipment:
- Thermocycler

Reagents:
- RNA (see RNA extraction/purification above)
- H_2O (RNase and DNase free)
- Random Primer Hexamer
- dNTP

- 0.1M DTT
- 5x First Strand Buffer

1. Start Thermocycler (so cover heats up)
    a. cDNA Superscript III -> View -> Run
2. Put tubes of Random Primer Hexamer, dNTP, DTT, Buffer, RNAse Out and Superscript III (stored at -20ºC) and put in metal tube holder on ice.
3. Using information from NanoDrop on RNA concentration, calculate maximum consistent ng of RNA (should be above 500ng) such that volume of RNA + H_2O = 11.5uL
    a. Ex. For RNA at 43.9 ng/µL, 11.4 µL is 500 ng, plus 0.1 µL H_2O
4. Add RNA, water, Random Primer Hexamer (0.5 µL) and dNTP (1 µL). Put in Thermocycler. Press Run.
5. Make Master Mix of remaining 4 reagents. Add in Superscript III last! (Always add enzyme last)
    a. Ex. For 3 samples, make x4 Master Mix
        i. 5x RT Buffer: 4 µL x 4 = 16 µL
        ii. 0.1M DTT: 1 µL x 4 = 4 µL
        iii. RNAse Out: 1 µL x 4 = 4 µL
        iv. Super III: 1 µL x 4 = 4 µL
6. Add 7 µL Master Mix to each tube. Put back in Thermocycler. Press “Skip.” Wait 1.5 hrs.
7. Dilute final product with 20 µL water for 40 µL total.

v. qPCR of cDNA

Equipment:
- Applied Biosystems 5500 Fast Thermocycler
- 96 well plates that fit 5500 Fast Thermocycler, specifically

Primer Sequences:
Table 5. qRT-PCR primers

Primer	Left (5’-3’)	Right (5’-3’)
Insulin Receptor	GAG GCT GCA CTG TGA TCA AC	TAG GAG CGG CGG ATC TTT AG
18S	GTA ACC CGT TGA ACC CCA TT	CCA TCC AAT CGG TAG TAG CG

1. Make a layout of samples in each well. Decide how many replicates, which samples/RNA, etc. Negative control should have Master Mix but no RNA. 18S RNA used to assess quantity of overall good RNA in each sample.
2. Make Master Mix of each RNA you want to quantify
Ex.

	Forward	Reverse	Water	SYBR green	Total
1 reaction	0.6 µL	0.6 µL	6.8 µL	10 µL	18 µL
3 samples x 3 replicates + 1 extra = x10	6 µL	6 µL	68 µL	100 µL	180 µL

3. Add 18 µL Master Mix to each well.
4. Add 2 µL of cDNA (from the 40 µL of sample in Step 7, above) to each well.
5. Seal plates. Add plastic covering, then rub thoroughly with plastic spatula. Overdone is better than underdone.
6. Vortex plates briefly, then centrifuge very briefly at 300g. (Wait until centrifuge hits 300g, then hit stop.)
7. Put plate in Applied Biosystems 5500 Fast Thermocycler.
8. Run plate
    a. Note: in Jacoby lab, go to Users/AD/Desktop/Old 7500 Computer Files/Templates/Templates and click the “Use this - Generic”
    b. Run will take ~4 hours

M. Visualization of Insulin Receptor RNA in Tissue Sections

a. BaseScope Protocol

(Modified from Advanced Cell Diagnostics)

This technique allows for visualization of RNA targets with single cell resolution and improved signal amplification and sensitivity compared to standard techniques. Paired oligo ("ZZ") probes amplify the mRNA signal and reduce non-specific background.

Reagents:

- BaseScope™ Detection Reagent Kit v2 – RED (Cat# 323900)

Day before:

- Turn on the incubator to 60°C.
  - In hall right outside first door

Day 1:

- Turn on a water bath to 40°C.
  - Under whiteboard
- Turn on the HybEZ Oven or a dry 40°C incubator and prepare the humidified chamber. Put it in the oven/incubator to be warm. 30 min prior to use
  - By RNAscope station near Ubaldo + Gina's benches

Needed later:

- 1X Wash buffer (980 mL distilled H_2O + 20 ml RNAscope Wash buffer (50x)) in a bottle.
  - Make 4x this, should be enough for whole experiment
    - Can keep for 1 month at RT.
    - NOTE: Warm the 50x wash buffer to 40°C 10-20 min before preparation.

START:

Write on slides to indicate which slides get what probe (with a slide pen – ImmPrint)

Bake slides! 1 hr at 60°C.
****optional stopping point**** Use immediately or store at RT with desiccants for ≤1 week

Deparaffinize:
Prep - In the fume hood:

- Fill two Tissue-Tek Clearing agent dishes with ~at least 200 ml fresh xylene
- Fill two Tissue-Tek clearing agent dishes with ~at least 200 ml fresh 100% ethanol

Protocol:

- Xylene 5 min RT (↓↑; lift slide rack up and down several time when you first put in the slides)
- Xylene 5 min RT (↓↑)
- 100% etOH 2 min RT (↓↑)
- 100% etOH 2 min RT (↓↑)
- Remove the slides from the rack and put on paper towels (section face up). Allow to dry.
    - 5 min drying oven 60º or until completely dry
    - While the slides are drying – start to boil the Target Retrieval Reagent (see next step)

Pretreat:

Start to boil the 1X RNAscope Target Retrieval Reagent

- 400ml RNAscope 1x
    - 360ml distilled H_2O + 40ml 10X Target Retrieval Reagents in a 2 L beaker
    - mix well
    - put on hot plate in a beaker and put foil on the beaker
    - DO NOT BOIL THE 1X SOLUTION MORE THAN 15 MIN BEFORE USE!!!
- Lay slides on bench.
- Add 5-8 drops of RNAscope hydrogen peroxide.
    - # of drops depends on size of tissue, sometimes 2 drops is plenty. That is okay.
- Incubate 10 min at RT
- Flick off hydrogen peroxide and place slides in rack containing diH_2O.
- Move slides up and down 3-5 times.
- Repeat with fresh diH_2O.
    - Here – Transfer the slides to a rack with a low-profile (often used with antigen retrieval steps) in the fresh H_2O. This rack allow to minimize the amount of target retrieval needed.
- Once the Target Retrieval Reagent has reached 99-102°C, add the slides in the low-profile slide rack. 15min (no more!)
- Put slides in a rack containing H_2O (do not let the slides cool before adding them to the water).
    - Here – use the low-profile bin used specifically for this rack.
- Move the slides up and down 3-5x. And transfer the slides back to the gray, high-profile rack in a container of H_2O for 15 sec.
- Put slides in 100% etOH for 3 min. RT
- Remove the slides and allow them to dry using a 60°C oven for 5 min (or completely at RT approx. 10 min)

Protease:

- Grab HybEZ slide rack first so you can set slides in it after using the pen
- Add the hydrophobic pen. Let it dry at RT. (this can be overnight if you want a stopping point)
    - If continuing – warm probes during this protease step.

- Remove the HybEZ slide rack from the tray in the HybEZ oven. Put the tray back in the oven to keep warm.
- Put the slides on the HybEZ slide rack.
- Add ~5 drops of RNAscope Protease III to the section.
- Put the slide rack into the tray. Close the lid, seal and insert the tray back in the oven.
- Incubate 40°C for 30 min.
    - During this incubation, prep the next reagents.
    - In the last 10 minutes of this incubation, remove the probes from the fridge and place in a 40°C in a water bath or incubator. Swirl gently to mix before use.
- Remove the tray from the oven. Remove the rack from the tray. Put the tray back in the oven.
- Flick off the protease solution and put the slides in a rack containing distilled H_2O.
- Move slides up and down 3-5 times to rinse.
- (It is essential to move from the protease step to the probe step, because the RNA is most exposed at this point.)

Add the probe:

Probes:

Insulin Receptor: BaseScope insulin receptor (Cat# 719141)
Negative Control: BaseScope™ Negative Control Probe-DapB-3ZZ (Cat# 701011)
Positive Control: BaseScope™ Positive Control Probe-Mouse (Mm)-PPIB-1ZZ (Cat# 701081)

- Flick water from the slides.
- Place slides in HybEZ slide rack.
- Add ~4 drops of probe.
- Put the slides in the tray, seal, and place in the oven for 2 hr at 40°C.
    - If doing whole protocol in one day, take AMP 1-6 out of the fridge now (not recommended)
- QUICKLY, remove the probe from the slide and put the slide in a rack containing 1x Wash buffer.
- Rinse 2 min at RT, moving the slides up and down in the dish.
- Repeat with fresh 1X Wash buffer.

Optional stopping point: Put slides in a container of 5x SSC at RT overnight. (225ml dH_2O + 75ml 20X SSC)

- Instead, use 65 mL 20X SSC + 195 mL H2O to get 260 mL of solution in the small, rectangular wash buckets
- Turn off HybEZ oven and let the tray dry overnight
- Okay to leave water bath on, probably won't need it unless run out of the wash buffer or spill it
- Leave incubator in hall on overnight

(Next day – Day 2):
Prepare:

- Pull out AMP1-8 from the fridge and put on bench to warm to RT.
- Turn on the incubator to 60°C.
- Turn on a water bath to 40°C.
- Turn on the HybEZ Oven or a dry 40°C incubator and prepare the humidified chamber. Put it in the oven/incubator to be warm.
  - At least 20 minutes
  - Start filtering hematoxylin. Use folded piece of filter paper in a funnel into an Erlenmeyer flask

START:

If the slides were in 5x SSC overnight, wash slide the next day in 1x wash buffer 2 times, 2 min each.

Amplification:

- Flick the buffer off the slide.
- Put the slide in the HybEZ slide rack in the tray.
- Add ~4 drops of AMP1.
- Put the tray in the HybEZ oven.
- Incubate 30 min at 40°C.
- QUICKLY, remove AMP1 from the slide and put the slide in a rack containing 1x Wash buffer.
- Rinse 2 min at RT, with occasional agitation. (Keep the tray in the oven to keep warm)
- Repeat with fresh 1X Wash buffer.

- Repeat with AMP2. Incubate 30 min at 40°C. Repeat wash steps above.
- Repeat with AMP3. Incubate 15 min at 40°C. Repeat wash steps above.
- Repeat with AMP4. Incubate 30 min at 40°C. Repeat wash steps above.
- Repeat with AMP5. Incubate 30 min at 40°C. Repeat wash steps above.

- Repeat with AMP6. Incubate 15 min at 40°C. Repeat wash steps above. Do not put the tray back in the oven to keep warm.

- Repeat with AMP7. Incubate 30 min <u>at RT</u>. Put the slides in the tray and seal – but do not put in the oven. Just leave on bench top. Repeat wash steps above.

- Repeat with AMP8. Incubate 15 min <u>at RT</u>. Put the slides in the tray and seal – but do not put in the oven. Just leave on bench top. Repeat wash steps above. During this step – prepare the RED-A and RED-B (below).

Detection:

- Briefly spin down the contents of the Fast RED-B tube.

- Prepare enough RED working solution:
    - 1:60 ratio Fast RED-B to Fast RED-A.
    - (Example: for a 0.75 x 0.75-inch barrier, add 2ul Red B + 120 ul Red A into a tube.)
    - Mix well.
    - NOTE: Use Fast RED-B solution within 5 min. Do not expose to direct sunlight or UV light.
  - Do this step in the dark microscope room
- Flick the buffer from the slide.
- Put the slide in the slide rack.
- Pipette ~120 ul of RED solution onto each slide.
- Place rack in the HybEZ tray and seal.
- Incubate 10 min at RT.
- Remove the RED solution by tilting the slide and placing it in a waste container.
- **Immediately,** put the slide in a container containing tap water.
- Rinse again with fresh tap water.

If performing IHC – put the slides in blocking and continue with a regular IHC protocol. (No need for the antigen retrieval or hydrogen peroxide steps. After DAB detection, continue to the counterstain – below)

Counterstain:

- Use orange slide holder in big top drawer of the same dresser that has the water baths
- Move the slides to a container of 50% Gills hematoxylin (see below for details).
- Incubate 2 min at RT. Slides will be purple.
- **Immediately,** transfer the slides back to the slide rack containing tap water.
- Wash the slides 3-5 times by moving the slides up and down.
- Keep repeating with fresh tap water until the slides are clear, while the sections remain purple.
- Replace the tap water with 0.02% ammonia water.
- Move the rack up and down 2-3 times. Sections should turn blue.
- Replace ammonia water with tap water.
- Wash slides 3-5 times.
    - Use 3 tri-pours with tap water in them
    - Order should be hematoxylin (2 min) -> Tri-pour 1 -> Tri-pour 2 -> 0.02% Ammonia water -> Tri-pour 2 -> Tri-pour 3

Mount the slides:

- Remove the slides from the container and dry the slides in a 60°C dry oven for 15 min.
- (Do not use alcohols – it will remove the RED substrate)
- Put 1-2 drops of EcoMount (Biocare Medical cat# EM897)
- Add a coverslip.
    - Wipe back of slide off w/ chem wipe
- Air dry slides at least 5 min. (Dry O/N before using oil objective)

Prepare the counterstaining reagents Do this at the beginning of day 2
In fume hood, filter 30ml of Gill's Hematoxylin.

- Hematoxylin is in the cabinet underneath the scale on Becky's bench
- Use small Erlenmeyer flask and funnel w/ folded filter paper

Make 50% Gill's 1 Hematoxylin (20ml Gills Hematox + 20 ml distilled H_2O in a Copland jar)

- can be reused up to 1 week
- get as much hematoxylin out as you can using the long electric pipette, then match that amount in water to make 50/50

In fume hood, make 0.02% (w/v) ammonia water.

- Add water first, then base

Stock ammonium hydroxide = ~7.63 M
To make 50 ml of 1M (or 1N) ammonium hydroxide: 6.55 ml of 7.63 M ammonium hydroxide + 43.45 ml distilled H_2O. Mix well.

N. Quantification of Insulin Signaling Pathways

a. Western Blot Protocol

Prep:

1. Make transfer buffer and store cold.
    a. 100ml of 10x BioRad Transfer buffer (Cat #161-0734)
    b. 200ml MeOH (cold)
    c. 700ml diH_2O
    d. 1g SDS (BioRad 161-0301; on chemical shelf; for proteins bigger than 80kaD)*
        i. *I use for all my proteins (~65 kaD)
2. Warm a heating block to 95°C (this will take ~20 min do this FIRST thing in morning)

Running Samples:

1. Make running buffer: 100ml of BioRad 10X running buffer + 900 ml diH_2O.
2. Add gel to the cassette:
    a. Mini-protean TGX BioRad Cat#456-1083 4-5%
    b. Remove the tape from the bottom of the gel.
    c. Take the gel holder out of the box and add the gel to one side.
    d. Add the plastic gel place holder to the other side
    e. Slide the contraption back into the holder
    f. Carefully close the little gates
    g. Add the whole thing to the box.
3. Add Running buffer – on the inside such that the gel wells are covered and on the outside.
4. Remove comb from gel once the buffer is on
5. Set up the samples
    a. Based on Bradford assay – add 15ug of protein to a 1.5ml tube.
    b. For Licor: must use orange running buffer (4x) – add 10 Add 100 µL of β-mercaptoethanol to 90 µL of 4X Protein Loading Buffer and mix well.
        i. 1 µL buffer per 3 µL sample
    c. Cap the tubes and boil samples 95°C for 5 min.
    d. Spin samples 16,000x g for 1 min.
6. Add the standard (10 µL) and samples to the well.
7. Run at 50V for 5 min.
8. Run at 100V for 1 hr.

Transferring Samples:

1. Remove the gel – put in transfer buffer for 15min.
2. Prep the membrane (Immobilon Sigma P4188-10EA; PDVF)

    a. Cut size to match the gel
    b. Notch the corner
    c. MeOH for 15 sec
    d. H_2O for 2 min
    e. Transfer buffer for minimum 5 min.
3. Sandwich
    a. Black side of cassette down.
    b. Pre-wet (transfer buffer) the fiber pads, filter papers.
    c. Add 1 fiber pad to the gray side of the cassette
    d. Then add 1 filter paper (pre-wet)
    e. Add the gel
    f. Add pre-wet membrane
    g. Roll the membrane with glass rod to get air bubbles out.
    h. Add 1 filter paper (pre-wet)
    i. Add pre-wet fiber pad)
    j. Close the sandwich.
4. Add the sandwich to the holder such that the clear side is toward the red electrode side.
5. Drop in thin “X” shaped spinner into the bottom of the box (or small round – doesn’t need to be “x”)
6. Add the ice block to the box.
7. Place box into ice (make sure to surround box fully with ice to keep cold) & ice box on top of spinner
    a. Do not let box/buffer get warm! (it will cause bubbles)
8. Run 100V for 1 hour

<u>Protein detection-on blot:</u> (Using the REVERT total protein stain from Licor)

1. Rinse membrane briefly in H_2O
2. Put into 5mL of total protein stain for 5min on rotator
3. Rinse 2x30sec in ~5mL Wash Solution
4. Briefly rinse in H_2O
5. Image immediately on 700 channel, 84um, low resolution
6. Incubate in 5mL Reversal Solution for 5-10min (until stain is no longer visible to the eye)
    a. This is optional – I skip if not imaging in the 700 channel
7. Rinse briefly in H2O & proceed directly to blocking step, **skipping the washing steps**

<u>Blocking Blot</u>

1. Block Blot in 5-10 mL Odyssey TBS Intercept Blocking Buffer for 1 hour at RT on rotator (or sometimes I block overnight in cold room)

1° Antibody application

1. Add the following antibodies in 5 mL Odyssey Blocking Buffer:
   5 µL rb anti-AKT (1:1,000)
   Cell Signaling cat# 9272S
   5 µL rb anti-phospho AKT (Ser473) (1:1,000)
   Cell Signaling cat# 4060S
   and
   5 µL rb anti-GSK3β (1:1,000)
   Cell Signaling cat# 9315S
   5 µL rb anti-phospho GSK3β (Ser9) (1:1,000)
   Cell Signaling cat# 9323S
   or
   5 µL rb anti-P44/42 MAPK (Erk1/2)* (1:1,000)
   Cell Signaling cat# 4695S
   5 µL rb anti-phospho P44/42 MAPK (Erk1/2) (Thr202/Tyr204)* (1:1,000)
   Cell Signaling cat# 4377S
   or
   5 µL rb anti-P38 MAPK* (1:1,000)
   Cell Signaling cat# 9212S
   5 µL rb anti-phospho P38 MAPK (Thr180/Tyr182)* (1:1,000)
   Cell Signaling cat# 4511S

2. Incubate blot overnight in cold room on rotator

*Cannot do both GSK3B & ERK at the same time because they are the same molecular weight – must strip and re-probe

**Test antibodies separately before using multiple at one time to check for nonspecific bands

2° Antibody application

1. Wash blot 3X in ~10 mL 0.1% PBS-Tween20 (10 min each)
   Add the following antibodies in 5 mL Odyssey PBS Blocking Buffer:
   1. 0.5 uL Licor anti-Rabbit IR 800 (1:10,000)
2. Incubate blot for 1 hr at room temperature on the rotator
3. Wash blot 2X in ~10 mL 0.1% PBS-Tween20 (10 min each)
4. Wash blot 1X in PBS (15 min)
   *Store in PBS @ 4°C if not imaging right away
5. Image on Licor on 800 channels, auto detection, 84um-169um, low resolution

To stain the gel with coomassie:

1. Wash gel 3x 5 min H_2O
2. Add 50ml Coomassie (BioRad) – Rocker, RT, 1hr.

3. Dump off coomassie
4. Wash H_2O 30min Rocker, RT.

<u>For stripping/re-probing:</u>
Follow directions on PDVF stripping buffer from LiCor (NewBlot PVDF 5X Stripping Buffer (P/N 928-40032) (modified below):

Reagents:
- 1X PBS wash buffer
- Ultrapure water
- Incubation Box
- Completed Western blot to be stripped (wet)

Warning: Keep the blot moist at all times. If it dries during the incubation, washing, scanning, or stripping step, it can reduce the ability to successfully strip and reprobe the blot.

1. Prepare a 1X working solution of NewBlot™ PVDF 5X Stripping Buffer by mixing one part stripping buffer with four parts water.
2. Transfer the working solution to a clean incubation container.
3. Place the blot into the incubation container. Ensure it is fully submerged and can move freely within the container. Place the container on a rotator and shake briskly (70-80 rpm) for 20 minutes at room temperature.
4. Immediately rinse the blot by removing it from the stripping buffer and completely submerging it in a fresh container of 1X PBS. Repeat rinse two more times, using fresh 1X PBS each time.
   *Note: Allow the blot to remain in 1X PBS after the last rinse until further processing. **Do not allow the blot to dry.**
5. Reprobe the blot with the desired primary and secondary antibodies.

Chapter 3. Hyperinsulinemia Potentiates Bronchoconstriction in Response to Parasympathetic Nerve Stimulation

A. Abstract

Obesity increases incidence and severity of asthma but the molecular mechanisms are not fully understood. Hyperinsulinemia in obese male rats potentiates vagally-induced bronchoconstriction. Here I test whether sex affects airway vagal nerve-induced bronchoconstriction. Furthermore, I tested whether insulin or insulin like growth factor-1 (IGF-1) change agonist-induced airway smooth muscle contraction. My results demonstrate that vagally-induced bronchoconstriction was potentiated only in male rats, which gained more body weight, body fat, and had increased levels of fasting insulin compared to females after a five-week high-fat diet feeding. Insulin, but not IGF-1, significantly increases methacholine-induced contraction of rat isolated airway smooth muscle. This is further confirmed by human *ex vivo* studies, suggesting that insulin is the mediator for increased methacholine-induced bronchoconstriction. These findings may explain the contribution of parasympathetic nerves and airway smooth muscle in obesity-related airway hyperreactivity and give insights into future targets for asthma treatment.

Work in this chapter has been published as part of the following manuscripts:

Calco GN, Proskocil BJ, Jacoby DB, Fryer AD, Nie Z. Metformin prevents airway hyperreactivity in rats with dietary obesity. Am J Physiol Lung Cell Mol Physiol. 2021 Dec 1;321(6):L1105-L1118. doi: 10.1152/ajplung.00202.2021. Epub 2021 Oct 20. PMID: 34668415; PMCID: PMC8715020.

Proskocil BJ, **Calco GN**, Nie Z. Insulin acutely increases agonist-induced airway smooth muscle contraction in humans and rats. Am J Physiol Lung Cell Mol

Physiol. 2021 Apr 1;320(4):L545-L556. doi: 10.1152/ajplung.00232.2020. Epub 2021 Jan 27. PMID: 33501891; PMCID: PMC8238158.

B. Introduction

The worldwide prevalence of obesity has nearly tripled in the last forty years with 13% of the adult population considered obese[211]. Obese individuals are more than twice as likely to be diagnosed with asthma and make up the majority of asthmatic patients with severe or difficult-to-treat asthma[82, 83]. These obese asthmatic individuals respond poorly to typical asthma medications, such as corticosteroids, leading to higher healthcare costs and reduced quality of life[4, 85]. Therefore, in order to develop effective treatment strategies, it is imperative to define the underlying characteristics and mechanisms driving obesity-related asthma.

Airway vagal nerves contain parasympathetic nerves, which provide the dominant autonomic control of airway tone. Parasympathetic nerves release acetylcholine (ACh) that activates M_3 muscarinic receptors on airway smooth muscle, resulting in smooth muscle contraction and bronchoconstriction. Acetylcholine also provides inhibitory feedback on M_2 muscarinic receptors, located on the parasympathetic nerves, to limit further acetylcholine release[212].

Studies in humans have revealed the importance of insulin resistance and hyperinsulinemia in obesity-related asthma[135, 213, 214]. Obese male rats have increased parasympathetic nerve-mediated bronchoconstriction compared with lean animals, and that this bronchoconstriction is insulin-dependent[138]. One of mechanism leading to this potentiated bronchoconstriction is due to the loss of normal neuronal M_2 receptor function on preganglionic parasympathetic nerves[138]. However, the contribution of M_3 receptors on smooth muscle to this potentiated bronchoconstriction response is not yet

clear due to sudden cardiac death truncating the dose-response curve[138]. Because muscarinic agonists can induce sudden cardiac death in obese rats with high circulating insulin[138], I tested the effect of insulin on M_3 receptors *ex vivo*.

Studies in both humans and animals have also described sexual dimorphism as an important factor in respiratory physiology and asthma[215]. A potential barrier to treating and preventing severe asthma may be due to a lack of understanding the sex differences in this disease. Asthma is more common in pre-pubescent males[216, 217], but following puberty, the trend reverses, and adult females more commonly have asthma[218]. Currently all data investigating the effects of obesity-related airway hyperreactivity has been done in male rats. Therefore, it is imperative to test if the same effects are seen in female rats.

Furthermore, similar to insulin, circulating insulin-like growth factor-1 (IGF-1) is also elevated in obese individuals[6] and has a role in the development of asthma[7]. IGF-1 regulates the proliferation of airway smooth muscle cells[8]. The effects of IGF-1 on airway parasympathetic nerve function, however, are unknown. IGF-1 and insulin are closely related hormones with homologous structures. They can fully activate their own receptors and are also able to bind to and activate each other's receptors, although with reduced affinity[9]. Thus, IGF-1 might also contribute to obesity-related airway hyperreactivity with similar mechanisms to insulin. This has not yet been studied.

In this chapter, I tested whether sex differences exist in obesity-related airway hyperreactivity and to what degree insulin or IGF-1 contribute to airway smooth muscle

contraction. I measured vagal-nerve stimulated bronchoconstriction in male and female rats on a high or low fat diet in obese-prone and obese-resistant rats. My data indicate that male, but not female, obese-prone rats are susceptible to body weight and fat gain on a high fat diet and subsequently develop hyperinsulinemia-potentiated airway hyperresponsiveness. IGF-1 does not appear to be involved in this mechanism. These results provide supporting evidence for the role of insulin in the parasympathetic and airway smooth muscle contribution to obesity-related asthma.

C. Specific Methods

Animals

Obese-prone and obese-resistant male and female rats were originally developed by selectively breeding Sprague Dawley rat pairs who gained the most weight or least weight, respectively. Rats were originally purchased from Charles River Labs (Wilmington, MA) and subsequently bred in-house. Wild-type Sprague–Dawley were purchased from Charles River Labs (Wilmington, MA). Wild-type Sprague–Dawley rats were used for *ex vivo* experiments. Animals were handled in accordance with the standards established by the United States Animal Welfare Acts set forth in NIH guidelines and approved by the Institutional Animal Care and Use Committee at Oregon Health & Science University.

Diet and Physiology

Obese-prone and obese-resistant rats were fed either a high- (60% of calories come from fat, Test Diet 58126) or low-fat diet (10% of calories come from fat, Test Diet 58124) for 5 weeks. After 5 weeks, some animals were treated with 3 units of insulin in 100 µL PBS s.c. (Lantus), during which they had free access to food to avoid hypoglycemia. Control animals were treated with PBS alone (100 µL s.c.) and fasted overnight. After a 16-h treatment with either insulin or PBS, airway function, blood glucose, body fat were measured as previously described in Chapter 2. Food intake (g) was calculated by subtracting remaining food (g) from food administered (g). Consumption of calories was calculated by multiplying the amount of food consumed (g) by calorie content per gram of food. Because eating increases blood glucose and

insulin, all rats were fasted for 16 hours prior to testing airway physiology in order to get accurate measurement of fasting glucose, fasting insulin and airway responses.

Measurements of Pulmonary Inflation Pressure, Heart Rate, and Blood Pressure

Bronchoconstriction in response to electrical stimulation of both vagus nerves was measured as previously described in Chapter 2. Briefly, rats were anesthetized with urethane (1.4 g/kg ip for female rats and 1.6 g/kg ip for male rats; Sigma-Aldrich) to induce deep anesthesia, evidenced by loss of foot withdrawal reflex, and ventilated via a tracheal cannula using a Harvard Apparatus ventilator (South Natick, MA, tidal volume 2.5 mL, 100 breaths/min). Body temperature was maintained at 37°C using a heating blanket. Heart rate and blood pressure were measured by a pressure transducer attached to a cannula inserted into the internal carotid artery. All animals were chemically sympathectomized with guanethidine (5 mg/kg iv; Sigma-Aldrich, 30 min before physiological data collection) and paralyzed with succinylcholine (1.155 mL/min iv bolus then 0.155 mL/min continuous infusions into jugular vein; Sigma-Aldrich). Pulmonary inflation pressure (P_{pi}) was measured from a pressure transducer attached to a sidearm of the tracheal cannula. Bronchoconstriction was measured as the increase in pulmonary inflation pressure (mmH_2O) above baseline pressure induced by the ventilator. Bradycardia was measured as a fall in heart rate in beats/min. Heart rate, blood pressure, and pulmonary inflation pressure were recorded using the Lab Chart software (AD Instruments, Colorado Springs, CO).

Vagally Induced Bronchoconstriction and Bradycardia

Anesthetized, paralyzed, and ventilated rats were vagotomized by cutting both vagus nerves to remove input from the central nervous system and eliminate reflex responses. Distal ends of both vagus nerves were placed on platinum electrodes and immersed in warm mineral oil. Electrical stimulation of both vagus nerves (2–30 Hz, 20 V, 0.4 ms pulse duration, for 6 s at 40 s intervals) produced frequency-dependent bronchoconstriction and bradycardia that recovered upon cessation of electrical stimulation.

Methacholine and Acetylcholine-Induced Bronchoconstriction and Bradycardia

Increasing doses of nebulized (AG-AL1100, Kent Scientific Corporation) methacholine (MCh, 1–10 mM in 20 µL, for 20 sec, Sigma-Aldrich) or intravenous acetylcholine (ACh, 1, 5, and 10 µg/kg) were delivered to vagotomized rats. In the absence of intact vagi, inhaled methacholine-induced bronchoconstriction is mediated only by M_3 muscarinic receptors on smooth muscle[186, 219-221] and bradycardia is mediated by M_2 muscarinic receptors on cardiac muscle[222, 223].

Human Tracheal Smooth Muscle

De-identified human tracheas were obtained from non-asthmatic organ donors from the Pacific Northwest Transplant Bank (Portland, OR). Tracheal smooth muscle strips (1.5 cm × 0.5 cm) were used for *ex vivo* experiments 6–20 hours after harvest.

Measurement of Rat and Human Tracheal Smooth Muscle Function *Ex Vivo*

Rat or human tracheal tissue was isolated for *ex vivo* studies. Wild type Sprague–Dawley rats were euthanized with 30 mg/kg pentobarbital i.p. (Vortech Pharmaceuticals,

Dearborn, MI) and tracheas were removed. For cranial vs. caudal studies, the trachea was cut just below the larynx (cranial) and just above the bifurcation (caudal) and divided into 2 pieces, each consisting of 4 cartilage rings. For all other studies, rat tracheal rings above the bifurcation (spanning 4–5 cartilage rings) and human tracheal smooth muscle strips were placed in 5 mL organ baths (Radnoti, Colorado Springs, CO) containing Krebs buffer as described in Chapter 2. Rat tracheal epithelium was removed from some segments by inserting and rotating a plastic catheter inside the tracheal lumen before placing the segments in the organ bath. After tissues equilibrated and stabilized, ascending doses of methacholine (0.1–100 μM, A2251 Sigma-Aldrich) or electrical field stimulation (EFS) (100 V, 0.2 ms, for 5 s duration, 1–50 Hz at 1-min intervals) were cumulatively delivered to the organ baths, followed by a series of washes, and then another ascending dose of methacholine or frequency of EFS (Figure 9). Changes in tension were measured as force (in grams) and recorded by Lab Chart software (ADInstruments). Tracheal smooth muscle was then treated with 1 μM insulin (I9278 Sigma-Aldrich)[224], 13.1 nM IGF-1 (100 ng/mL), or PBS for 10 min–2 h. Rat IGF-1 (4326-RG, R&D Systems, Minneapolis, MN) and human IGF-1 (I3769, Sigma-Aldrich) were used for rat and human tissue, respectively, and the PBS control was used to ensure tissue viability did not change over time. After treatment with insulin, IGF-1, or PBS, ascending doses of methacholine were again added to the organ bath and then repeated after washing the tissue. The average of the two methacholine dose-response curves before treatment was compared to the average of the two methacholine dose-response curves after treatment. For longer treatments with insulin (4 and 16 h), rat tracheal smooth muscle was treated with either 1 μM insulin or PBS for 4 h or 16 h. In all the organ bath experiments, each tissue was contracted with 0.1 M KCl at the end of

each experiment to control for variations between samples due to tissue mass or contractibility, and this change in tension was used to normalize contractions induced by methacholine.

Statistical Analysis

Bronchoconstriction and bradycardia in response to vagal nerve electrical stimulation and inhaled nebulized methacholine were analyzed using two-way repeated-measures analysis of variance [225]. Physiological baselines (blood pressure and heart rate), body weight, body fat, and fasting blood glucose and insulin were analyzed by one-way ANOVA with Bonferroni correction. All data were analyzed with Prism (GraphPad, La Jolla, CA). P value < 0.05 was considered significant.

D. Results

High-fat diet induced obesity and airway hyperreactivity in male rats

Resting inflation pressure, heart rate, and blood pressure were not different among male and female rats on either high- or low-fat diets for 5 weeks (Table 6). Male rats weighed more than age matched females before starting a high- or low- fat diet feeding (Figure 15A). Five weeks later, male rats still weighed more than age matched females independent of dietary interventions (Figure 15B). Body weight in male rats on high-fat diet increased by 15% compared to male rats on a low-fat diet, while female rats on a high-fat diet increased by only 9% compared to low-fat diet fed females. However, only males on high-fat diet significantly increased in body weight compared to males on low-fat diet (Figure 15B). Females had significantly higher overall body fat than males (Figure 15C), but body fat was not significantly increased by a high-fat diet. In contrast, body fat was significantly increased in males on a high-fat diet compared to males on a low-fat diet (Figure 15C). Body fat was increased by 23% and 9% in male and female rats respectively, by a high-fat diet vs. a low-fat diet. Calorie intake was higher overall in males independent of diet (Figure 15D). Fasting glucose was not different between males and females and was not changed by diet (Figure 15E). In contrast, a high-fat diet feeding significantly increased fasting insulin in males (3.25 ± 0.24 ng/ml compared to 1.81 ± 0.27 ng/ml in those on a low-fat diet) but not in females (1.13 ± 0.25 ng/ml compared to 0.72 ± 0.12 ng/ml on a low-fat diet) (Figure 15F).

Electrical stimulation of both vagal nerves produced frequency-dependent bronchoconstriction (Figure 16A-B) in all groups. In males, vagally-induced bronchoconstriction was significantly greater in rats on a high-fat diet, than in rats on a

low-fat diet (Figure 16A). In contrast, feeding female rats high-fat diet for the same period of time did not potentiate vagally-induced bronchoconstriction (Figure 16B). Female rats on high-fat diet were still responsive to heightened insulin levels since exogenous insulin increased vagally induced bronchoconstriction (Figure 17). Methacholine caused dose-dependent bronchoconstriction in vagotomized rats that was not different between rats on a high- or low- fat diet, regardless of sex (Figure 16C-D).

In the heart, electrical stimulation of both vagus nerves or inhaled methacholine, induced frequency-dependent or dose-dependent falls in heart rate (Figure 16E-H). In male rats, vagally induced bradycardia was greater in rats on a high-fat diet than in rats on a low-fat diet (Figure 16E). Conversely, vagally induced bradycardia in female rats was greatest in those on a low-fat diet (Figure 16F). Thus, similar to vagally-induced bronchoconstriction, the effect of a high-fat diet on vagally induced bradycardia in females was opposite to that in males. Although none of the differences in females were statistically significant, identical trends in female lung and heart function that are opposite of males are important to acknowledge. Inhaled methacholine also induced dose-dependent falls in heart rates that were not significantly different among groups (Figure 16G-H).

Bronchoconstriction in response to intravenous acetylcholine, which stimulates airway smooth muscle contraction indirectly in vagotomized animals, was used in conjunction with methacholine results to determine whether acetylcholinesterase activity between males and females contributed to differences in the vagal nerve-induced bronchoconstriction response. Because acetylcholine is shorter-acting after intravenous

injection[226], it caused bronchoconstriction that was reversible to baseline in all tested animals (Figure 18). No significant differences in response to acetylcholine were measured between male and female rats on a high fat diet (Figure 18). Airway response to acetylcholine in the obese male rats came from previously published work[138].

High-fat diet (HFD) did not cause obesity or airway hyperreactivity in obese-resistant rats

In obese-resistant rats, male rats weighed slightly, but significantly, more than female rats at baseline before any diet (Figure 19A). Male rats remained heavier than females after 5 weeks and again weighed slightly, but significantly, more on a high-fat diet than females (Figure 19B). Fasting glucose was similar in all groups and unchanged by diet (Figure 19C). Electrical stimulation of both vagal nerves produced frequency-dependent bronchoconstriction (Figure 19D-E) in all groups of obese-resistant rats. There were no differences in bronchoconstriction, however, between low- and high-fat diets regardless of sex. Methacholine also induced dose-dependent bronchoconstriction in vagotomized rats that was not different between rats on a high- or low- fat diet, regardless of sex (Figure 19F-G).

Insulin potentiated methacholine-induced rat tracheal smooth muscle contraction *ex vivo*

I used an organ bath experimental setup to determine the effect of insulin on methacholine-induced smooth muscle contraction. Methacholine-induced contractions of rat tracheal smooth muscle rings were measured before and after incubation with either PBS or insulin in organ baths (Figure 20A-E). Methacholine caused dose-

dependent contractions in tracheal smooth muscle from wild type rats. When airway epithelium was intact, methacholine-induced contraction after a 10 minute incubation with 1 μM insulin was slightly increased compared to methacholine-induced contraction before insulin incubation (Figure 20A). Methacholine-induced contractions were significantly potentiated after a 30 minute incubation with 1 μM insulin (Figure 20B) but did not significantly change the EC50 (EC50 before insulin EC50 = 3.67 ± 0.82 μM, after insulin EC50 = 3.59 ± 0.65 μM; p = 0.9417 unpaired t-test). Methacholine-induced contraction after incubation with PBS [227] for 10 minute (Figure 20C) or 30 minute (Figure 20D) was not significantly different from methacholine-induced contractions before incubation with PBS, indicating that smooth muscle contractibility was not changed over time. When the airway epithelium was removed (Figure 20E), methacholine-induced contractions were still significantly potentiated after a 30 minute incubation with 1 μM insulin (after insulin EC50 = 3.02 ± 0.22 μM).

Insulin potentiated methacholine-induced human tracheal smooth muscle contraction *ex vivo*

Methacholine dose-dependently contracted human tracheal smooth muscle strips isolated from organ donors (Figure 20F-G). Methacholine-induced contraction after a 2-hour incubation with 1 μM insulin was significantly potentiated compared the methacholine-induced contractions before incubation with insulin (Figure 20F). Methacholine-induced contractions were similar before and after a 2 hour incubation with PBS, the vehicle control for insulin (Figure 20G), indicating that there was no change in smooth muscle contractibility over time.

IGF-1 did not potentiate methacholine-induced contraction of rat or human tracheal smooth muscle *ex vivo*

Incubation with 13.1 nM (100 ng/mL) rat IGF-1 for 30 minutes to 2 hours or 20 ng/mL human IGF-1 for 30 minutes did not potentiate methacholine-induced tracheal smooth muscle contraction in either rat tracheal smooth muscle (Figure 21A-B) or human tracheal smooth muscle strips (Figure 21D), respectively. Again, methacholine-induced rat tracheal smooth muscle contractions were not different after administration of PBS (the vehicle control for IGF-1), indicating that the tissue does not become fatigued over this interval (Figure 21C). Furthermore, IGF-1 did not potentiate contractions induced by electrical field stimulation (EFS). Parasympathetic nerves mediate contraction of airway smooth muscle *ex vivo* under EFS. My data show this mechanism was not affected by acute IGF-1 incubation (Figure 21E-F). Because the cranial tracheal has fewer nerves and therefore may be less responsive if IGF-1 has an effect on parasympathetic nerves[228], I tested if there were differences in response to EFS in cranial versus caudal sections of trachea. No difference was found between the sections after incubation with IGF-1 (Figure 22A-B). For consistency, all sections of trachea used in IGF-1 EFS experiments came from the caudal trachea.

Table 6. Pulmonary inflation pressure (Ppi) and cardiovascular parameters at baseline in obese-prone rats on a high or low-fat diet.

Diet and Treatment Group	Ppi mmH_2O	Heart rate Beat/min	Systolic BP mmHg	Diastolic BP mmHg	Number of animals
Low-fat diet 5 weeks (female)	93 ± 3	427 ± 17	92 ± 4	31 ± 2	10
Low-fat diet 5 weeks (male)	77 ± 3	403 ± 14	95 ± 5	36 ± 1	8
High-fat diet 5 weeks (female)	90 ± 4	437 ± 8	77 ± 6	41 ± 3	12
High-fat diet 5 weeks (male)	80 ± 2	376 ± 15	89 ± 5	49 ± 3	22

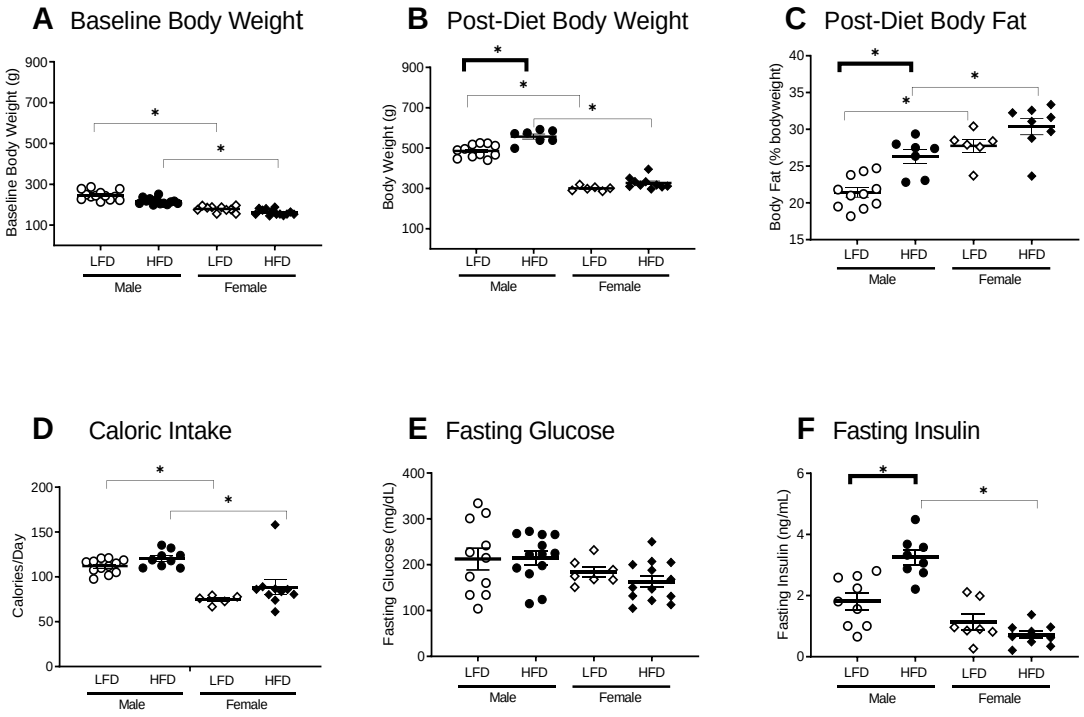

Figure 15. Male rats on a high-fat diet (HFD) gained more body fat and had higher fasting insulin than female rats. (A) Male rats weighed slightly, but significantly, more than female rats at baseline before diet treatment. (B) Male rats remained heavier than females after 5 weeks and weighed significantly more on a high-fat diet than females. (C) Male rats on the high-fat diet weighed significantly more (B) and had greater body fat (C) than male rats on the low-fat diet (LFD). (C) Female rats had a higher percent body fat than males independent of diet, and this did not significantly change with diet. (D) Although male rats ate more calories per day than females, diet fat content did not change caloric intake. (E) Fasting glucose was similar in all groups. (F) Fasting insulin was increased in males on a high-fat diet compared to males on a low-fat diet and females on a high-fat diet. Each data points represent an individual animal; mean ± SEM shown. (n = 7-13) * $p < 0.05$. Reprinted from Calco et. al, 2021.

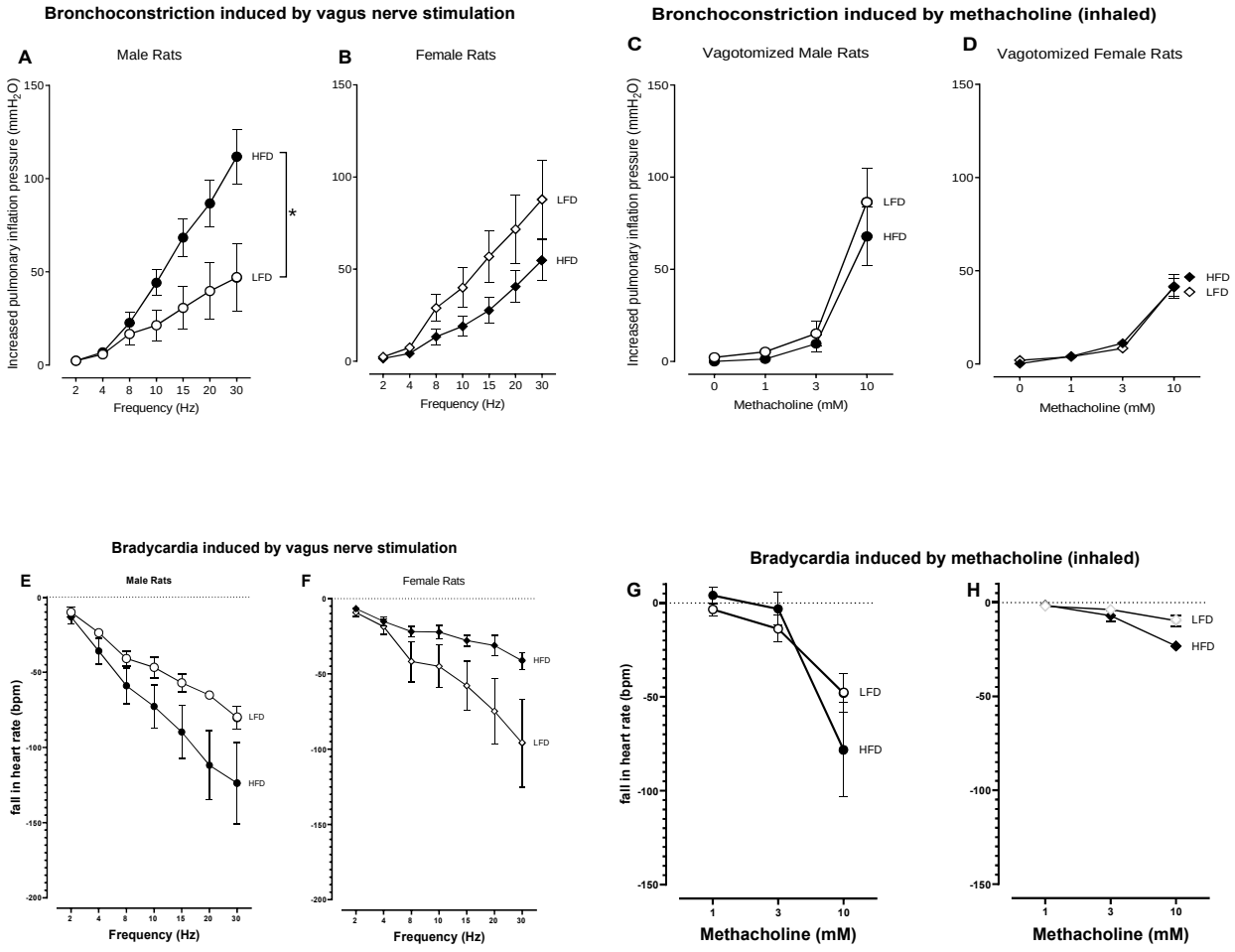

Figure 16. High-fat diet (HFD) induced airway hyperreactivity in obese-prone male rats. (A) Bronchoconstriction induced by electrical stimulation of both vagus nerves (2-30 Hz, 20 V, 0.4-ms pulse duration for 6 s with 40 s pause) was significantly potentiated in high-fat diet fed male rats (HFD; filled circles) vs low-fat diet fed male rats (LFD; empty circles). (B) In contrast, there was a trend of reduced vagally-induced bronchoconstriction in female rats fed high-fat diet (filled diamonds) vs female rats on a low-fat diet (empty diamonds) that was not significant. (C-D) Bronchoconstriction in response to inhaled methacholine was not affected by sex or

by a high- or low-fat diet. (E) High-fat diet had a trend of increased vagus nerve stimulation induced bradycardia in male rats but (F) reduced vagus nerve stimulation induced bradycardia in female rats. Bradycardia induced by inhaled methacholine was not affected by sex or by a high- or low-fat diet. Data presented as mean ± SEM. (n = 6-8) *$p < 0.05$. Reprinted from Calco et. al, 2021.

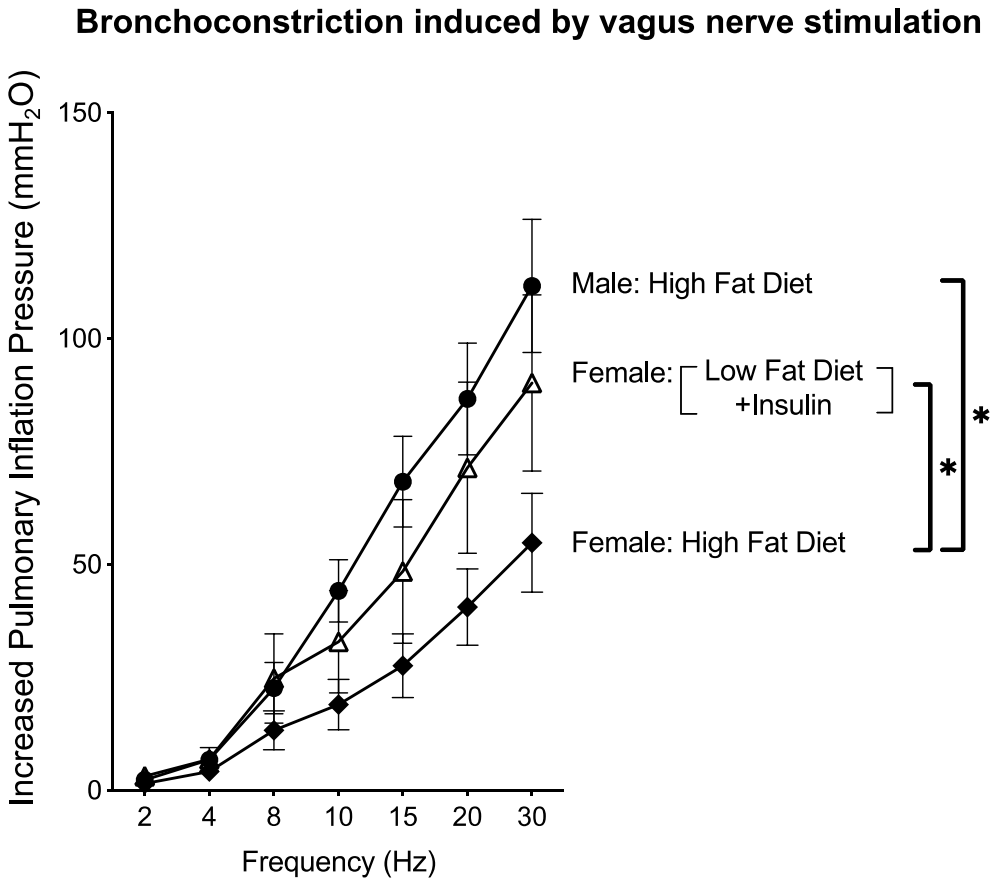

Figure 17. Supplemental insulin potentiated vagally-induced airway hyperreactivity in female rats. Female rats were fed a low-fat diet for 5 weeks. Sixteen hours before measuring airway function, rats were treated with supplemental insulin (Lantus, 3 units/rat subcutaneously) with free access to food. Bronchoconstriction induced by electrical stimulation of both vagus nerves (2-30 Hz, 20 V, 0.4-ms pulse duration for 6 s with 40 s pause) was significantly potentiated in female rats given insulin (empty triangles) vs. high-fat diet fed female rats (filled diamonds). Male high fat diet (filled circles) shown for comparison. Data presented as mean ± SEM. (n = 4-7) *$p < 0.05$.

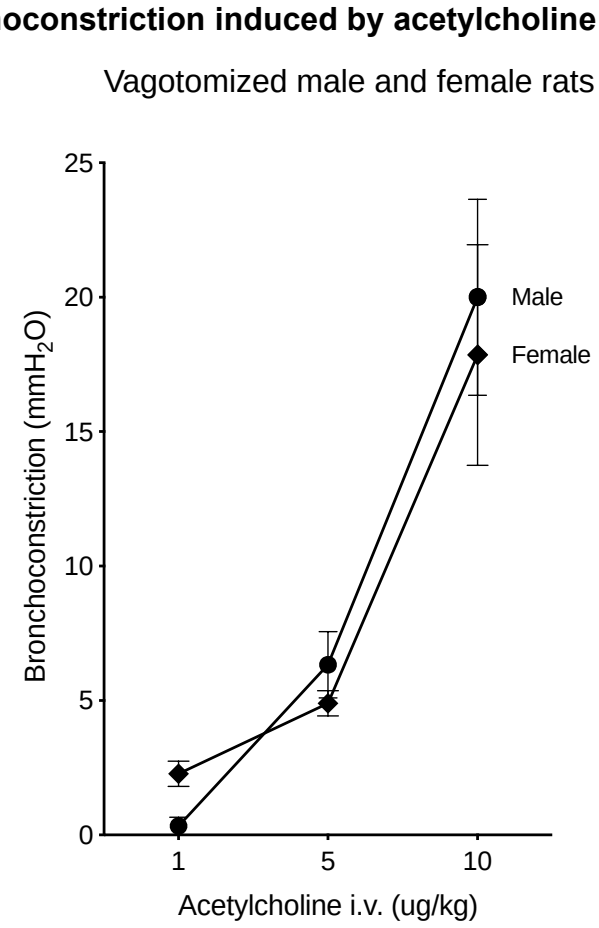

Figure 18. Bronchoconstriction induced by intravenous M_3 muscarinic receptor, acetylcholine, was not significantly different between male and female rats on a high fat diet. ACh cause bronchoconstriction reversible to baseline in all tested animals. No significant differences in response to acetylcholine were measured between male and female rats on a high fat diet. Data presented as mean ± SEM. (n = 3-6). Data from male rats adapted from Nie et al., 2014.

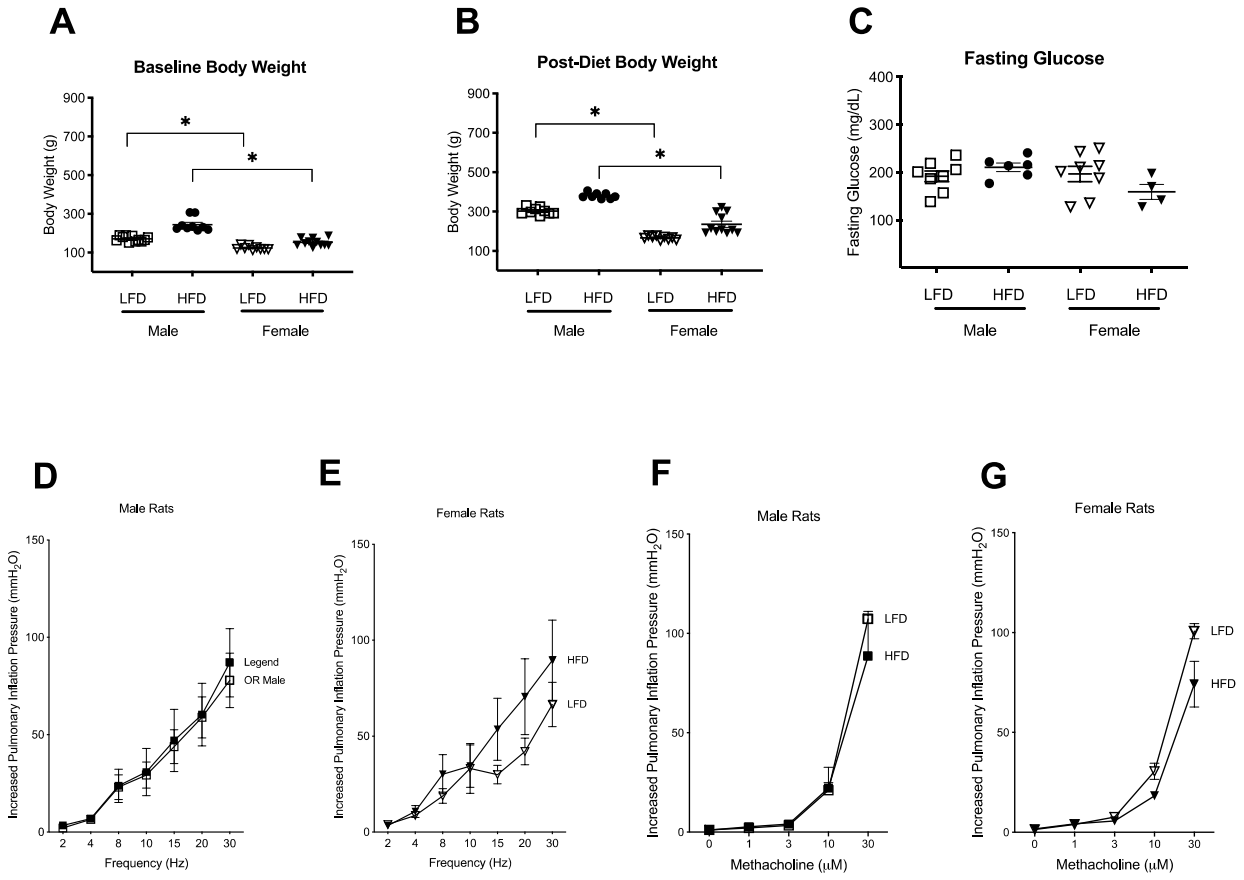

Figure 19. High-fat diet (HFD) did not cause obesity or airway hyperreactivity in obese-resistant rats. Male and female obese resistant rats were fed a high- or low-fat diet for 5 weeks. (A) Male rats weighed slightly, but significantly, more than female rats at baseline before diet treatment. (B) Male rats remained heavier than females after 5 weeks and weighed significantly more on a high-fat diet than females. (C) Fasting glucose was similar in all groups. (D) Bronchoconstriction induced by electrical stimulation of both vagus nerves (2-30 Hz, 20 V, 0.4-ms pulse duration for 6 s with 40 s pause) was similar in males given high-fat diet (HFD; filled squares) and low-fat diet (LFD; empty squares) and (E) in females given high-fat diet (HFD; filled triangles) and low-fat diet (LFD; empty triangles). (F-G) Bronchoconstriction in

response to inhaled methacholine was not affected by sex or by a high- or low-fat diet. Data are presented as mean ± SEM. (n = 4-8) *p < 0.05.

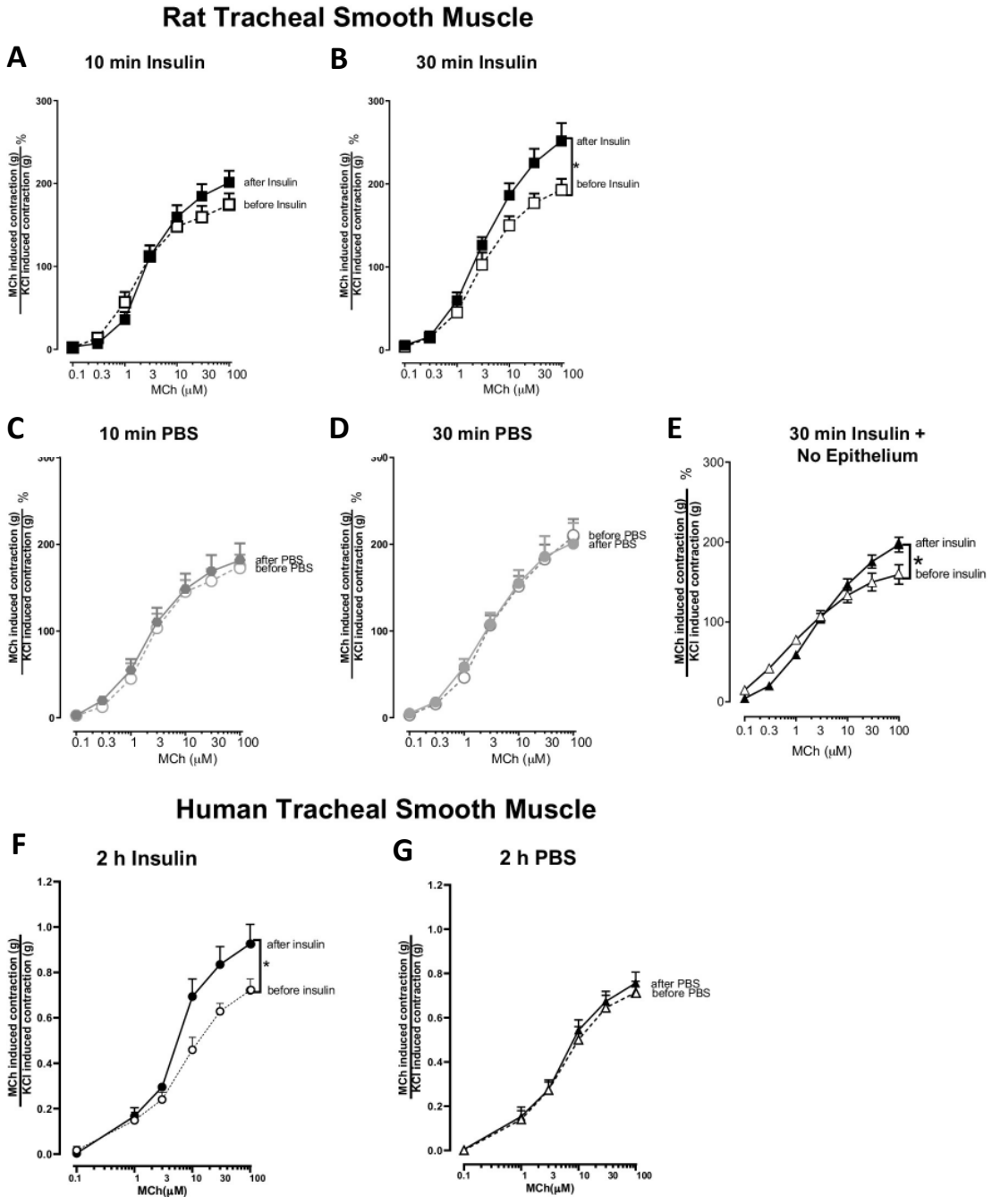
Rat Tracheal Smooth Muscle
A
10 min Insulin
B
30 min Insulin
MCh induced contraction (g) / KCl induced contraction (g) %
after Insulin
before Insulin
*
MCh (μM)
C
10 min PBS
D
30 min PBS
E
30 min Insulin + No Epithelium
after PBS
before PBS
after insulin
before insulin
Human Tracheal Smooth Muscle
F
2 h Insulin
G
2 h PBS
MCh(μM)

Figure 20. Methacholine (MCh)-induced contraction of tracheal smooth muscle is potentiated by insulin, in both rats and humans. Methacholine-induced contraction was measured before and after treatment with 1 μM insulin. [2] In intact rat tracheal rings, methacholine-induced contraction was measured before and after a 10- or 30-min treatment with 1 μM insulin or (C-D) PBS. (E) In rat tracheal rings without airway epithelium, methacholine-induced contraction was measured before and after a 30-min treatment with 1 μM insulin. (F) In intact human tracheal smooth muscle strips, methacholine-induced contraction was measured before and 2 h after treatment with 1 μM insulin or (G) PBS. Methacholine-induced contractions were normalized to contractions induced by 100 mM KCl. Data shown are means ± SE of two replicates each from 6–9 smooth muscle strips ($n = 6–10$). *$P < 0.05$. Modified from Proskocil et al, 2021.

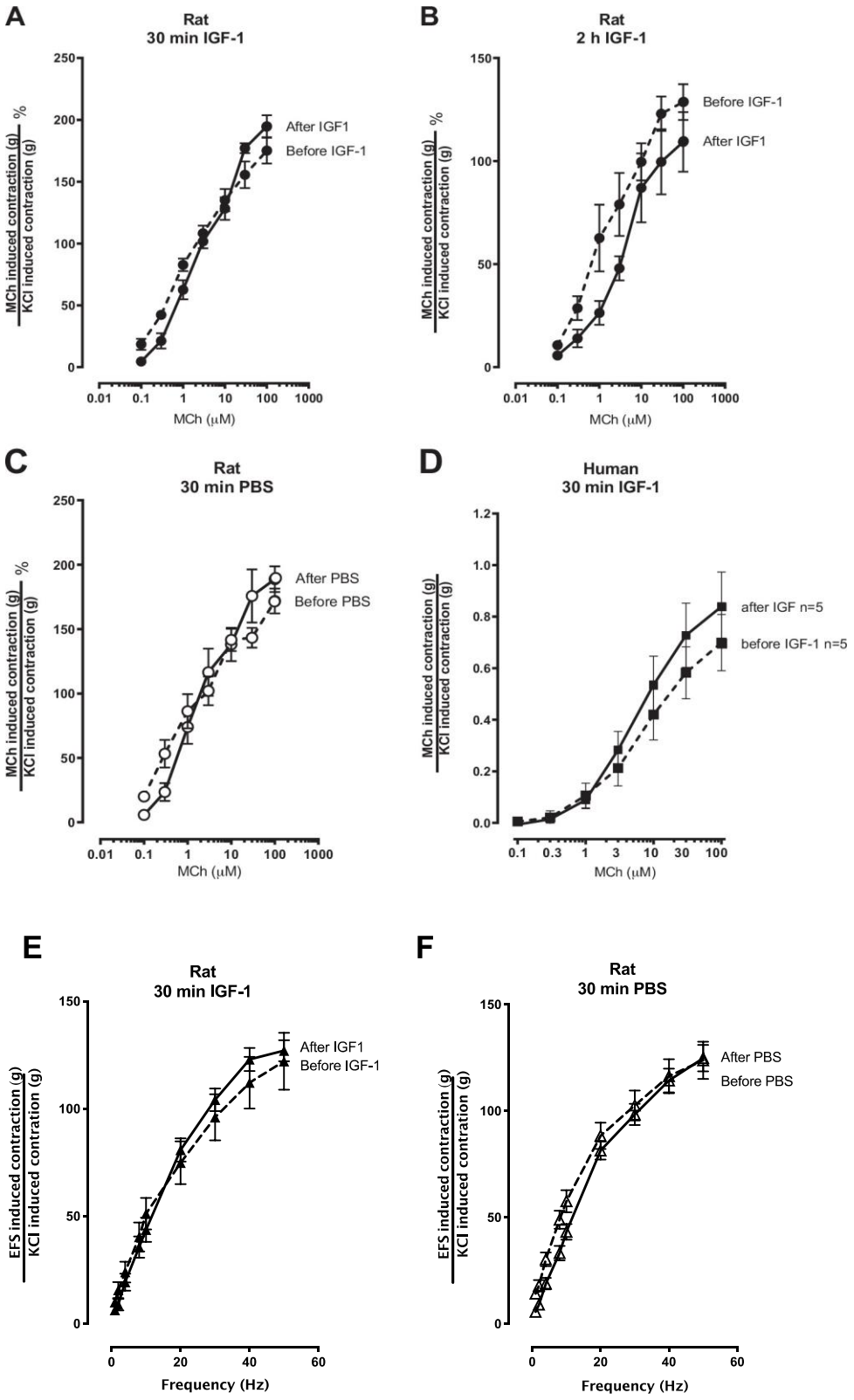
A
Rat
30 min IGF-1
MCh induced contraction (g) / KCl induced contraction (g) %
After IGF1
Before IGF-1
MCh (μM)
B
Rat
2 h IGF-1
Before IGF-1
After IGF1
C
Rat
30 min PBS
After PBS
Before PBS
D
Human
30 min IGF-1
after IGF n=5
before IGF-1 n=5
E
Rat
30 min IGF-1
EFS induced contraction (g) / KCl induced contration (g)
Frequency (Hz)
F
Rat
30 min PBS
After PBS
Before PBS

Figure 21. IGF-1 did not potentiate methacholine(MCh)- or electrical field stimulation(EFS)-induced contraction of rat or human tracheal smooth muscle. (A) Methacholine-induced smooth muscle contraction was measured in rat tracheal rings before and after a 30-min or (B) 2-h exposure to 100 ng/mL rat IGF-1 and (D) in human tracheal smooth muscle strips before and after a 30-min exposure to 20 ng/mL human IGF-1. (C) Methacholine-induced smooth muscle contraction in rat tracheal rings was also measured before and after a 30-min treatment with PBS (vehicle for IGF-1). (E-F) EFS-induced smooth muscle contraction in rat tracheal rings was measured before and after a 30-min treatment with 100 ng/ml IGF-1(E) or PBS (F). All contractions were normalized to contraction induced by 100 mM KCl. Data shown are means ± SE of two replicates each from 3-5 rat tracheas (n = 3; A–C, E-F) and 2 replicates each from 5 human donors (n = 5; D). PBS, phosphate-buffered saline. Modified from Proskocil et al, 2021.

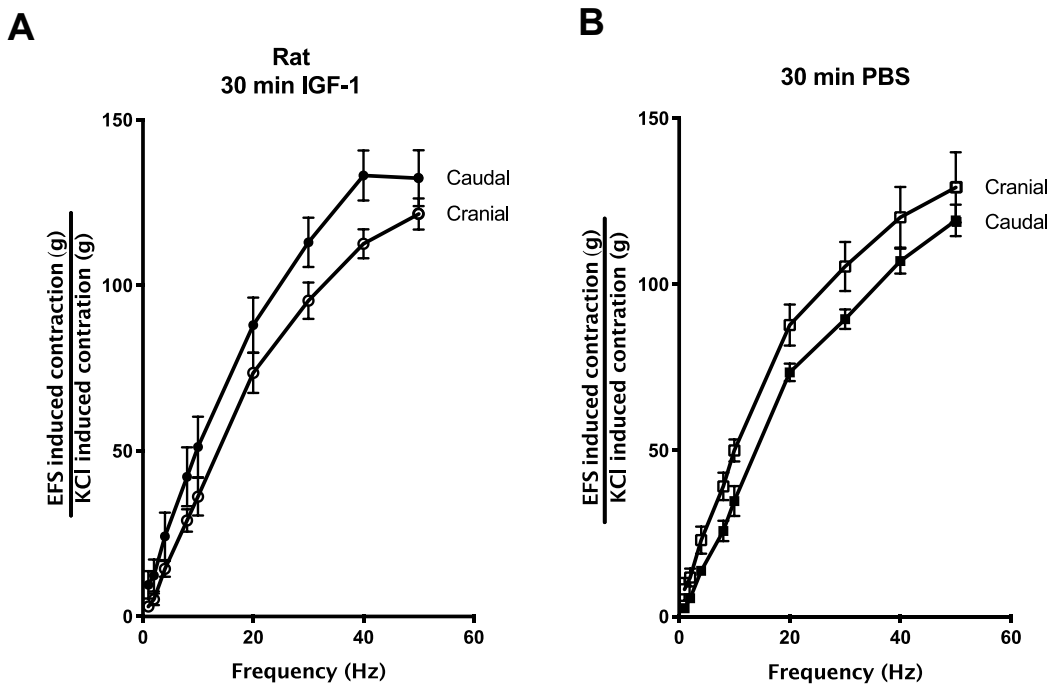

Figure 22. Rat tracheal rings incubated with IGF-1 showed no difference in response to electric field stimulation (EFS) in cranial vs. caudal sections. (A) EFS-induced smooth muscle contraction was measured in cranial and caudal rat tracheal rings after 30-min exposure to 100 ng/mL rat IGF-1. (B) Tracheal rings exposed to PBS showed no difference in response to EFS in cranial vs. caudal sections. Data shown are means ± SE of two replicates each from 3-5 rat tracheas (n = 4-5) PBS, phosphate-buffered saline.

E. Discussion

Here I show that diet-induced obese rats with high insulin levels have potentiated bronchoconstriction in response to parasympathetic nerve-stimulation, which is consistent with previous results[138]. Vagally-induced bronchoconstriction is significantly increased by high-fat diet only in hyperinsulinemic male rats. My findings suggest that this difference is due to greater weight gain and hyperinsulinemia in male, but not female rats. Furthermore, insulin, but not IGF-1, significantly increases methacholine-induced contraction of rat and human isolated airway smooth muscle. Despite this finding, insulin does not seem to contribute significantly to airway smooth muscle contraction *in vivo*.

In human studies, how the relationship between obesity and asthma is affected by sex is, as of yet, still unresolved. Early studies reported an increased asthma incidence in obese women and that weight gain was a risk factor for women with asthma but not men[229-231]. Other studies, however, showed a greater risk of asthma in men[232, 233] or no relationship with sex at all[83]. Most studies, however, examined the relationship between asthma, sex, and obesity using body mass index (BMI) to define obesity-related asthma[234]. BMI, however, is not solely responsible for the obesity-asthma connection[9, 86, 235]. Studies investigating metabolic dysfunction, including insulin resistance, and obesity-related asthma have shown a positive correlation in both men and women[135], independent of sex[136]. Thus, despite the sex differences described in asthma incidence and prevalence, the exact effect modification of sex on obesity-related asthma remains unclear.

Male/female differences in asthma are further complicated by obesity and metabolic syndrome. The incidence of insulin resistance is lower in pre-menopausal women than in men of a similar age[236]. In mice, 17β-estradiol protects neurons from developing insulin resistance[237]. Conflicting data make it difficult to ascribe a role for sex in adult obesity-related asthma[83, 230, 238 231, 233]. My data show that female rats on a high-fat diet did not have significantly higher body weight and body fat compared to female rats on a low-fat diet, which is consistent with a previous study showing female rats were slower to gain weight when fed a high-fat diet compared to their male counterparts[239]. Sex differences were apparent in my data when feeding both sexes of rats high-fat diet for the same period of time. However, the sex difference may not be significant if the high-fat diet is continued for a longer period of time. The underlying mechanisms of sex differences on high-fat diet response may also be related to age and sex hormones[240]. Juvenile male mice on a high-fat diet gain more weight than females mice, but if the diet is initiated in middle-aged mice, the sex difference is reversed, and females gain more weight than males[240]. I am using male and female rats between 5-10 weeks, therefore, the diet was begun in adolescence and all were around peri-adolescence at diet completion[241].

The difference in airway hyperreactivity between males and females may also be due to different insulin levels. My data show female rats on a high-fat diet had lower circulating insulin levels than males independent of diet likely due to this slower weight gain in response to high-fat diet. When females on low-fat diet were administered exogenous insulin, these female rats were capable of developing increased airway response to vagus-nerve stimulation. This indicates that normal circulating insulin levels in female

rats on high-fat diet may explain their normal bronchoconstriction responses compared to the potentiated bronchoconstriction response in obese male rats with hyperinsulinemia.

In obese-resistant rats, which are bred to be resistant to diet-induced obesity[207, 242], there were no differences between males and females. Therefore, differences in response to electrical stimulation of the vagus nerve between males and females in the obese-prone rats is likely not due to the obese-prone rat strain and more likely due to the difference in insulin level. Because of the differences in response to high-fat diet between male and female obese-prone Sprague-Dawley rats, care should be taken when developing experiments investigating vagal nerve-mediated obesity-related airway hyperresponsiveness in obese animals. Only those animals with defined metabolic dysfunction, including hyperinsulinemia, may be relevant to the disease model and warrant further study. Understanding this model of obesity-related asthma will allow for better experimental design and avoidance of bias in future investigations of human airway disease.

Ex vivo, a thirty minute exposure to insulin was sufficient to significantly potentiate smooth muscle contraction induced by methacholine. The potentiation effect on agonist-induced airway smooth muscle contraction is specific to insulin, and not related to IGF-1, which is elevated in obese individuals[243] and may play a role in the development of asthma[244] via increasing proliferation of airway smooth muscle cells[245]. IGF-1 and insulin have homologous structures and activate their own receptors, but also bind to and activate other receptors[246]. Despite these similarities, my data showed no

potentiation of methacholine-induced or parasympathetic nerve-mediated airway smooth muscle contraction by IGF-1. Despite insulin potentiating airway smooth muscle contraction *ex vivo*, the *in vivo* data did not support a significant contribution of airway smooth muscle to airway hyperreactivity in obese rats. Thus airway hyperreactivity in obese rats is likely due to functional changes in airway nerves.

In summary, my work here supports the hypothesis that male rats prone to obesity are susceptible to developing hyperinsulinemia when fed a high fat diet, leading to a stronger bronchoconstriction in response to airway nerve stimulation. Moreover, insulin appears to be the main driver of agonist-induced potentiation of airway smooth muscle, however, despite an acute effect present *ex vivo*, this has a limited effect on overall airway contraction *in vivo*. Discovery of the multifaceted effects of insulin on potentiating vagally mediated bronchoconstriction and airway smooth muscle may help direct the development of therapeutic targets for treatment of asthma in patients with hyperinsulinemia, type II diabetes, or obesity.

Chapter 4. Insulin Increases Reflex Bronchoconstriction and Airway Epithelial Sensory Nerve Innervation

A. Abstract

Obesity increases the incidence and severity of asthma that frequently responds poorly to treatment. The underlying mechanisms of obesity-induced asthma are unclear, hampering development of new therapies. Insulin resistance and hyperinsulinemia are common in obese individuals and increase the risk of asthma. In these studies, I used a mouse model of diet-induced obesity to study the mechanisms of airway hyperreactivity. I found that obese mice had increased insulin and potentiated bronchoconstriction in response to inhaled 5-HT or methacholine that was mediated by a neural reflex, as it was eliminated by vagotomy. Airway sensory innervation was increased in obese animals, as measured in 3D in optically cleared, whole-mount tracheas. Deleting insulin receptors specifically on sensory nerves prevented diet-induced airway hyperreactivity and hyperinnervation. My data in this chapter demonstrate the importance of insulin receptors on airway epithelial sensory nerves in obesity-related airway hyperreactivity.

B. Introduction

There are over 250,000 new obesity-related asthma cases per year in the United States[4, 77-81]. Over 60% of the adults with severe asthma are obese[82,83], and respond poorly to typical asthma medications, such as corticosteroids, leading to higher healthcare costs[84] and a substantially reduced quality of life[4,85]. However, the mechanisms driving obesity-related asthma are unclear, limiting our ability to develop new treatments.

Dysfunctional airway nerves lead to airway hyperreactivity, the excessive bronchoconstriction response to stimuli that is a defining feature of asthma. In the airways, sensory neurons in the epithelium detect stimuli in the lumen and relay this signal through the central nervous system. This relay activates parasympathetic nerves, which are the dominant autonomic nerves controlling airway smooth muscle[186]. Parasympathetic nerves release acetylcholine, which activates M_3 muscarinic receptors on airway smooth muscle, causing bronchoconstriction. The release of acetylcholine is reduced by inhibitory M_2 muscarinic receptors on prejunctional parasympathetic nerves. Loss of M_2 muscarinic receptor function has been demonstrated in allergic asthma in humans, and in every animal model of asthma studied[247], including in rats with obesity-induced asthma[138, 248]. Activation of sensory nerves and subsequent reflex bronchoconstriction is also increased in asthmatic patients[249,250] along with abnormal structural changes,[170] however, the architecture and function of airway sensory nerves have never been investigated in obese individuals. Here I studied the contribution of sensory nerves to increased activation of neural reflexes in obesity-related asthma.

Insulin resistance and compensatory hyperinsulinemia are common in obese individuals and increase the risk of asthma, independent of other variables[86,135]. Disruption of insulin signaling by obesity has been linked with airway hyperreactivity and asthma[9]. Insulin potentiates parasympathetic nerve-mediated bronchoconstriction in obese rats by impairing M_2 muscarinic function[138]. At physiological levels, insulin also enhances sensory neurite outgrowth and acts directly on sensory nerves to promote axon growth and regeneration[122]. Thus, hyperinsulinemia may increase nerve-mediated reflex bronchoconstriction by affecting the structure or function of sensory nerves and parasympathetic nerves as both are components of the reflex bronchoconstriction pathway.

In this chapter, I tested the effects of insulin on airway nerve-mediated reflex bronchoconstriction in a diet-induced obese mouse model, which has increased circulating insulin[102]. My data demonstrated that airway epithelial sensory innervation and airway nerve-mediated reflex bronchoconstriction were increased in hyperinsulinemic obese mice. Furthermore, selectively depleting insulin receptors on sensory nerves of these hyperinsulinemic obese mice prevented this increase.

C. Specific Methods

Animals

Adult male and female mice (10-30 weeks-old) were used for experiments. Wild type C57BL/6 mice were purchased from Jackson Laboratory (Bar Harbor, ME) and bred in-house. Transgenic mice with loxp sites flanking exon 4 of the insulin receptor gene ($IR^{lox/lox}$, B6.129S4(FVB)-Insrtm1Khn/J; #006955) and mice expressing Cre recombinase driven by mouse sensory nerve specific advillin promoter elements ($Avil^{icre/+}$, Tg(Avil-icre/ERT2)AJwo/J; #032027; Jackson Laboratory) were purchased from Jackson Laboratory and bred in-house. $Avil^{icre/+}$ mice were on a mixed C57BL/6 and B6129SF1/J genetic background. Insulin receptor floxed mice were on a 129S4/SvJae background. I bred $IR^{lox/lox}$ with $Avil^{icre/+}$ mice to create creERT2 tamoxifen-inducible sensory neuron insulin receptor knockout (SNIRKO) mice as described by Grote et al[153] (Figure 23). SNIRKO mice were treated with 75 mg/kg tamoxifen (20 mg/ml in corn oil, i.p.) for five consecutive days to induce cre expression. Additional control mice are listed in Table 7. Although tamoxifen is known to be toxic, short-term tamoxifen treatment has not been shown to interfere with adult neurogenesis[251]. Mice were given ad libitum access to food and water and housed on a 12-hour light/dark cycle. Animals were handled in accordance with standards established by the US Animal Welfare Acts set forth in NIH guidelines and approved by the Institutional Animal Care and Use Committee at Oregon Health & Science University.

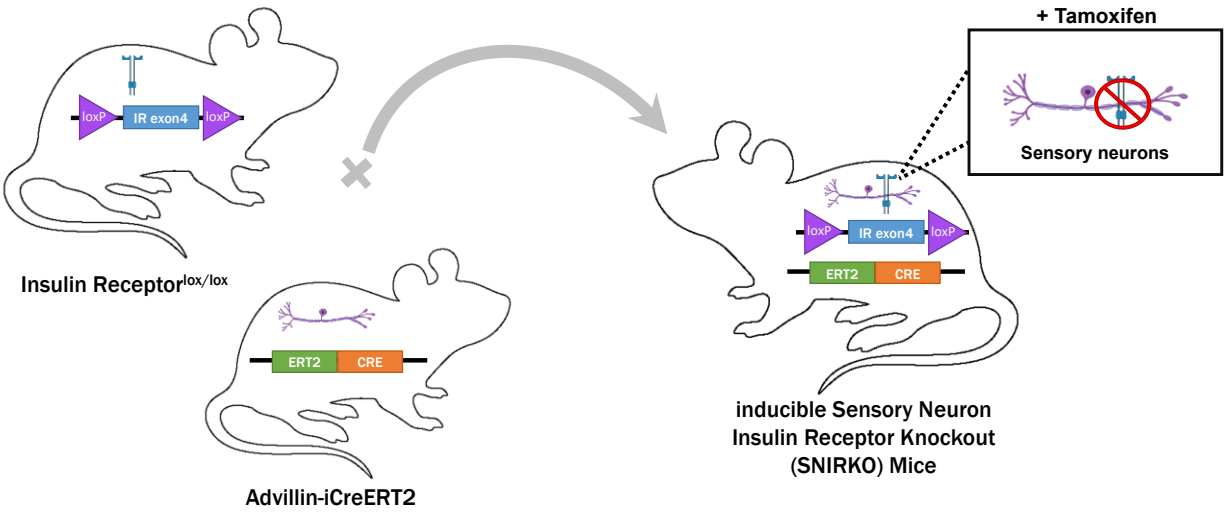

Figure 23. SNIRKO breeding scheme. Diagram showing the result of breeding mice with loxp sites flanking exon 4 of the insulin receptor gene ($IR^{lox/lox}$) with Advillin Cre (Advil-Cre) mice expressing a tamoxifen-inducible cre recombinase directed by mouse advillin promoter elements. Breeding $IR^{lox/lox}$ with tamoxifen Advil-Cre mice results in deletion of exon 4 leading to sensory neuron insulin receptor knockout (SNIRKO) mice.

Table 7. Mouse Diet, Genotype, and Treatment Groups.

Genotype	Diet	Advil iCRE	IRKO	Tamoxifen	Justification
Wild Type	NC	-	-	-	Control lean animals
	HFD	-	-	-	Test effect of high fat diet
	HFD	-	-	+	Test the toxic effect of tamoxifen
SNIRKO	NC	+	+	+	Test effect of diet in IR knockout
	HFD	+	+	+	Test if IR knockout prevents effect of high insulin on nerves
	HFD	+	+	-	Test leaking of cre without tamoxifen
Advil	HFD	+	-	+	Test the toxic effect of free Cre, but IR knockout

Normal Chow (NC); High-fat diet (HFD); Insulin Receptor (IR); Sensory Insulin Receptor Knockout (SNIRKO); Advillin (Advil).

Diet

Ten- to twelve-week-old male and female mice were given access to either a pelleted high-fat diet (61.6% fat, 18.1% protein, and 20.3% carbohydrate, TestDiet 58Y1, St. Louis, MO), or a pelleted normal chow diet (13.4% fat, 29.3% protein, and 29.3% carbohydrate, ResearchDiet 5L0D) for 19 weeks (Table 1, Figure 26A). Mice were housed 2-5 per cage. Food intake for each cage of mice was measured once a week by subtracting the remaining food from the food given. Caloric intake was calculated by multiplying the amount of food consumed by the calorie content per gram of food. The caloric intake data points represents the average number of calories consumed by a single mouse in each cage.

Body Fat, Glucose, and Insulin Measurements

After 19 weeks on a high-fat or normal chow diet, body fat was measured using a nuclear magnetic resonance (NMR)-based body composition analyzer (EchoMRI, Houston, TX) as previously described[248]. Briefly, awake mice were placed into a holding tube and then into a calibrated EchoMRI system. This system uses nuclear magnetic resonance relaxometry to detect and calculate grams of body water, and fat and lean mass based on the different spin relaxation rates in variable tissues. Blood samples were withdrawn from the inferior vena cava to measure blood glucose (OneTouch Ultra2, LifeScan, Inc, Milpitas, CA) and plasma insulin (mouse insulin ELISA, 10-1247-01, Mercodia, Winston Salem NC). Mice were fasted for 16 hours before collecting blood and testing airway physiology. Increase in body weight and fat was calculated by taking the difference between diet groups and dividing by the average of the normal chow control group.

Bronchoalveolar Lavage

Mice were killed by anesthetic overdose and leukocytes were harvested from bronchoalveolar lavage (BAL) fluid as previously described[252]. Briefly, BAL cells were washed, resuspended in PBS, spun onto slides, and stained with Wright stain solution (Sigma-Aldrich, St. Louis, MO) to obtain a differential cell count.

Ventilation

Mice were anesthetized with ketamine (100 mg/kg i.p.) and xylazine (10 mg/kg i.p.), tracheotomized, and ventilated as previously described[252]. A 20-gauge catheter was inserted into the cricothyroid membrane to the level of the fourth cartilage ring. Mice were mechanically ventilated with 100% oxygen at 120 breaths/min with a tidal volume of 200 µl and a positive end-expiratory pressure of 2 cm H_2O. Mice were paralyzed with succinylcholine (10 mg/kg i.m.) to eliminate respiratory effort. Body temperature was maintained at 37°C with a heat lamp and homeothermic blanket, and measured by rectal probe. Heart rate and rhythm were measured by electrocardiogram recorded with electrodes placed subcutaneously on the right foreleg, right back shoulder, and left rear leg. Airway pressure, tidal volume, air flow, heart rate, and body temperature were all measured using LabChart Pro acquisition software (ADInstruments, Colorado Springs, CO).

Measuring Airway Resistance

Airway resistance was measured as previously described[252]. Briefly, two deep inspirations at 25 cmH_2O were given, followed by an inspiratory pause for 225 ms at

peak inspiration for four breaths in a row. For each breath, both peak pressure and end-inflation pressure (plateau pressure) were recorded, and resistance was calculated as the average ($P_{peak}-P_{plateau}$)/inspiratory flow of these four breaths (Figure 24).

Baseline airway resistance was measured at the beginning of each experiment. It was measured again 10 s before and 35 s after each dose of either aerosolized saline, 5-hydroxtryptamine (5-HT, 10 µL, 0–300 mM) (Figure 25), or methacholine (10 µL, 0–1,000 mM). Change in airway resistance (bronchoconstriction) is graphed as the difference between airway resistance after aerosolized challenge and that immediately before challenge ($cmH_2O \cdot mL^{-1} \cdot s^{-1}$). Two deep inspirations were given between each dose to ensure return to baseline between treatments.

Measuring Airway Nerve-Mediated Reflex Bronchoconstriction

Neuronal contribution to bronchoconstriction was measured by comparing changes in airway resistance in response to inhaled 5-HT (10 µL, 10–300 mM, Sigma) and methacholine (10 µL, 10–300 mM, Sigma) with and without vagotomy, as previous described[16]. Vagotomy and atropine (3 mg/kg i.p.) were used to test whether responses were vagally mediated. Two dose-response curves to 5-HT were recorded, the first with the vagi intact and the second after both vagus nerves were isolated and cut to eliminate reflex (neuronal) bronchoconstriction. In other animals, after a first dose-

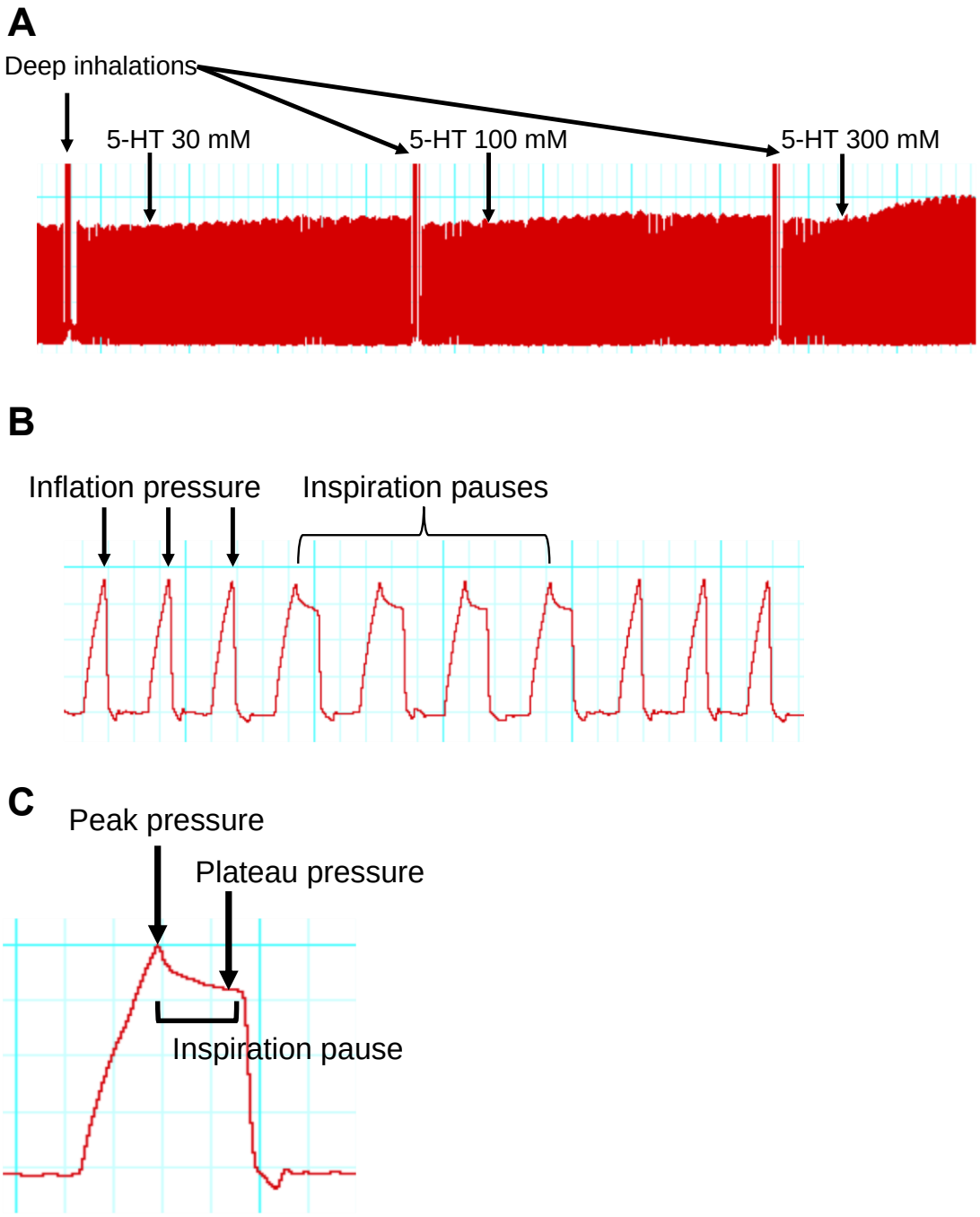

Figure 24. Measurement of airway resistance in a mouse. (A) inflation pressure before and after each dose of aerosolized serotonin (5-HT) (B) inspiration pause after each dose of 5-HT and a magnified view of inflation pressure (C) airway resistance calculated by: $(\text{pressure}_{peak} - \text{pressure}_{plateau})/\text{airway flow}$.

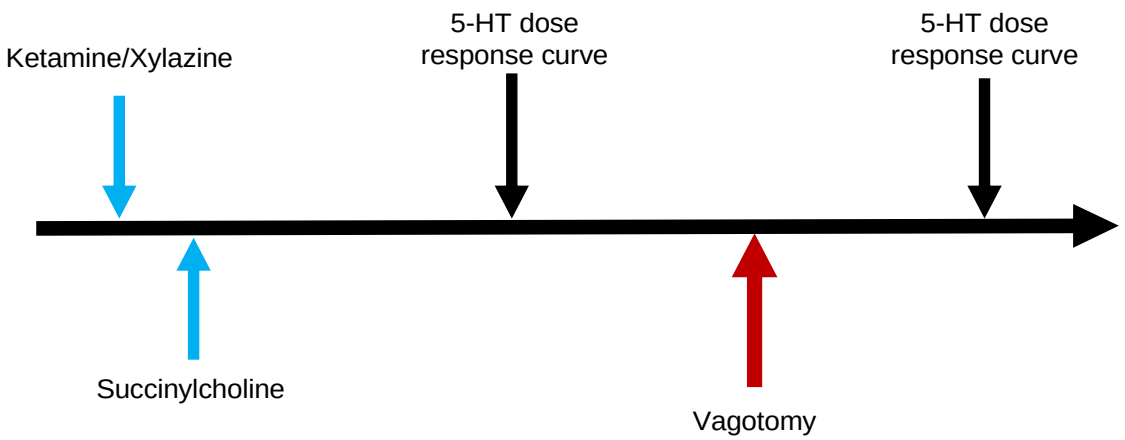

Figure 25. Airway physiology experimental protocol. Ketamine/Xylazine mixture is given to anesthetized animal. When deep anesthesia is reached (no response to toe pinch), paralytic succinylcholine is administered. Increasing doses of serotonin (5-HT) (10-300 mM 5HT) are given both before and after vagotomy to test reflex bronchoconstriction.

response curve, atropine was given and the response to the highest dose of 5-HT was again tested.

Measuring M_3 Muscarinic Receptor Function

The function of M_3 muscarinic receptors on airway smooth muscle was measured using the change in airway resistance in response to increasing doses of aerosolized methacholine (10 µL, 10–300 mM, Sigma) in animals that were vagotomized to eliminate the reflex component of MCh induced bronchoconstriction[253, 254].

Tissue Optical Clearing and Imaging and Quantification of Airway Nerves

Mice were perfused with phosphate buffered saline (PBS) and airways were excised. Tracheas were left at 4°C in Zamboni fixative (Newcomer Supply) overnight. Tracheas were blocked overnight with 4% normal goat serum, 1% Triton X-100, and 5% powdered milk, and then incubated with antibodies to pan-neuronal marker protein gene product 9.5 (PGP9.5, rabbit IgG, 1:200; Amsbio) and substance P (rat IgG_{2A}, 1:500; BD Pharmigen) on a shaker at 4°C overnight. Tissues were washed and incubated overnight in secondary antibodies: Alexa goat anti-rabbit 647 (1:1,000; Invitrogen) and Alexa goat anti-rat 555 (1:1,000; Invitrogen) and counterstained using the nuclear stain 4′6-diamidino-2-phenylindole, dilactate (DAPI, Molecular Probes). Tracheas were then optically cleared in N-methylacetamide/Histodenz (Ce3D) for 12 hours[205] and mounted in Ce3D on slides in 120 µm deep imaging wells (Invitrogen).

Images were acquired using a Zeiss LSM900 confocal microscope and 63×/1.4 oil PlanApo DIC M27 objective with a 0.19 mm working distance. Samples were illuminated with 401 nm, 553 nm, and 653 nm light, and images were acquired as z-stacks. Two to three randomized images were taken of each mouse trachea using DAPI to locate the epithelium. Airway nerves were modeled in 3D using Imaris semi-automatic filament tracing software (Imaris 9.7, Oxford Instruments). Users were blinded to study group at the time of nerve modeling. A 3D filament model was created around tracheal epithelial nerves to quantify nerve length and number of branch points. Neuronal substance P expression was quantified by creating a surface around the substance P-positive voxels and using Imaris software to colocalize the voxels in contact with PGP9.5-positive nerve axons. Two to three images were quantified per mouse trachea.

Confirmation of Insulin Receptor Knockout using qRT-PCR

Mice were euthanized with anesthetic overdose and perfused with PBS, and tissue was dissected and snap frozen in liquid nitrogen. Total RNA was isolated from control and SNIRKO liver, nodose and jugular ganglia, and dorsal root ganglia (DRG) using the RNeasy Mini Kit (Qiagen, Germantown, MD). cDNA was generated using Superscript III Reverse Transcriptase (Thermo Fisher Scientific). Insulin receptor mRNA expression was quantified using QuantiTect SYBR Green (Qiagen) and real time qRT-PCR (7500 Fast Real-Time PCR System, Applied Biosystems, Foster City, CA). Insulin receptor primers were: left primer 5'- GAGGCTGCACTGTGATCAAC-3' and right primer (located within exon 4) 5' – TAGGAGCGGCGGATCTTTAG-3'. Primers for the housekeeping gene 18S rRNA were 5′- GTAACCCGTTGAACCCCATT and 18S 3'

CCATCCAATCGGTAGTAGCG). Insulin receptor expression data were analyzed using the delta-delta CT (ddCT) method[255] and normalized to 18S rRNA.

Insulin Receptor mRNA Localization using BaseScope

Tissues were fixed in 10% Neutral Buffered Formalin overnight at room temperature. BaseScope assays were performed on paraffin sections (5 µm thickness Superfrost plus slides, Fisher Scientific, Loughborough, UK) using guidelines provided by the supplier (Advanced Cell Diagnostics, Newark, CA). Briefly, slides were baked at 60 °C for 1 h before deparaffinizing in xylene (2 × 5 min) and ethanol (2 × 2 min), then dried at 60 °C for 5 min. RNAScope hydrogen peroxide was applied for 10 min at RT, then target retrieval was applied for 15 min at 100 °C. RNAScope protease III was then applied for 30 min at 40 °C. BaseScope insulin receptor (#719141), positive control (#01071), and negative control probes (#701011) were purchased from Advanced Cell Diagnostics and in situ hybridized to tissue sections with BaseScope Detection Reagent Kit v2 - Red (Advanced Cell Diagnostics, Newark, CA). Slides were counterstained with 50% Gill's hematoxylin and then 0.02% ammonia water before drying for 15 min at 60 °C and mounting in EcoMount (Biocare Medical, Pacheco, CA).

Statistical analysis

Increases in airway resistance in response to inhaled nebulized methacholine and 5-HT data were analyzed using two-way repeated-measures analysis of variance[225]. Body weight and fat, caloric intake, fasting blood glucose and insulin were analyzed by Student's t-test and one-way ANOVA. Nerve length, branching, and substance P data were analyzed by one-way ANOVA with Bonferroni post hoc test. All data were

analyzed with Prism 8.0 software (GraphPad, La Jolla, CA). A p value < 0.05 was considered significant.

D. Results

High-fat diet fed mice were obese, hyperinsulinemic, and hyperglycemic

Wild type mice were started on either high-fat diet or normal chow diet for 19 weeks (Figure 26A-B). Both animal groups had similar initial body weights (Figure 26C). Body weight in mice fed a high-fat diet increased by 77% compared with age-matched mice on a normal chow diet (Figure 26B, D). Body fat also increased by 345% in mice on a high-fat diet compared to those on a normal chow diet (Figure 26E). Despite an increase in both body weight and fat in the high-fat diet group, mice on both diets ate a similar number of calories per day (Figure 26F). High-fat diet significantly increased fasting insulin (2.27 ± 1.66 ng/ml compared to 0.40 ± 0.17 ng/ml in those on a normal chow diet) and fasting glucose (214 ± 82.4 mg/dl compared to 140 ± 42.5 mg/dl in those on a normal chow diet) (Figure 26G-H).

High-fat diet-fed mice had increased reflex bronchoconstriction

5-HT-induced bronchoconstriction was significantly greater in mice fed a high-fat diet compared to mice fed a normal chow diet (Figure 27A). This increased bronchoconstriction in response to 5-HT was blocked by vagotomy (Figure 27B) or by atropine (Figure 27C), indicating that the increased bronchoconstriction was due to a potentiated vagal reflex. Bronchoconstriction in response to inhaled methacholine (MCh), a M_3 muscarinic receptor agonist, was significantly increased in mice with intact vagus nerves on a high-fat diet compared to normal chow (Figure 27D). This increased response to MCh was also eliminated by vagotomy, indicating that increased bronchoconstriction was due to a potentiated vagal reflex. In vagotomized mice, inhaled methacholine acts directly on airway smooth muscle to cause contraction. My data

demonstrated there was no difference in bronchoconstriction response to methacholine between vagotomized mice on a high-fat diet compared to those fed normal chow (Figure 27E).

Male and female mice had similar physiological responses to high-fat diet

Male mice gained more weight than female mice on either a high-fat diet or normal chow diet; however, both male and female mice gained significant body weight on high-fat diet (Figure 28A-B). There were no differences in body fat percentage between male and female mice and both sexes gained a significant amount of body fat after a high-fat diet feeding (Figure 28C). Male and female mice within each diet group had similar fasting glucose, fasting insulin, and reflex bronchoconstriction in response to 5-HT (Figure 28D-F).

High-fat diet fed mice did not have airway inflammation

Both normal chow and high-fat diet fed mice had similar total number of cells in their bronchoalveolar lavage fluid (Figure 29A). Both diet groups also had similar numbers of macrophages, lymphocytes, neutrophils, and eosinophils (Figure 29B-E). Neither group had an infiltration of inflammatory cells typically present in allergic asthma[256].

Selectively depleting insulin receptors on sensory neurons in SNIRKO mice via tamoxifen treatment

Male and female SNIRKO mice were treated with five consecutive days of tamoxifen (20 mg/ml i.p.) or corn oil (vehicle control) to induce Cre recombinase activity and delete insulin receptors on sensory neurons (Figure 30A). Insulin receptor mRNA expression in

sensory neurons was determined by BaseScope in-situ hybridization technique, which was used to locate mRNA expression at the single cell level (Figure 30B-G). mRNA expression was visualized via pink dots present in images in Figure 30B-G. Insulin receptor mRNA quantification was confirmed by qRT-PCR in liver, dorsal root ganglia, and nodose and jugular ganglia (Figure 30H). After treatment with tamoxifen, insulin receptor mRNA expression in SNIRKO mice was significantly decreased in nodose and jugular ganglia and dorsal root ganglia compared to that found in wild type mice (Figure 30B-E, and 4H). In liver, tamoxifen resulted in a non-significant decrease, possibly due to deletion of insulin receptors on sensory nerves in the liver (Figure 30F-H).

Selectively depleting insulin receptors on sensory neurons increased circulating insulin

Selectively depleting insulin receptors on sensory neurons significantly increased fasting insulin in SNIRKO mice compared to control mice (wild type mice on a normal chow), regardless of diet [WT NC: 0.40 ± 0.17 ng/ml; SNIRKO NC: 4.12 ± 3.22 ng/ml ($p < 0.0001$); SNIRKO HFD: 2.03 ± 1.63 ng/ml ($p = 0.0314$)]. SNIRKO mice treated with tamoxifen on a high-fat diet had similar fasting insulin levels those on normal chow diet (Figure 31F). This indicated that selectively depleting insulin receptors on sensory nerves caused hyperinsulinemia. High-fat diet SNIRKO mice also had slightly, but significantly, higher fasting glucose levels compared to SNIRKO mice on normal chow (286 ± 83.0 mg/dl on high-fat diet compared to 204 ± 91.5 mg/dl on normal chow diet) (Figure 31G). All mice had similar body weights when the diet treatment started (Figure 31B). However, mice with insulin receptors selectively depleted on sensory neurons gained more body weight and body fat on a high-fat diet compared to those on a normal

chow diet (Figure 31C-D). Daily caloric intake was similar in both diet groups (Figure 31E). Control groups with wild type mice treated with tamoxifen and SNIRKO mice without tamoxifen had similar initial body weights before starting high-fat diet and after diet completion (Figure 32A-B). High fat diet induced similar increases in fasting insulin in wild type mice treated with tamoxifen and SNIRKO mice without tamoxifen [WT HFD with tamoxifen: 1.65 ± 1.53 ng/ml; SNIRKO HFD without tamoxifen: 1.77 ± 1.09 ng/ml] (Figure 32C). Both groups also had similar final fasting glucose (Figure 32D).

SNIRKO mice had normal reflex bronchoconstriction

When fed a high-fat diet, SNIRKO mice without tamoxifen treatment (ie, with intact insulin receptors on sensory nerves) had increased reflex bronchoconstriction to inhaled 5-HT, similar to that seen in the wild type high-fat mice without tamoxifen (Figure 33A). This increased bronchoconstriction in response to 5-HT was blocked by vagotomy (Figure 33B), indicating the response to 5-HT was neurally-mediated. Wild type animals on high-fat diet with and without tamoxifen had similarly increased reflex bronchoconstriction, demonstrating tamoxifen alone did not inhibit reflex bronchoconstriction. Advillin (Advil) mice without floxed insulin receptors on a high-fat diet, also had increased reflex bronchoconstriction, indicating free Cre-recombinase did not affect reflex bronchoconstriction (Figure 33A). In contrast, tamoxifen treatment in SNIRKO mice, effectively depleted insulin receptors on sensory nerves and completely prevented the increased reflex bronchoconstriction to inhaled 5-HT in mice on a high-fat diet. Vagotomized SNIRKO mice with and without tamoxifen had similar bronchoconstriction responses to MCh (Figure 33C). Therefore, the reduced bronchoconstriction in SNIRKO mice treated with tamoxifen was not due to changes in

smooth muscle function. Furthermore, airway resistance directly correlates with fasting insulin in wild type but not SNIRKO mice (Figure 34A-B). This means as fasting insulin increases, airway resistance increases. This is only true in mice with intact insulin receptors.

High-fat diet mice had increased airway epithelial sensory innervation

Airway epithelial nerves were imaged using laser scanning microscopy and modeled on 3D software (Figure 35A-H). The total length of airway epithelial nerves and the total number of nerve branch points were significantly increased in wild type mice on a high-fat diet (Figure 35I-J). The total amount of neuronal substance P expression, determined by colocalization of substance P immunostaining with PGP9.5 positive neurons, was significantly higher in wild type mice on a high-fat diet (Figure 35K). A high-fat diet, however, did not lead to an increase in the ratio of neuronal substance P expression to PGP9.5 expression, which indicates that the increase in colocalized substance P was due to an increase in total epithelial nerves, including those that express substance P (Figure 35L). Depleting the insulin receptor on sensory nerves in SNIRKO mice on high-fat diet prevented increased airway epithelial nerve length and branching and nerve-associated substance P expression (Figure 35I-L).

Insulin-stimulated signaling activation was pathway and tissue dependent

Insulin signaling was quantified using Western blots of activated Akt (p(Ser473)Akt/total Akt), ERK1/2 (p(Thr202/Tyr204)ERK1/2/total ERK1/2), and p38 (p(Thr180/Tyr1820p38/total p38) in liver, nodose and jugular ganglia, and dorsal root

ganglia (DRG) (Figure 36). Mice on a normal chow diet showed a significant increase in Akt phosphorylation after insulin treatment in liver and nodose and jugular ganglia tissues; however, dorsal root ganglia were not very responsive to insulin (Figure 37A-C). The phosphorylation of Akt in the liver by insulin in these mice was far greater than that of neural tissue. This exemplifies that responses to insulin via the PI3K/Akt pathway are tissue dependent. In the liver, nodose and jugular ganglia, and dorsal root ganglia of high-fat diet fed obese mice, Akt phosphorylation and activation was not observed after insulin treatment. Obesity, therefore, induced insulin resistance in the Akt phosphorylation pathway in liver and nodose and jugular ganglia.

A similar pattern was observed when examining phosphorylation and activation of ERK1/2 via the MAP kinase pathway. In the liver and nodose and jugular ganglia of normal chow fed mice, phosphorylation of ERK1/2 was significantly increased by insulin, while there was little change in the DRG. In high-fat diet fed animals insulin-induced phosphorylation of ERK1/2 was trending toward, but not significantly increased, in liver and nodose and jugular ganglia, indicating that high-fat diet induced a weaker activation of MAPK-ERK pathway in those tissue. DRG from high-fat animals had no difference in phosphorylation from baseline (Figure 37D-F).

In normal chow fed animals, the nodose and jugular ganglia had a significant increase in p38 phosphorylation after insulin treatment, while the liver trended toward an increase. The DRG, however, had little response to insulin in the normal chow animals. In liver, nodose and jugular ganglia, and DRG of high-fat diet fed mice, p38 trended toward an increase in insulin-induced phosphorylation (Figure 37G-I). Overall, this data

indicates that activation of the insulin receptor is dependent on the tissue, signaling molecule, and obesity status of the animal.

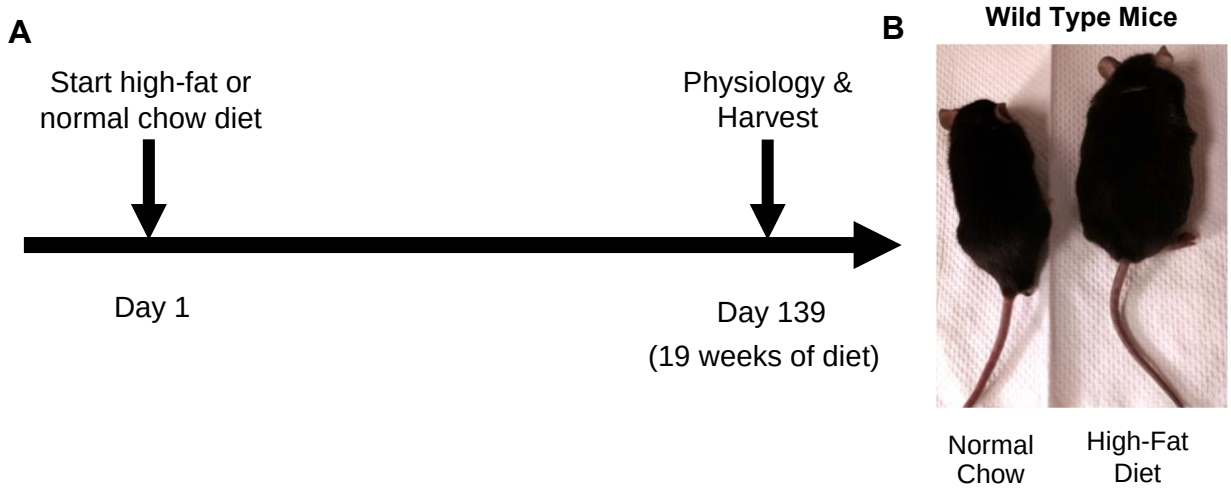
A
Start high-fat or
normal chow diet
Physiology &
Harvest
Day 1
Day 139
(19 weeks of diet)
B
Wild Type Mice
Normal
Chow
High-Fat
Diet

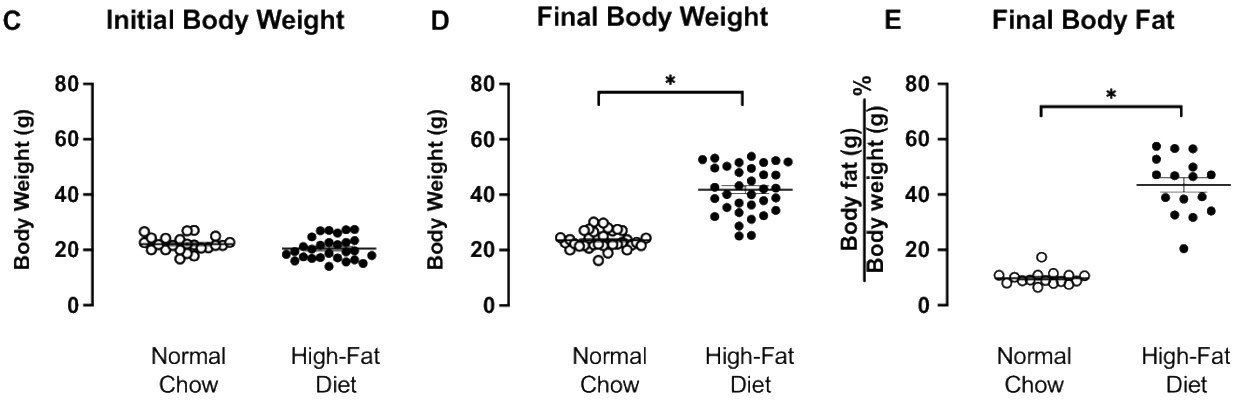
C
Initial Body Weight
Body Weight (g)
80
60
40
20
0
Normal
Chow
High-Fat
Diet
D
Final Body Weight
Body Weight (g)
*
E
Final Body Fat
Body fat (g) / Body weight (g) %
*

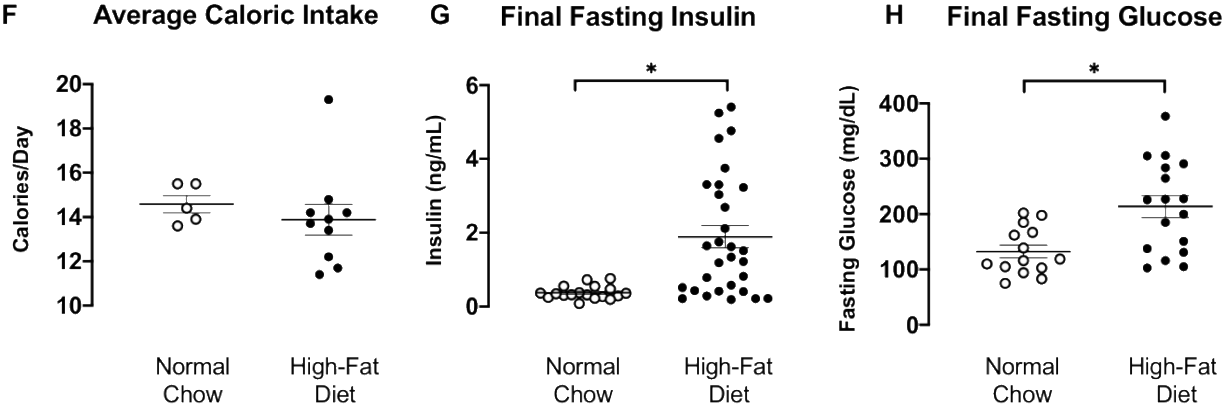
F
Average Caloric Intake
Calories/Day
20
18
16
14
12
10
Normal
Chow
High-Fat
Diet
G
Final Fasting Insulin
Insulin (ng/mL)
6
4
2
0
*
H
Final Fasting Glucose
Fasting Glucose (mg/dL)
400
300
200
100
0
*

Figure 26. High-fat diet fed mice were obese, hyperinsulinemic, and hyperglycemic. (A) Wild type mice were started on either high-fat diet (HFD) or normal chow diet for 19 weeks. (B) Representative pictures of normal chow and high-fat diet mice after 19 weeks of diet. (C) Both animal groups had similar initial body weights. Wild type high-fat diet fed mice (closed circles) had a significant increase in post-diet body weight (D) and percent body fat (E) compared to wild type normal chow fed mice (open circles). (F) Caloric intake was similar among animals. High-fat diet fed mice had significantly increased fasting insulin (G) and fasting glucose (H). Each data point represents an individual animal; mean $\pm$ SEM are shown. (n = 14-23) *$p < 0.05$.

Bronchoconstriction induced by 5-HT

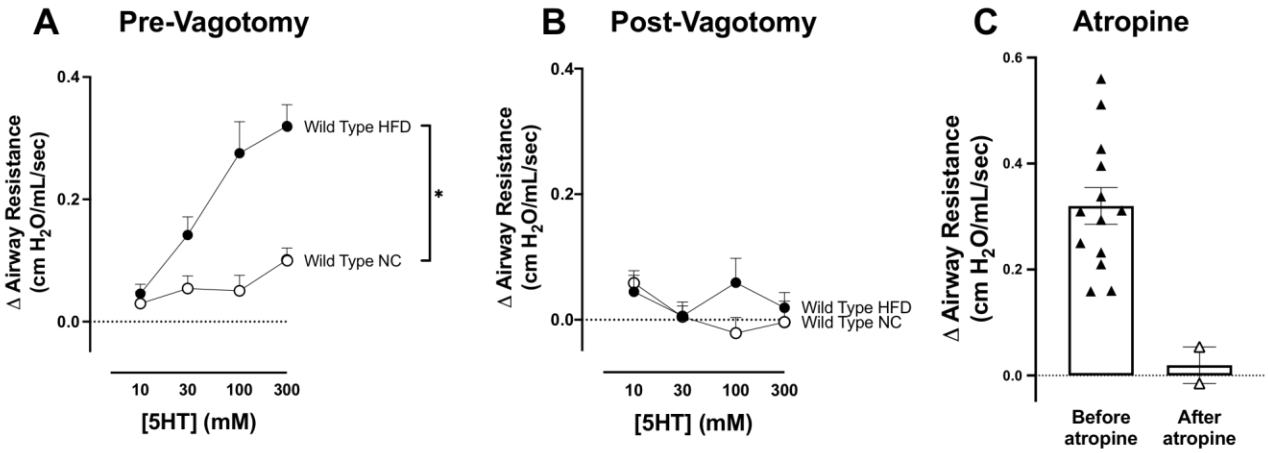

Bronchoconstriction induced by MCh

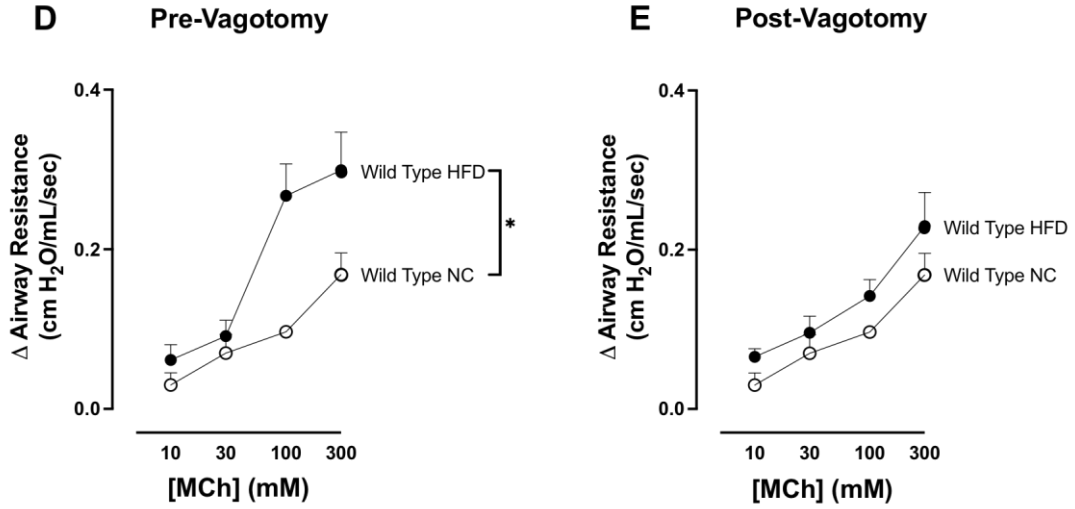

Figure 27. High-fat diet (HFD) fed mice had increased reflex bronchoconstriction. Change in airway resistance was measured in anesthetized and mechanically ventilated mice. (A) 5-HT induced dose-dependent bronchoconstriction that was significantly greater in mice fed high-fat diet (filled circles) than in mice fed normal chow mice (open circles). (D) Mice on a high-fat diet also had increased bronchoconstriction in response to inhaled methacholine (MCh) compared to normal chow mice. The increased bronchoconstriction in response to either 5-HT (B) or MCh (E) was blocked by vagotomy or atropine (C) in mice on a high-fat diet, indicating this increase was mediated by a reflex response. Each data point represents the mean ± SEM. ($n = 6\text{-}12$) $^*p < 0.05$.

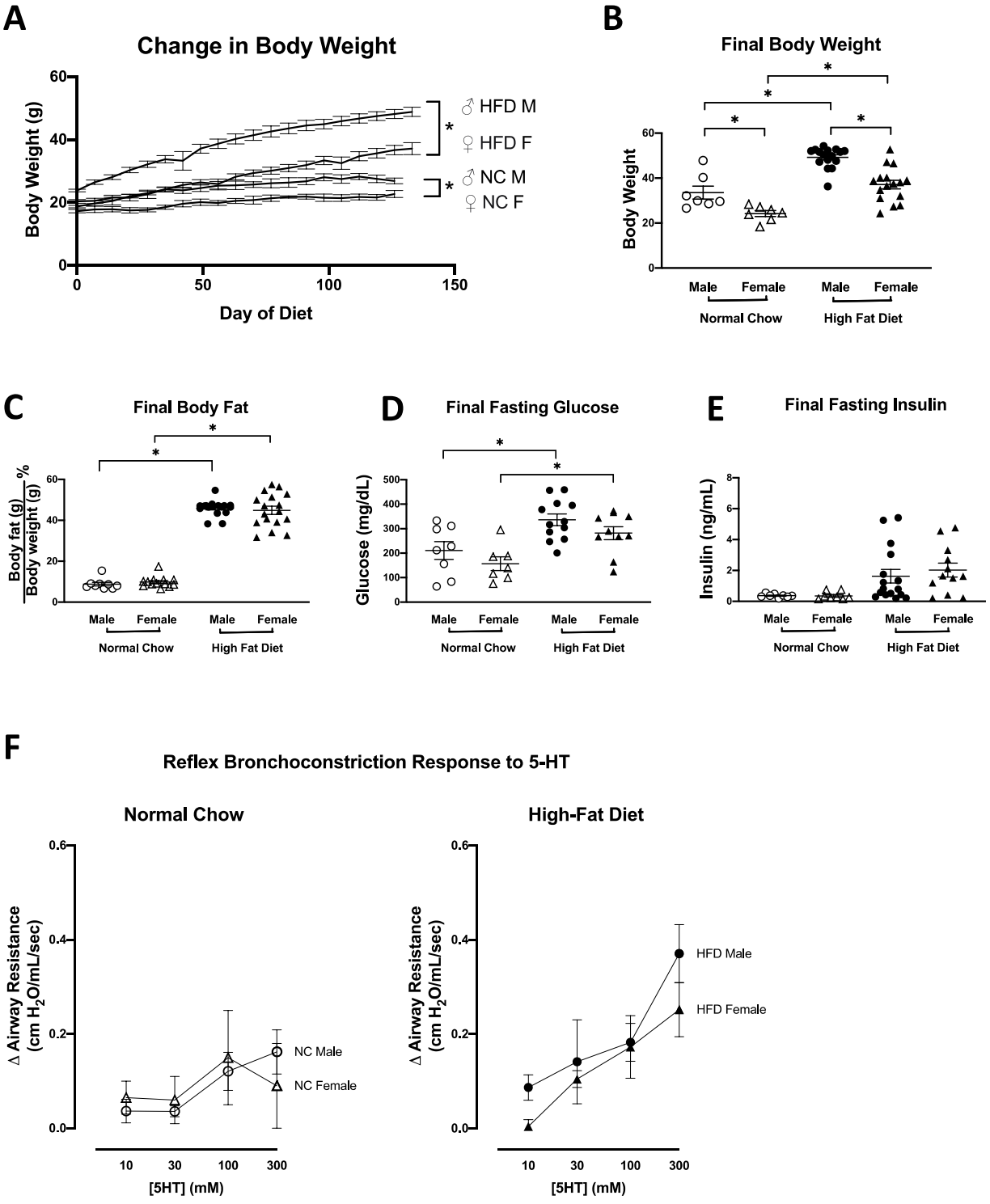
A
Change in Body Weight
Body Weight (g)
Day of Diet
♂ HFD M
♀ HFD F
♂ NC M
♀ NC F
B
Final Body Weight
Body Weight
Male
Female
Normal Chow
High Fat Diet
C
Final Body Fat
Body fat (g) / Body weight (g) %
D
Final Fasting Glucose
Glucose (mg/dL)
E
Final Fasting Insulin
Insulin (ng/mL)
F
Reflex Bronchoconstriction Response to 5-HT
Normal Chow
High-Fat Diet
Δ Airway Resistance (cm H2O/mL/sec)
[5HT] (mM)
NC Male
NC Female
HFD Male
HFD Female

Figure 28. Male and female mice had similar physiological responses to high-fat diet. (A) Male mice on a high-fat diet gained more weight than female mice on a high-fat diet; however, male mice also gained more weight than female mice on a normal chow diet. (B) Male mice weighed more than female mice, regardless of diet. Both male and female mice gained significant body weight (B) and body fat (C) on high-fat diet. Male and female mice within each diet group had similar fasting glucose (D), fasting insulin (E), and reflex bronchoconstriction (F) in response to 5-HT.

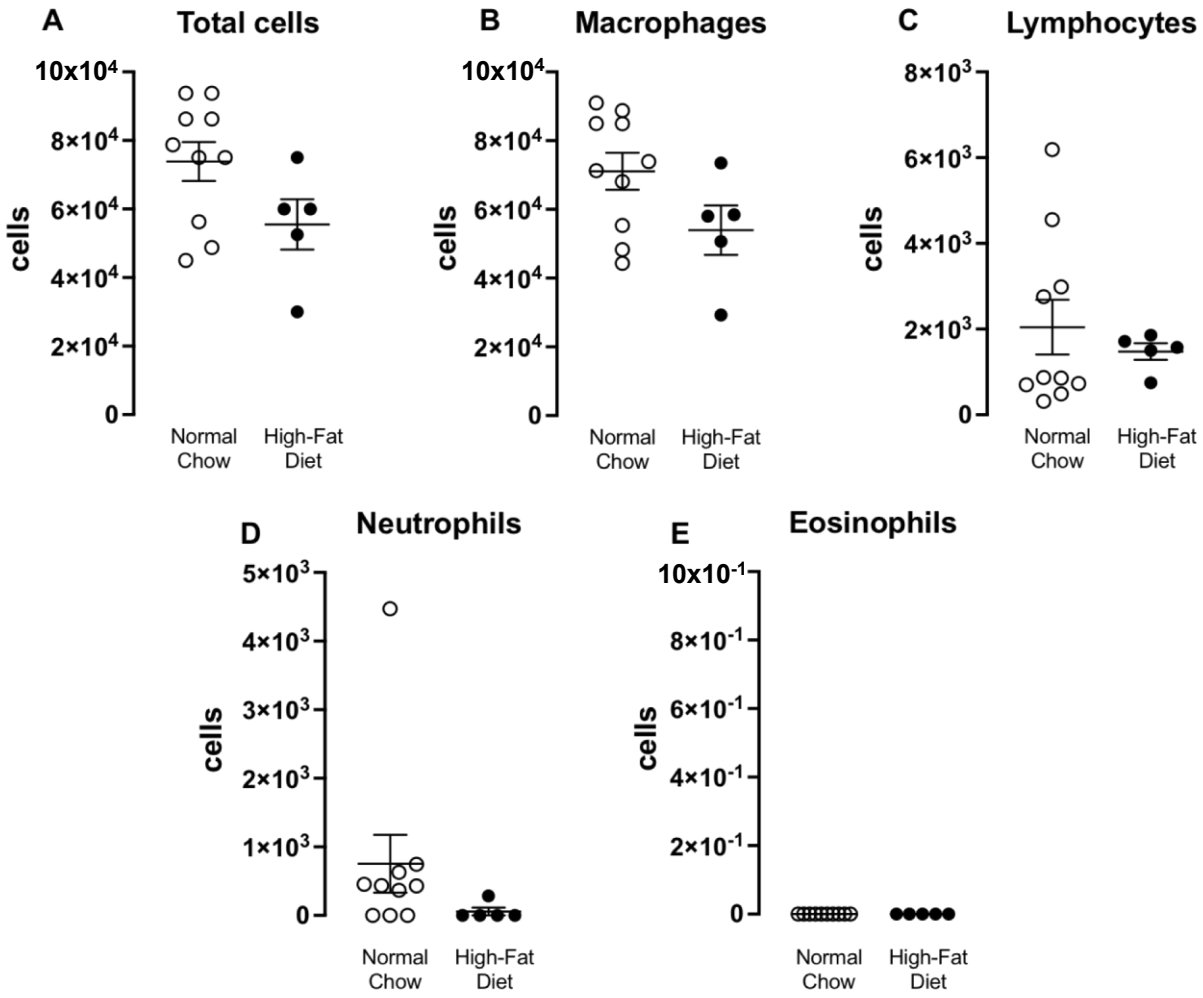

Figure 29. High-fat diet fed mice did not have airway inflammation. (A) Normal chow (open circles) and high-fat diet (filled circles) fed mice have similar total cell numbers in their bronchioalveolar lavage fluid. There was no diet-induced difference in macrophages (B), lymphocytes (C), neutrophils (D), or eosinophils (E). Each data point represents an individual animal; mean ± SEM are shown. (n = 5-10).

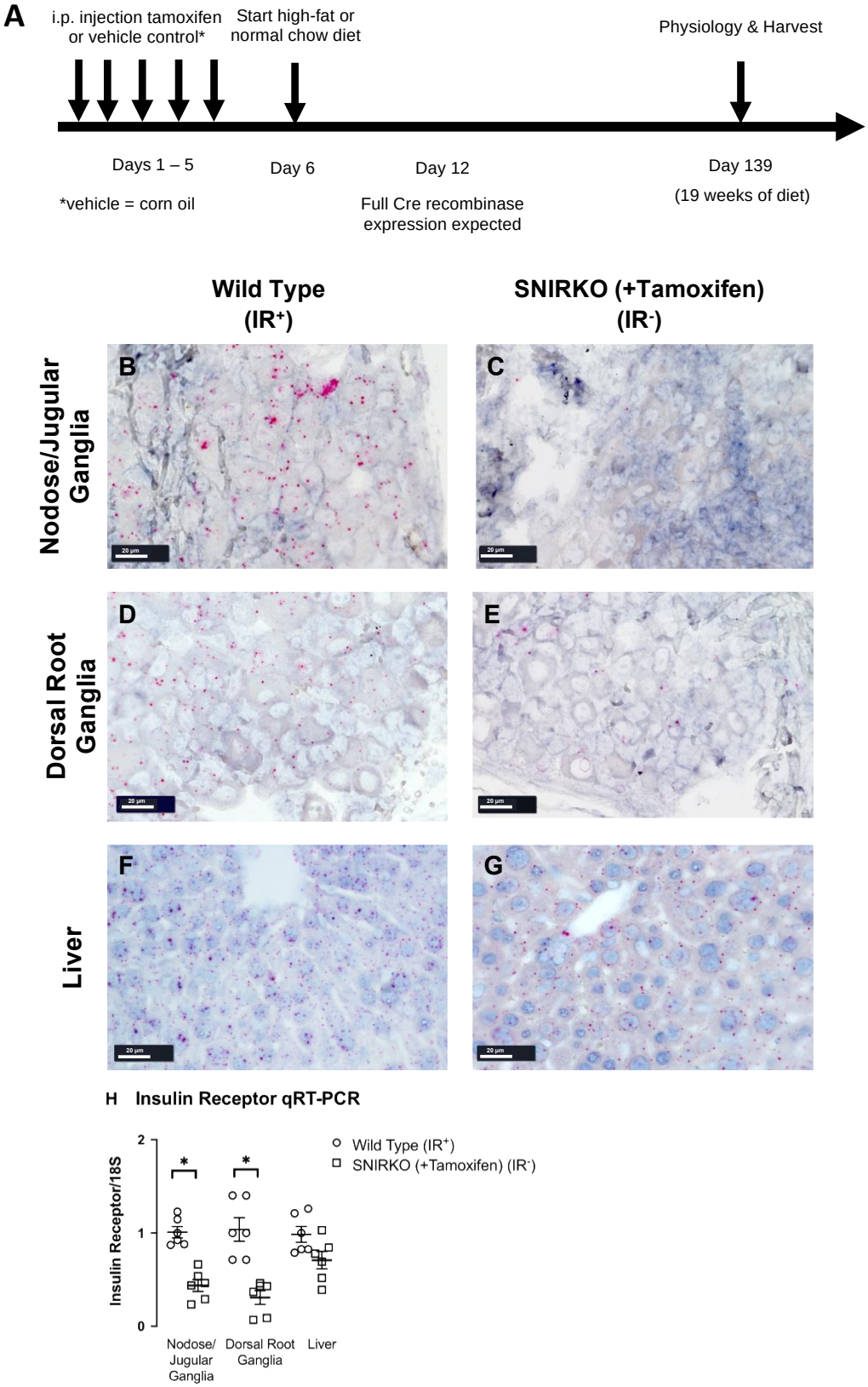
A
i.p. injection tamoxifen or vehicle control*
Start high-fat or normal chow diet
Physiology & Harvest
Days 1 – 5
Day 6
Day 12
Day 139
(19 weeks of diet)
*vehicle = corn oil
Full Cre recombinase expression expected
Wild Type (IR+)
SNIRKO (+Tamoxifen) (IR-)
Nodose/Jugular Ganglia
Dorsal Root Ganglia
Liver
B
C
D
E
F
G
H Insulin Receptor qRT-PCR
Insulin Receptor/18S
Wild Type (IR+)
SNIRKO (+Tamoxifen) (IR-)
Nodose/ Jugular Ganglia
Dorsal Root Ganglia
Liver

Figure 30. Creation and characterization of sensory neuron insulin receptor knockout (SNIRKO) mice. (A) Male and female SNIRKO mice were treated with 5 consecutive days of i.p. tamoxifen (20 mg/ml) or corn oil (vehicle control) to induce Cre recombinase activity and delete the insulin receptors on sensory neurons. On day 6 they were started on either a high-fat diet or normal chow diet for 19 weeks. Full Cre recombinase expression in SNIRKO mice was expected by day 12. (B-G) Representative images of insulin receptor mRNA expression shown in by Fast Red staining (pink dots) in wild type mice with intact insulin receptors (IR^+) and SNIRKO mice with selectively deleted insulin receptors (IR^-). Tamoxifen treated SNIRKO mice (IR^-) had decreased insulin receptor mRNA detected in the dorsal root ganglia (C) and nodose and jugular ganglia (E) compared to mice with intact insulin receptors (B,D). (F, G) Liver of both mice groups had similar insulin receptor mRNA expression. (H) The relative changes in the amount of mRNA in sensory neurons and liver cells were measured by qRT-PCR. Each data point represents an individual animal; mean ± SEM are shown. (n = 10-15) *$p < 0.05$.

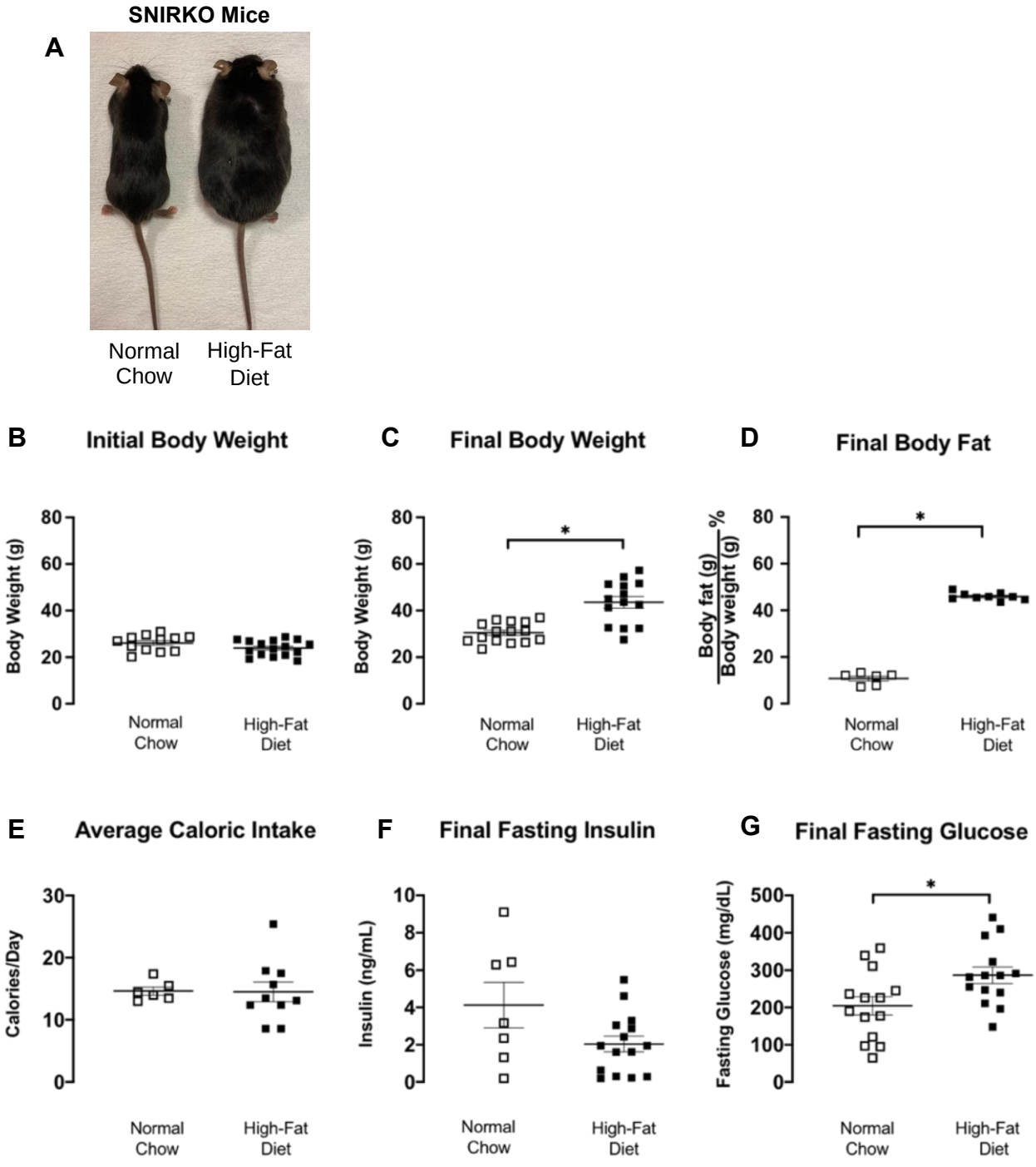
SNIRKO Mice
A
Normal Chow
High-Fat Diet
B
Initial Body Weight
Body Weight (g)
0
20
40
60
80
Normal Chow
High-Fat Diet
C
Final Body Weight
Body Weight (g)
0
20
40
60
80
*
Normal Chow
High-Fat Diet
D
Final Body Fat
Body fat (g) / Body weight (g) %
0
20
40
60
80
*
Normal Chow
High-Fat Diet
E
Average Caloric Intake
Calories/Day
0
10
20
30
Normal Chow
High-Fat Diet
F
Final Fasting Insulin
Insulin (ng/mL)
0
2
4
6
8
10
Normal Chow
High-Fat Diet
G
Final Fasting Glucose
Fasting Glucose (mg/dL)
0
100
200
300
400
500
*
Normal Chow
High-Fat Diet

Figure 31. Characterization of SNIRKO mice treated with tamoxifen on normal chow or high-fat diet. (A) SNIRKO mice had similar initial body weights before starting specific diets. (B) Representative pictures of normal chow and high-fat diet mice after 19 weeks of diet. SNIRKO mice had significantly increased body weight (C) and body fat (D) after a high-fat diet. (E) Mice consumed a similar number of calories per day regardless of diet. (F) Both diet groups had similar fasting insulin. (G) High-fat fed diet mice had slightly, but significantly higher glucose levels. Each data point represents an individual animal; mean ± SEM are shown. (n = 10-15) *$p < 0.05$.

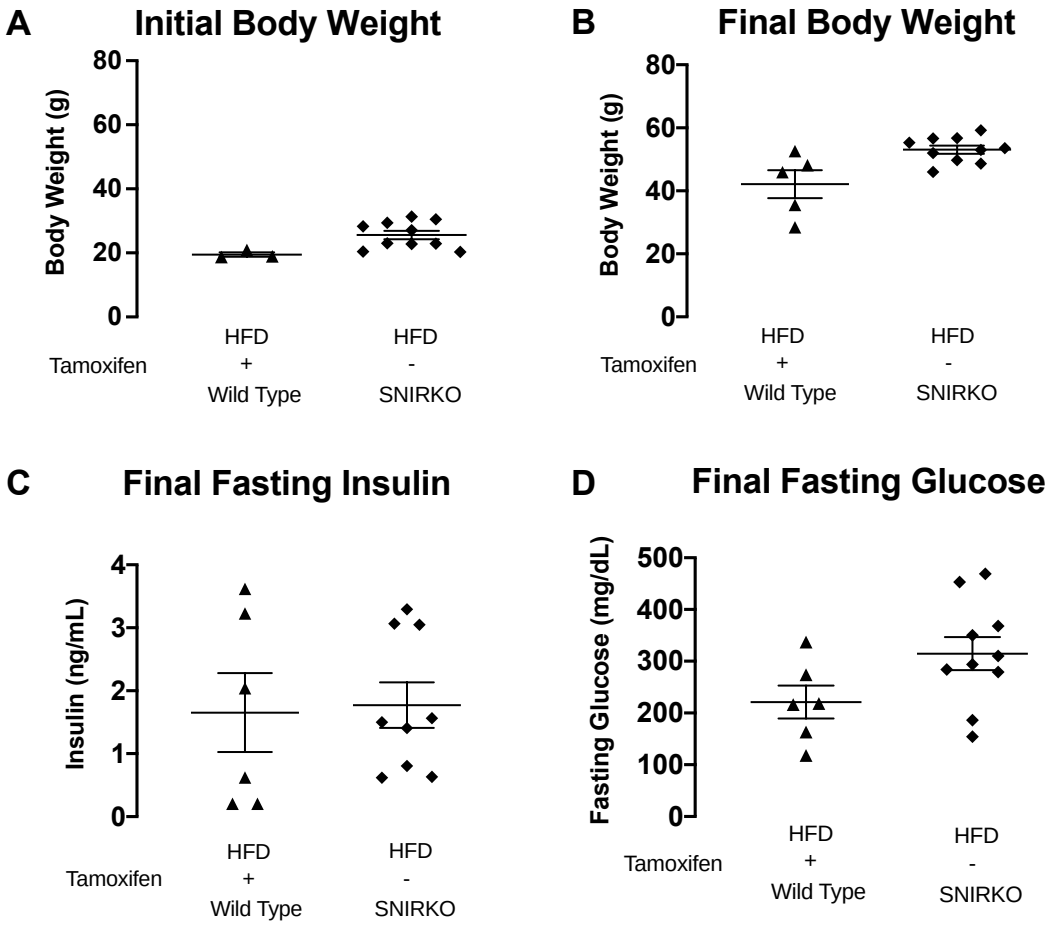

Figure 32. Characterization of high-fat diet wild type and SNIRKO control mice. Wild type mice treated with tamoxifen and SNIRKO mice without tamoxifen had similar initial body weights before starting the diet (A) and after diet completion (B). Both groups also had similar final fasting glucose (C) and insulin levels (D). Each data point represents an individual animal; mean ± SEM are shown. (n = 6-9).

Bronchoconstriction induced by 5-HT

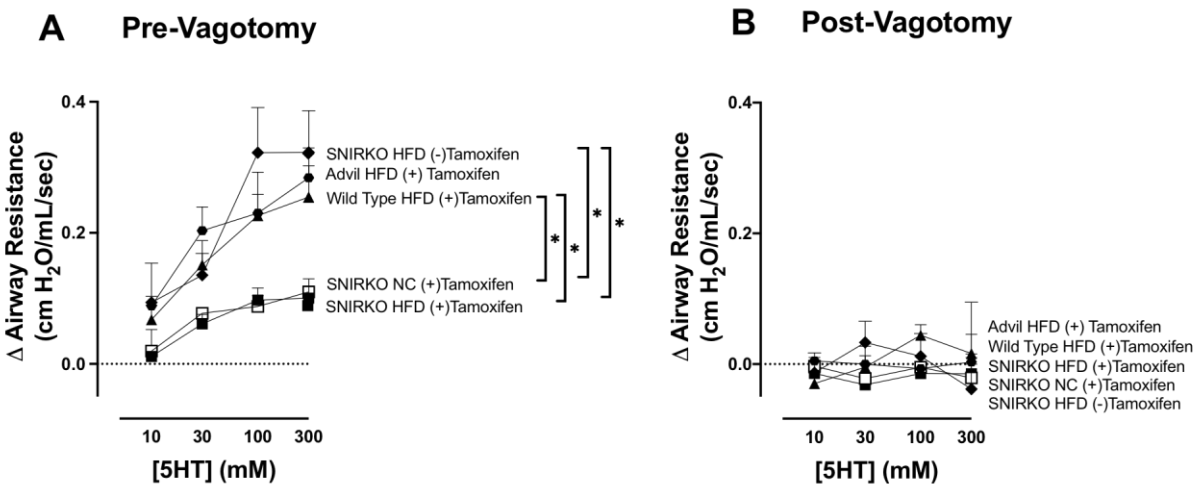

Bronchoconstriction induced by MCh

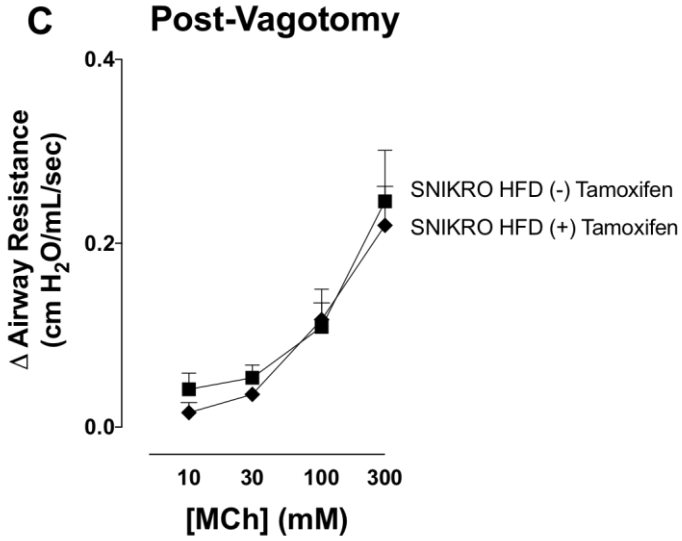

Figure 33. Specific knockout of insulin receptor in sensory neurons prevented potentiated reflex bronchoconstriction in mice on a high-fat diet. (A-D) Airway resistance was measured in anesthetized and mechanically ventilated sensory insulin receptor knockout (SNIRKO) mice. (A) 5-HT induced dose-dependent bronchoconstriction in high-fat diet fed SNIRKO mice without tamoxifen treatment (A; filled diamonds) and Advil mice with tamoxifen (A; filled hexagons). Knocking out insulin receptors on sensory nerves with tamoxifen significantly inhibited 5-HT induced bronchoconstriction resulting from a high fat diet (A; filled squares). Tamoxifen alone did not inhibit 5-HT induced bronchoconstriction in wild type mice on a high fat diet (A; filled triangles), or inhibit 5-HT induced bronchoconstriction in SNIRKO mice on a normal diet (A; open squares). (B) Response to 5-HT was eliminated by vagotomy in all mice. (C) Following vagotomy, bronchoconstriction in response to inhaled methacholine (MCh) was similar in SNIRKO mice with and without tamoxifen on a high-fat diet. Each data point represents the mean ± SEM. (n = 6-7) *$p < 0.05$.

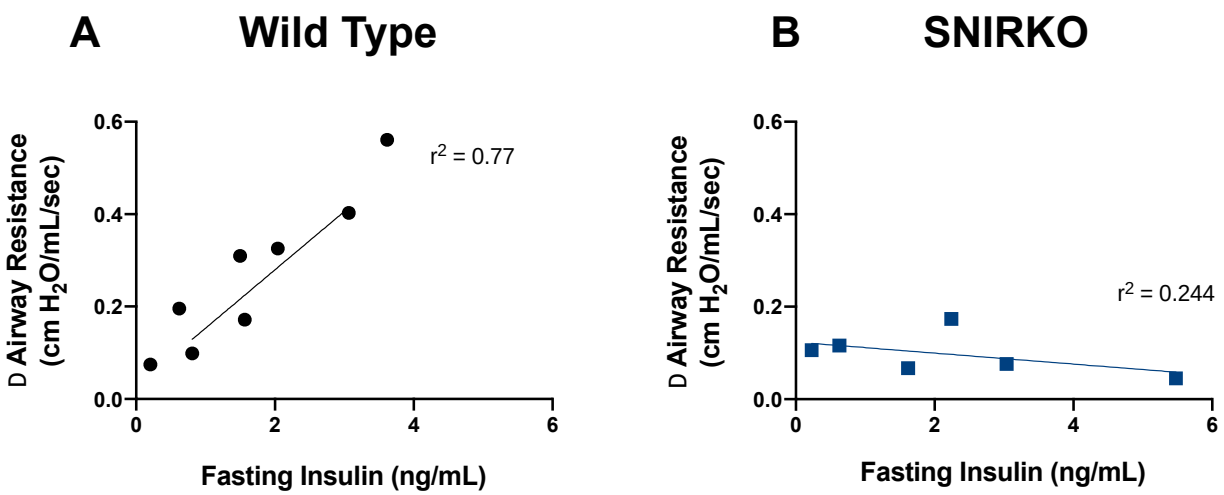

Figure 34. Change in airway resistance increased with fasting insulin in wild type but not SNIRKO mice. Airway resistance in response to 300 mM 5-HT directly correlates with fasting insulin in wild type (A) but not SNIRKO (B) mice. Each data point represents an individual animal. (n = 6-8).

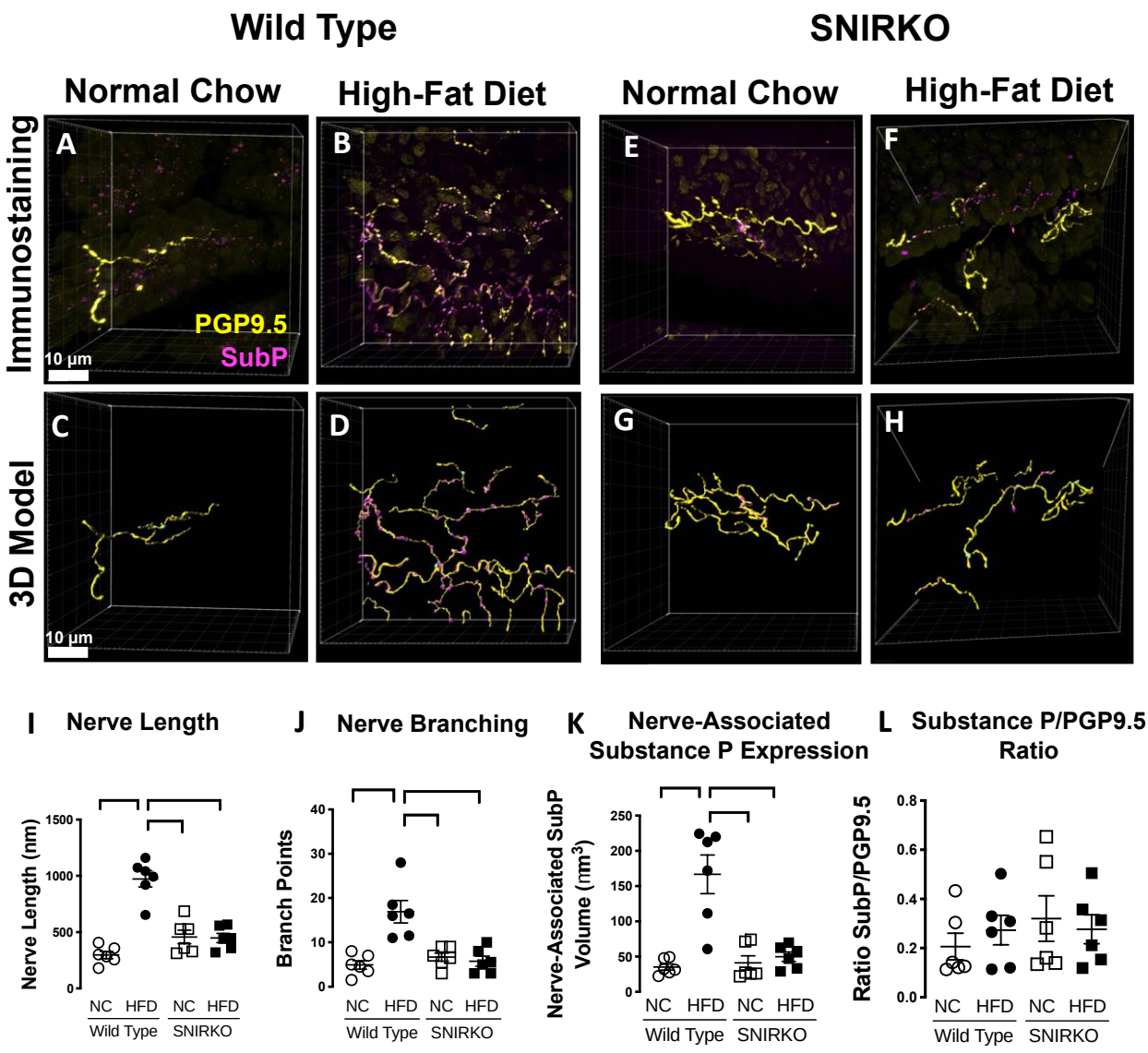

Figure 35. Airway epithelial sensory hyperinnervation induced by a high-fat diet was prevented by decreasing insulin receptors on sensory nerves. (A-B, E-F) Shown are representative images of whole mouse tracheas, labeled with antibody against pan-neuronal marker PGP9.5 (yellow) and neuropeptide substance P (magenta). Tracheas were optically cleared, imaged using laser scanning microscopy, and imaged as a z-stack. Imaris software was used to trace and identify epithelial nerves

(yellow), branch points (cyan), and substance p expression (magenta) in wild type mice fed normal chow (C) or high-fat diet (D) and SNIRKO mice fed normal chow (G) or high-fat diet (H). Wild type mice on a high-fat diet had increased airway epithelial nerve length (I) and number of nerve branch points (J). This increase in nerve length and branching was inhibited when insulin receptors were depleted from sensory nerves of SNIRKO mice. (K) High-fat diet mice had increased nerve-associated substance P expression, inhibited by selectively knocking out the insulin receptors. (L) All mice had a similar ratio of substance P to PGP. Each data point represents an individual animal; mean ± SEM are shown. (n = 6) *$p < 0.05$.

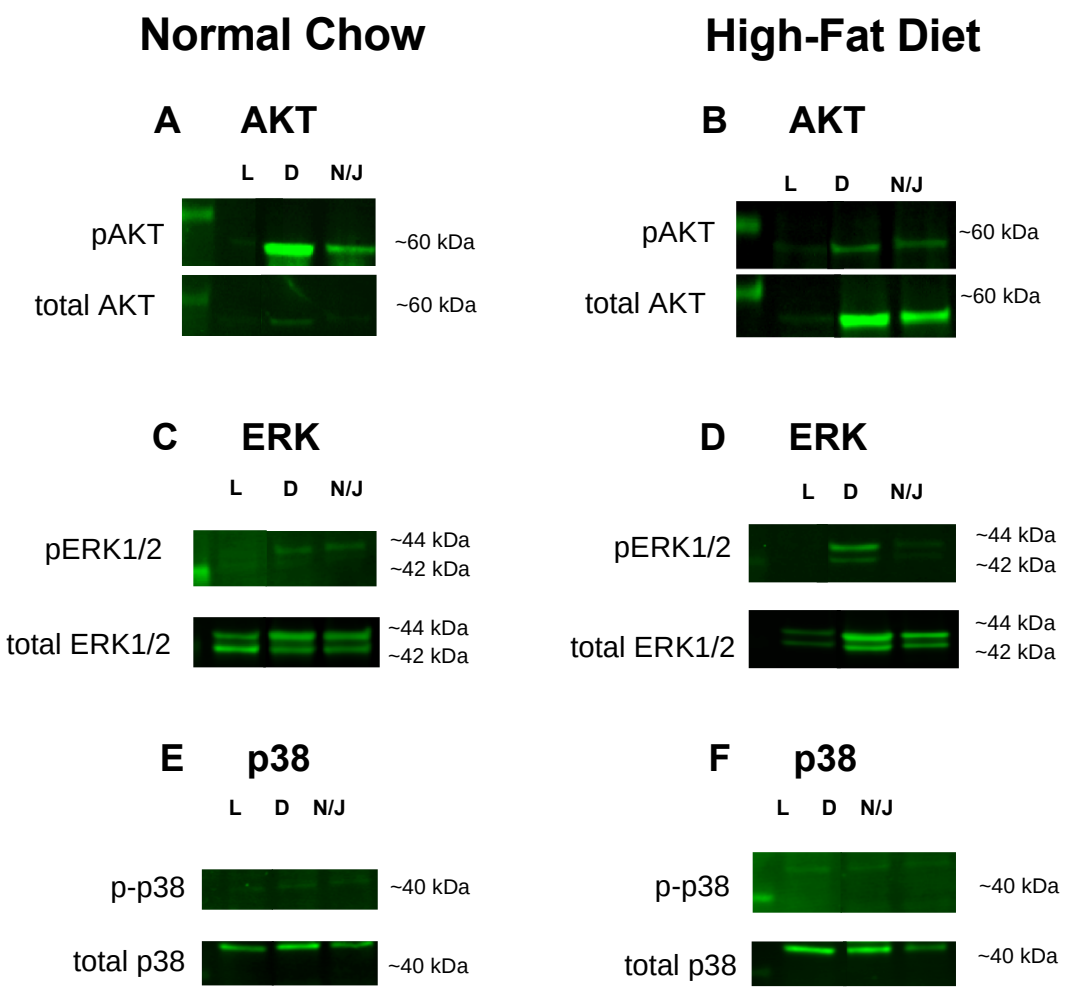

Figure 36. Representative Western blots of phosphorylated and total AKT, ERK1/2, and p-38 in normal chow and high-fat diet fed mice treated with insulin. Akt phosphorylation at serine 473 and total Akt levels in normal chow (A) and high-fat diet (B) fed mice. ERK phosphorylation at threonine 202/tyrosine 204 and total ERK1/2 levels in normal chow (C) and high-fat diet (D) fed mice. p38 phosphorylation at Threonine 180/Tyrosine 182 and total p38 in normal chow (E) and high-fat diet (F) fed mice. L, liver; D, dorsal root ganglia; N/J, nodose & jugular ganglia.

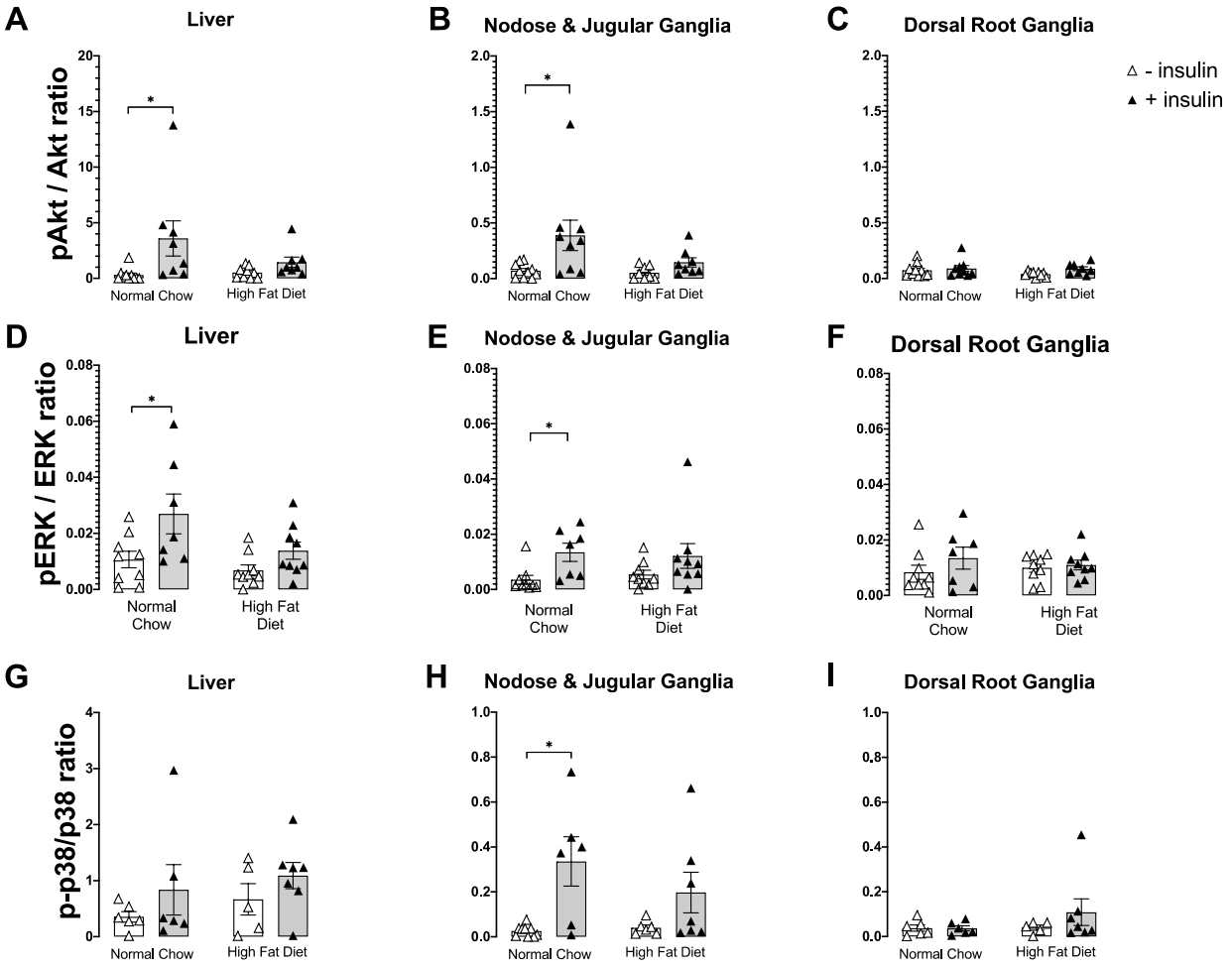

Figure 37. Insulin-stimulated signaling activation was tissue and pathway dependent. [2] Mice on a normal chow diet had significantly increased Akt phosphorylation with insulin stimulation (filled triangles) in the liver and nodose and jugular ganglia; however no significant increase in insulin-stimulated Akt phosphorylation was observed in high-fat diet fed mice. (C) Dorsal root ganglia were not responsive to insulin through the PI3K/Akt pathway, regardless of diet. (D-E) In high-fat diet animals, insulin-induced phosphorylation was not significantly increased in liver or nodose and jugular ganglia. (F) Insulin-induced ERK1/2 phosphorylation

was similar in DRGs of both normal chow and high-fat diet fed mice. Nodose and jugular ganglia of mice fed normal chow had significantly increased insulin-induced p38 phosphorylation. (G-I) There was no significant effect in either liver or DRG. Each data point represents an individual animal; mean ± SEM are shown. (n = 6-10) *$p < 0.05$.

E. Discussion

My data show that diet-induced obese mice have increased circulating insulin, airway epithelial sensory hyperinnervation, and hyperreactivity to both 5-HT and methacholine. Hyperreactivity was entirely reflex mediated, as when obese animals were vagotomized their response to both 5-HT and methacholine were the same as in lean animals. Hyperinnervation and hyperreactivity were prevented by selectively depleting insulin receptors on sensory nerves, despite high circulating insulin levels in these mice, demonstrating a direct effect of insulin on sensory nerves. Thus, hyperinsulinemia is a key factor in obesity-related airway hyperreactivity.

This study is the first to demonstrate the importance of airway sensory nerves in obesity-related airway hyperreactivity. Increased airway sensory innervation is present in patients with eosinophilic asthma and in mice that overexpress IL-5 in airway epithelium, causing airway eosinophilia[170]. While increased innervation and hyperreactivity in those previous studies were clearly related to inflammation, my current study shows that obesity-induced hyperinnervation and hyperreactivity occur in the absence of airway inflammation and eosinophilia. Although obesity and metabolic syndrome are associated with general systemic inflammation, four large clinical studies found no relationship between obesity-associated asthma and the cellular airway inflammation normally associated with allergic asthma[87-90]. Studies in diet-induced obese C57BL/6 mice also show increased bronchoconstriction does not rely on inflammatory cell infiltration[91]. Lack of airway inflammation in some obesity-related asthmatic patients may explain why corticosteroids are less effective in their treatment[92,93].

My current study clearly demonstrates a central role for hyperinsulinemia and for a direct effect of insulin on airway sensory nerves in obesity-induced hyperreactivity and hyperinnervation. Recent human birth cohort studies have shown that higher blood insulin in early childhood is associated with a later increased asthma risk and reduced lung function in adulthood independent of body mass index (BMI).[137] Furthermore, insulin binding to its receptor exerts trophic effects on neurons[122, 257, 258], which could explain the increased airway innervation in diet-induced obese mice. Sensory neurons express insulin receptors and, although their uptake of glucose is not insulin dependent, they respond to insulin signaling[259]. Insulin administration has also been shown to prevent sensory nerves atrophy in peripheral diabetic neuropathy[260] indicating an important role of insulin in neuron growth and maintenance.

Advillin expression has been found in most neural crest-cell derived neurons, including some sympathetic and parasympathetic neurons.[261] In fact, postganglionic parasympathetic cells in the trachea have been shown to express low levels of advillin[262]. Thus, in SNIRKO mice, the tamoxifen-induced Cre may be present in both sympathetic and parasympathetic neurons and deplete insulin receptors in these tissues. Because depleting insulin receptors in SNIRKO mice on a high-fat diet prevented increased reflex bronchoconstriction, this could mean insulin may act on nerves in the autonomic nervous system to cause airway hyperreactivity. Indeed, insulin also inhibits the function of neuronal M_2 muscarinic receptors on parasympathetic nerves in obese rats, leading to increased acetylcholine release and increased bronchoconstriction in response to vagal nerve stimulation[138]. Combined with the data

here, I have shown that insulin affects both the afferent and efferent pathways of the neural reflex, both causing airway hyperreactivity, and potentially having physiological consequences leading to obesity-related asthma.

Airway reflex hyperreactivity is determined by airway nerve function as well as airway smooth muscle contraction in animals with intact vagus nerves. In vagotomized animals, however, the inhaled methacholine-induced bronchoconstriction is mediated entirely by M_3 muscarinic receptors on smooth muscle. Inhaled methacholine acts both as a direct agonist of M_3 muscarinic receptors on airway smooth muscle and through activation of airway sensory nerves via a reflex mechanism[254]. While the response to methacholine is potentiated in obese animals, the normalization of this response after vagotomy shows that it is the reflex component that is increased, while the direct smooth muscle response is normal. This is consistent with other models of obesity-related airway hyperreactivity[138, 263]. My data also demonstrate that the direct smooth muscle response to inhaled methacholine is not altered by selectively depleting the insulin receptor on sensory nerves. Therefore, the normal airway response to 5-HT seen in these mice is not due to a reduction in the contractile response of airway smooth muscle to muscarinic receptor agonists.

Reflex bronchoconstriction in diet-induced obese mice could also be potentiated by increased airway epithelial nerve sensitivity. Increased airway epithelial nerve sensitivity is associated with increased expression of substance P, which has been shown in inflammatory and pain models[264, 265]. The number and length of substance P immunoreactive nerves are increased in asthmatic patients[170]. My data show that

substance P positive nerves had increased length and branching in hyperinsulinemic obese mice, which is consistent with previous reports that note substance P-expressing sensory neurons are one of the major subpopulations exhibiting enhanced insulin-induced neurite outgrowth[266,267]. My data indicate that increases in substance P were due to overall increased sensory innervation of the airway.

Activity of the insulin pathway is tissue dependent. Brain and muscle tissue have been shown to retain insulin sensitivity even after adipose and other peripheral tissues become insulin resistant[268,269]. Thus, airway nerves may remain responsive to insulin after other metabolically-sensitive tissues, such as the liver, have become insulin resistant in diet-induced obese mice. One explanation for increased airway innervation in individuals with obesity and insulin resistance is an imbalance in the PI3K/Akt and MAPK signaling pathways. Normal insulin signaling occurs through two major pathways, phosphoinositide-3 kinase (PI3K)/Akt and Ras/mitogen-activated protein kinase (MAPK) pathways[270]. In insulin resistance, the PI3K pathway is impaired, while the MAPK pathway continues to respond to insulin[271, 272]. The MAPK cascade, including extracellular signal-regulated kinases-1 and -2 (ERK1 and ERK2) and p38, has an important role in cell growth, survival, and differentiation. ERKs are activated in response to growth factors, including insulin and nerve growth factor (NGF)[273], to induce cell growth and regulate synaptic and structural plasticity in neurons[130, 274]. The MAPK-ERK cascade leads to p38 MAP kinase activation. p38 MAPKs are stress-activated kinases that have been implicated in both inflammation[275, 276] as well as neuronal plasticity[277-279]. Therefore, excessive insulin leading to aberrant ERK and p38 activation may contribute to neuronal remodeling in insulin resistant obese mice and increase

sensory innervation of the airways. Furthermore, increased systemic inflammation has been shown to elevate basal phosphorylation levels of p38 in adipocytes of type 2 diabetics with insulin resistance[280]. Increased basal phosphorylation of p38 in high-fat diet mice may explain why stimulating p38 phosphorylation with insulin in obese mice trended toward, but was not, significant.

Here I demonstrate an important role for insulin in altering airway sensory innervation leading to obesity-related airway hyperreactivity. Obese mice have increased nerve-mediated reflex bronchoconstriction and airway sensory nerve hyperinnervation via activation of insulin receptors on sensory nerves. When insulin receptors are selectively depleted from sensory nerves, reflex bronchoconstriction and airway innervation is normalized. These findings underscore the previously undefined role insulin plays in mediating obesity-related asthma. Insulin, or insulin receptors, may be considered as pharmacological targets for obesity-mediated asthma. Reducing insulin by using anti-diabetic drugs may be the key to improving asthma symptoms and control in individuals with obesity-related asthma.

Chapter 5. Increased Airway Epithelial Sensory Innervation and Reflex Bronchoconstriction in Adult Offspring of Obese Mothers

A. Abstract

Maternal obesity increases the risk of asthma in offspring. The mechanisms behind why children born to obese mothers are prone to developing asthma, however, remain elusive. Dr. Alina Maloyan's lab developed a mouse model of diet-induced maternal obesity. Despite being fed a regular diet (RD), adult offspring of high-fat diet (HFD)-fed mothers showed increased adiposity, hyperinsulinemia and insulin resistance, similar to the cardio-metabolic abnormalities seen in humans. Airway bronchoconstriction, induced by inhaled 5-HT, was significantly increased in male and female offspring of HFD-fed compared to RD-fed mothers. Increased bronchoconstriction was blocked by vagotomy, suggesting that airway nerves mediate this reflex hyperresponsiveness. Here I test if offspring of HFD-fed mothers have differences in their airway nerve structure compared to RD-fed offspring. I demonstrate that the offspring of HFD- fed mothers have increased nerve length, nerve branching, and expression of neuronal substance P, in the airway epithelium compared with offspring of RD-fed mothers. These results demonstrate that intrauterine exposure to maternal obesity increases airway sensory innervation in offspring.

Maternal obesity mouse model was developed and supplied by the Alina Maloyan lab.

B. Introduction

According to the World Health Organization, worldwide obesity has nearly tripled since 1975, with over 650 million adults or about 13% of the adult population being classified as obese as recently as 2016[281]. Consequently, the number of women of reproductive age classified as overweight or obese has increased; as many as 1 in 5 women are obese during pregnancy. Of particular concern is that the effects of maternal obesity do not simply target one generation; the increased nutrient abundance experienced by the fetus of an over nourished mother is the basis of the intergenerational cycle of obesity and affects the overall health of the next generation. The developmental origins of health and disease (DOHaD) hypothesis has demonstrated that the health of offspring is significantly impacted by pre- and perinatal health of their mothers[157]. Epidemiological studies have documented the offspring of overweight and obese mothers are at an increased risk of developing respiratory complications such as wheezing and asthma[158-161]. While several hypotheses have been proposed to explain this association, the exact mechanisms by which maternal obesity increases asthma risk in offspring remain unclear. With recent statistics showing there are 38.9 million overweight and obese (body mass index (BMI) $\geq$ 25) pregnant women and 14.6 million obese (BMI $\geq$ 30) pregnant women globally[282], this is an area that requires immediate and thorough investigation.

Increased neuronal reflex bronchoconstriction is a critical component of the pathophysiological mechanism of asthma. Sensory nerves are densely distributed in the airway, and detect stimuli, relay information to the central nervous system, and then stimulate parasympathetic efferent nerves to induce reflex bronchoconstriction.

Parasympathetic nerves regulate airway tone and induce bronchoconstriction by releasing acetylcholine, which activates M_3 muscarinic receptors on airway smooth muscle to stimulate contraction[283]. Acetylcholine release is normally limited by inhibitory M_2 muscarinic receptors located on parasympathetic nerves[283]. This sensory and parasympathetic nerve-mediated reflex bronchoconstriction occurs in response to a variety of stimuli including methacholine [254], histamine [284], cold air [285], exercise [286] and allergens [287], and is increased in patients with asthma [188, 288, 289]. Airway nerve-mediated hyperresponsiveness has been shown in every tested animal model of asthma, including antigen challenge[283], viral infection, and exposure to ozone or insulin[190]. Importantly, this reflex is increased in patients with asthma[288, 289]. Since the airway nerve-mediated reflex bronchoconstriction can be induced by activation of sensory afferent nerves or parasympathetic efferent nerves, changes in either the sensory afferent limb or parasympathetic efferent limb of this reflex pathway can inhibit or exacerbate bronchoconstriction. Thus, in humans, using anticholinergic treatment to reduce parasympathetic nerves induced bronchoconstriction has been recommended as an optimization step for patients with severe asthma[288, 290]. Furthermore, increased sensory innervation correlates with disease severity in patients with asthma[170].

Neuronal dysfunction is an important mechanism through which obesity-related asthma develops. Hyperinsulinemia in obese rats reduces the function of inhibitory M_2 muscarinic receptors on airway parasympathetic nerves, increasing acetylcholine release and potentiating vagally-induced bronchoconstriction[190]. Reducing circulating insulin levels inhibits vagally-mediated hyperresponsiveness in obese animals. Furthermore, insulin has neurotrophic effects[291-293], and nerve growth and increased

sensory innervation correlates with disease severity in patients with asthma[170]. Since diets rich in saturated fat are linked to obesity and metabolic disorder, which can result in increased insulin secretion from the offspring of obese mothers [294, 295], we created a murine model to investigate the effect of maternal high-fat diet (HFD) on adult offspring airway hyperreactivity (AHR), a key feature of asthma.

Results from Dr. Maloyan's lab show 16-week-old male offspring mice of mothers on a HFD (Off-HFD) had significantly increased body weight when compared to offspring of mothers on a regular diet (Off-RD) (Figure 38A). Offspring of mothers on a HFD had a higher percentage of body fat, and a reduced lean mass compared to offspring of mothers on a RD (Figure 38B-C). Additionally, offspring of mothers on a HFD were hyperinsulinemic and displayed increased insulin resistance measured by Homeostatic Model Assessment for Insulin Resistance (HOMA-IR) when compared to offspring of mother on a RD (Figure 38E-F). Both male and female Off-HFD mice had significantly increased airway response to inhaled 5-HT compared with the Off-RD controls (Figure 38G). Because no sex differences were observed in airway resistance, the data from both male and female offspring were combined in Figure 38G-H. Airway hyperreactivity was blocked by vagotomy, indicating that this was an airway nerve-mediated reflex hyperreactivity (Figure 38H). Given these finding, in this chapter, I tested whether

Figure 38. Offspring of obese mothers had increased insulin and reflex bronchoconstriction. Offspring of mothers on a high-fat diet (Off-HFD) had increased body weight (A), body fat percentage (B), and reduced lean mass (C) compare to offspring of mothers on a regular diet (Off-RD). (D) Fasting glucose was not significantly different among groups, but fasting insulin (E) and HOMA-IR (F) were both significantly increased in offspring of mothers on a HFD vs RD. (G) Inhaled 5-HT induced stronger bronchoconstriction and significantly increased airway resistance in offspring of mothers on a HFD. (H) The increased airway response was completely blocked by vagotomy, demonstrating that airway nerves are responsible for the reflex bronchoconstriction. Data from males and females were pooled in reflex bronchoconstriction experiments. Each data point represents an individual animal; mean ± SEM are shown (n = 9-13). *$p < 0.05$ vs. Off-RD; #, $p<0.05$ males vs. females within the same experimental group. *Data generated from the Maloyan (A-F) and Nie labs.*

B. Specific Methods

Animals

All mouse studies were conducted using wild type FVB/NJ mice that were housed in sterile conditions and have ad libitum access to food and water. Mice were kept on a nocturnal 12-hour light cycle. To model maternal obesity in mice, wild type females mice were randomly divided into a regular diet (RD, 17% kcal from fat) fed group and a high fat diet (HFD, 45% kcal from fat) fed groups starting at six weeks of age and continuing for eight weeks (Figure 39). After eight weeks of dietary intervention, all female mice were bred with RD-fed male wild type mice. The breeding couples were fed according to the maternal diet. Offspring were weaned at three-weeks old and were fed only a RD thereafter. All animal studies were carried out in accordance with a protocol approved by the Institutional Animal Care and Use Committee at Oregon Health and Science University.

Tissue Optical Clearing and Imaging and Quantification of Airway Nerves

Sixteen-week-old F1 male and female offspring mice were perfused with phosphate buffered saline (PBS) and airways were excised. Tracheas were left at 4°C in Zamboni fixative (Newcomer Supply) overnight. Tracheas were blocked overnight with 4% normal goat serum, 1% Triton X-100, and 5% powdered milk, and then incubated with antibodies to pan-neuronal marker protein gene product 9.5 (PGP9.5, rabbit IgG, 1:200; Amsbio) and substance P (rat IgG_{2A}, 1:500; BD Pharmigen) on a shaker at 4°C overnight. Tissues were washed and incubated overnight in secondary antibodies: Alexa goat anti-rabbit 647 (1:1,000; Invitrogen) and Alexa goat anti-rat 555 (1:1,000;

Invitrogen) and counterstained using the nuclear stain 4′6-diamidino-2-phenylindole, dilactate (DAPI, Molecular Probes). Tracheas were then optically cleared in N-methylacetamide/Histodenz (Ce3D) for 12 hours[205] and mounted in Ce3D on slides in 120 μm deep imaging wells (Invitrogen).

Images were acquired using a Zeiss LSM900 confocal microscope and 63×/1.4 oil PlanApo DIC M27 objective with a 0.19 mm working distance. Samples were illuminated with 401 nm, 553 nm, and 653 nm light, and images were acquired as z-stacks. Two to three randomized images were taken of each mouse trachea using DAPI to locate the epithelium. Airway nerves were modeled in 3D using Imaris semi-automatic filament tracing software (Imaris 9.7, Oxford Instruments). Users were blinded to study group at the time of nerve modeling. A 3D filament model was created around tracheal epithelial nerves to quantify nerve length and number of branch points. Neuronal substance P expression was quantified by creating a surface around the substance P-positive voxels and using Imaris software to colocalize the voxels in contact with PGP9.5-positive nerve axons. Two to three images were quantified per mouse trachea.

C. Results

Offspring from obese mothers had increased airway epithelial innervation and neuronal substance P expression

I measured the airway epithelial sensory innervation and substance P expression in whole-mounts of offspring's tracheas using immunostaining, tissue optical clearing, confocal microscopy, and digital three-dimensional (3D) reconstruction of airway nerves as previously described and detailed in chapter 5 specific methods[169, 296] (Figure 40A-J). The total length of airway epithelial nerves and the total number of nerve branch points were significantly increased in offspring of mothers on a high-fat diet compared to offspring of mothers on a regular-diet (Figure 40E-F), indicating that maternal high-fat diet caused hyperinnervation in airway epithelium of offspring. Substance P expression was detected on PGP9.5 positive nerve fibers. The total amount of neuronal substance P expression was significantly higher in offspring of mothers on a high-fat diet compare to that in offspring of mothers on a regular-diet (Figure 40K). Additionally, the maternal high-fat diet also caused an increase in the ratio of neuronal substance P expression to PGP9.5 expression, indicating that maternal high-fat diet not only caused hyperinnervation but also potentiated neuronal substance P expression (Figure 40L).

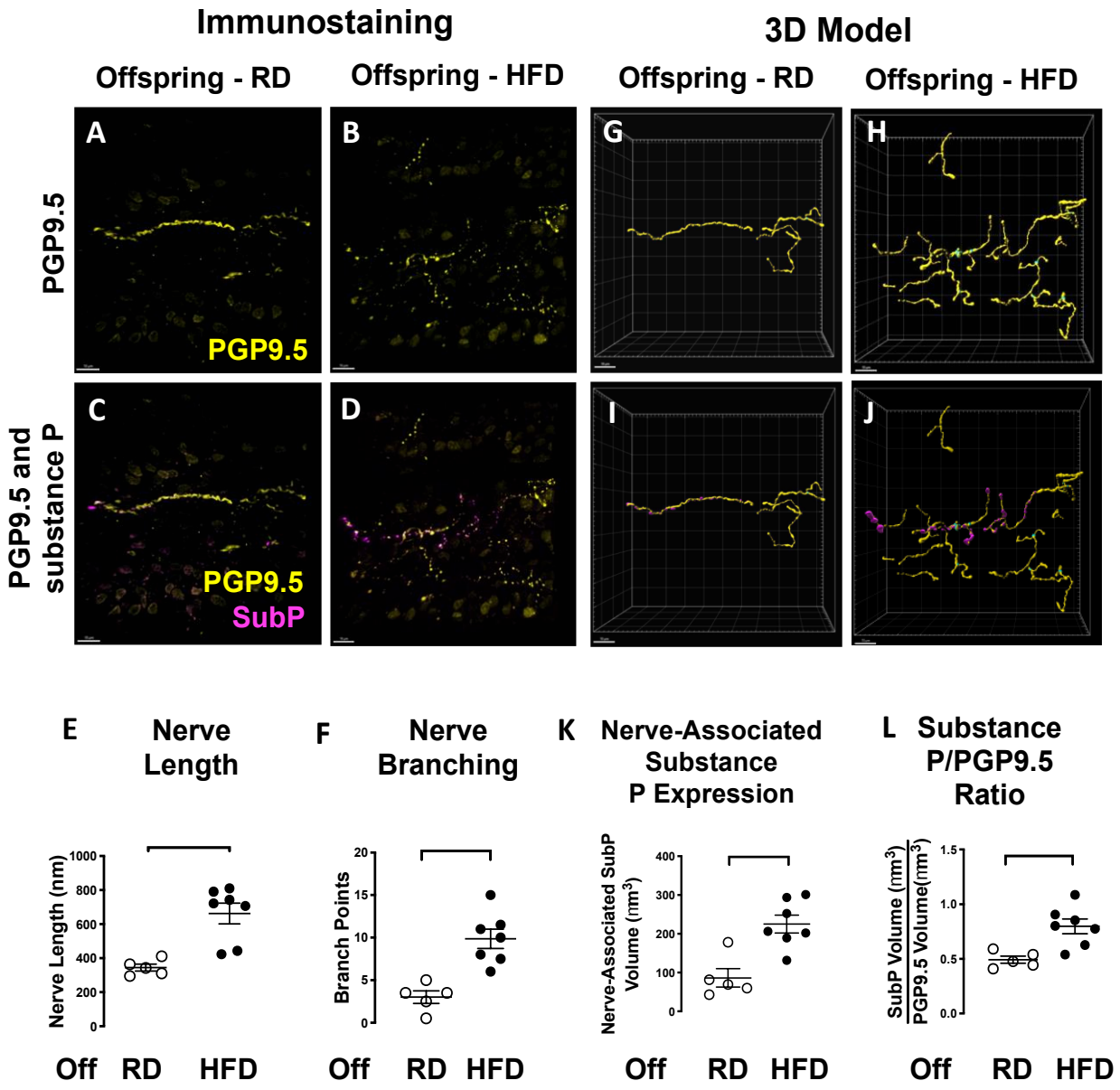

Figure 40. Airway sensory nerve length, branching, and substance P expression were increased in offspring of high-fat diet fed mothers. Whole tracheas were stained with antibodies against pan-neuronal marker PGP9.5 (yellow) and neuropeptide substance P (magenta), optically cleared, and imaged with a laser scanning confocal microscope. [2] Representative maximum intensity projection images of *z*-stacks with PGP9.5 and (C-D) both PGP9.5 and co-localized

substance P. Stained epithelial nerves shown in offspring from high-fat diet (B, D) and regular chow (A, C) mothers. Offspring mice of high-fat diet fed mothers (filled circles) had increased airway nerve length (E) and branching (cyan) (F) compared to offspring of mothers on a regular diet (empty circles). Imaris software was used to create digital 3D reconstructions of offspring from regular diet (G, I) and high-fat (H, J) diet fed mothers. Offspring mice of high-fat diet fed mothers (filled circles) had increased nerve-associated substance P expression (K) and ratio of substance P to PGP9.5 (L) compared to offspring of mothers on a regular diet (empty circles). Each data point represents an individual animal; mean ± SEM are shown. (n = 5-7) *p < 0.05.

D. Discussion

My data show that offspring of mothers on a high-fat diet have increased airway epithelial innervation, despite being fed a regular diet from birth. Intrauterine exposure to obesity induced by high-fat diet increased airway epithelial sensory hyperinnervation and enhanced expression of neural substance P in airway of offspring. These results reveal a possible mechanism by which maternal obesity increases the risk of asthma in offspring.

Because insulin has neurotrophic effects[293], the hyperinnervation of airway epithelial sensory nerves may be due to increased circulating insulin in the offspring of obese mothers. Hyperinsulinemia in obese rats reduces the function of inhibitory M_2 muscarinic receptors on airway parasympathetic nerves, which increases acetylcholine release and potentiates vagally-induced bronchoconstriction[190]. Furthermore, reducing circulating insulin levels inhibits vagally-mediated hyperresponsiveness in obese animals[248, 297]. All of these data suggest that inhibiting hyperinsulinemia could prevent airway nerve-mediated hyperresponsiveness. Since human cord blood hyperinsulinemia has been reported in infants born to obese mothers[298], maternal obesity may increase circulating insulin in offspring early in development. Therefore, nutritional interventions during pregnancy are necessary and important to prevent transgenerational programming of obesity and asthma. Furthermore, my novel finding that neural substance P expression was increased in offspring of diet-induced obese mothers suggest a therapeutic potential of targeting substance P or NK-1 receptors in maternal obesity related asthma.

Hyperinnervation of the airway epithelium may explain increased airway reflex bronchoconstriction in the offspring of high-fat mothers. Increased sensory innervation potentiates afferent nerve airway responses in mice, which indicates that changes in neural structure in the airways lead to increased reflex bronchoconstriction[299]. Airway hyperinnervation is also present in early postnatal monkeys exposed to ozone and house dust mite allergen[300] and in patients with asthma[170]. This airway nerve remodeling in human asthmatic patients was associated with worse lung function and increased sensitivity to environmental irritants. Similarly, mice with over-expression of interleukin-5 (IL-5) had increased nerve density and potentiated reflex bronchoconstriction.[170] Sensory innervation of the airways, therefore, is critical to normal airway function.

Increased reflex bronchoconstriction induced by inhaled 5-HT in offspring of mothers on a high-fat diet may be due to increased sensitivity of airway epithelial sensory nerves. Substance P is a neuropeptide known to increase sensory nerve sensitivity in inflammatory and pain models[264, 265]. Substance P expression on airway sensory nerves is also increased in patients with moderate persistent asthma[170]. Substance P causes bronchoconstriction both by directly binding to neurokinin-1 (NK1) receptors on airway smooth muscle[56] and also by indirectly potentiating nerve function through neurogenic inflammation. Sensory nerves mediate neurogenic inflammation via substance P binding to the NK-1 receptor[301]. Neurogenic inflammation is characterized by vasodilation, plasma extravasation, and changes in mucous secretion. This inflammation sensitizes airway nerves, thus increasing nerve excitability and activity[302].

Obesity during pregnancy is an important modifiable risk factor involved in the development of asthma even later into adulthood. Changes in nerve structure and function may contribute to this asthma phenotype. A healthy pregnancy weight and reducing hyperinsulinemia should be targeted throughout pregnancy in order to reduce the incidence of asthma in future generations. These insights deserve further investigation and verification in human studies.

Chapter 6. Summary and Conclusions

A. Summary

Obesity-related asthma is a major comorbidity exacerbated by the accelerating global obesity public health crisis. Despite the recent push to understand the mechanisms behind obesity-related asthma, we still have limited knowledge on the best ways to treat and prevent this disease. Hyperinsulinemia and insulin resistance have been identified as key risk factors for obesity-related asthma[136,235] and cause preganglionic M_2 muscarinic receptor dysfunction in obese rats[138]. There have been few investigations into mechanisms involving insulin and excessive nerve-mediated bronchoconstriction of the airways, a defining feature of asthma, in obesity-related asthma. Understanding the role of insulin and its effect on the development of obesity-related asthma is critical to targeting preventative interventions and treatments.

I hypothesized that hyperinsulinemia in obesity potentiates airway nerve-mediated reflex bronchoconstriction through structural and functional changes in parasympathetic and sensory nerves in the airways. In this dissertation, I test how hyperinsulinemia effects parasympathetic and sensory nerve-mediated bronchoconstriction. I used *in vivo* lung physiology measurements, novel quantitative imaging techniques, and an inducible knockout model to test the effects of high insulin levels on airway physiology and nerve growth, morphology, and specific neuropeptide expression in obese animals. My data demonstrates hyperinsulinemia, but not high-fat diet alone, potentiates parasympathetic nerve-induced bronchoconstriction. Insulin, but not IGF-1, increases agonist-induced smooth muscle contraction. Furthermore, sensory nerve hyperinnervation is present in the airway epithelium of obese mice with hyperinsulinemia and increased reflex bronchoconstriction.

My data demonstrates that male rats are prone to developing obesity and becoming hyperinsulinemic compared to female rats. Vagal nerve stimulated bronchoconstriction was potentiated only in hyperinsulinemic male rats, indicating high insulin levels lead to excessive parasympathetic nerve-mediated bronchoconstriction. Moreover, insulin, but not IGF-1, is involved in agonist-induced potentiation of airway smooth muscle. However, this effect has a limited impact on overall airway contraction *in vivo*. These data are important pieces in understanding the mechanisms behind obesity-related asthma and the potential therapeutic options available.

My data also show increased reflex bronchoconstriction in obese, hyperinsulinemic mice. These mice also had sensory nerve hyperinnervation in the airway epithelium. Selectively deleting the insulin receptor in sensory nerves prevented both reflex airway hyperreactivity and hyperinnervation. Mitogenic actions of insulin may underlie airway sensory nerve remodeling. Moreover, adult offspring mice born from obese mothers have airway hyperreactivity and airway epithelial sensory nerve hyperinnervation. Insulin signaling through its receptor clearly has an important role in airway nerve-mediated reflex bronchoconstriction in the setting of obesity. These experiments demonstrate the plasticity of airway nerves and how they change in response to environmental signals.

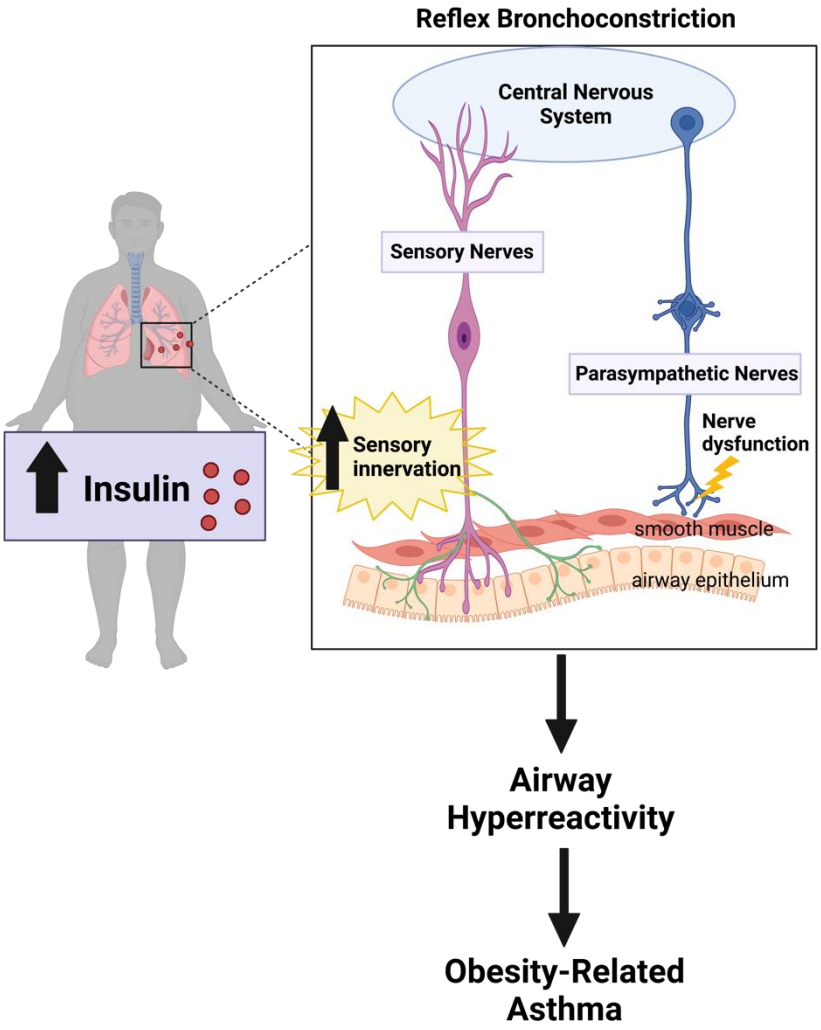

Figure 41. Summary of dissertation findings. I demonstrated that hyperinsulinemia in obesity potentiates parasympathetic nerve-mediated airway hyperreactivity and acts on airway smooth muscle (Chapter 3). Hyperinsulinemia increases airway hyperreactivity via nerve-mediated reflex bronchoconstriction. Further, both hyperinsulinemic diet-induced obese mice (Chapter 4) and hyperinsulinemic adult offspring of obese mothers (Chapter 5) had airway sensory nerve hyperinnervation. In summary, my data add to our understanding of the mechanisms driving airway hyperreactivity in obesity-related asthma. Image created with Biorender.com.

B. Future directions

a. Treatment of Obesity-Induced Asthma

Although I was able to show that selectively depleting insulin receptors on sensory nerves prevents obesity-induced reflex bronchoconstriction and epithelial hyperinnervation, we do not yet know if these changes are reversible. Using insulin-lowering drugs may be one way to test whether normal airway nerve structure and function can be restored. Metformin[214, 263], Pioglitazone[248], and the combination of Empagliflozin and Dulaglutide[303] appear to be potential candidates for restoring metabolic abnormalities in obesity-related asthma. Lifestyle modifications such as weight loss and physical activity in obese individuals may also important in asthma control and quality of life, but can be difficult to sustain and studies so far have been limited[304]. Furthermore, a recent study indicated that obese individuals with metabolic syndrome benefit less from bariatric surgery than those without metabolic syndrome[305]. Patients with metabolic syndrome did not have improvements in asthma control after the first year compared to those without. Likely, a multimodal approach that includes the combination of pharmacotherapy, weight loss, and exercise may be necessary to manage obesity-induced asthma.

b. Maternal Obesity Impacts on Offspring

I demonstrate that adult offspring mice of obese mothers with airway hyperreactivity have airway epithelial nerve hyperinnervation. Maternal obesity in pregnancy and increased maternal gestational weight is associated with an increased risk of asthma in their offspring[306, 307]. We do not know, however, when this airway nerve remodeling occurs. It is not known at this time whether changes in airway innervation are present at

birth or develop over time as offspring age. Ongoing experiments are underway investigating the time point at which changes in nerve morphology occurs. I will first be testing whether these neuronal changes are present at the time of birth.

c. Targeting Insulin Receptor Isoforms

My data suggest that insulin acts on sensory nerve remodeling through the mitogenic signaling pathway. The insulin receptor has two alternative splicing two isoforms at exon 11 into isoform A (IR-A) and isoform B (IR-B). IR-A is primarily involved in mitogenic actions, whereas IR-B plays a bigger role in metabolism and glucose regulation[114]. The predominant isoform present in neurons is IR-A[121], which may explain the propensity of growth in neurons during exposure to high insulin such as during obesity-induced insulin resistance. Dysregulation of the IR-A/IR-B ratio is also associated with insulin resistance, aging, diabetes, obesity, and increased cell proliferative leading to cancer[114, 121]. A high IR-A:IR-B ratio has been associated with insulin resistance of patients with myotonic dystrophy and possibly in patients with type 2 diabetes, although the evidence here is still discordant[308]. Future experiments could determine relative ratios of IR-A:IR-B and receptor subtype activation. Further delineating the role that insulin signaling has through each isoform will be helpful in creating targeted treatments for obesity-related asthma.

C. Conclusions

In summary, the data in this thesis show that high insulin levels increase airway nerve-mediated bronchoconstriction in obesity-related asthma by altering nerve function. The data also support my hypothesis that hyperinsulinemia increases airway epithelial

sensory innervation, which may lead to airway hyperreactivity. My hypothesis can also explain the high incidence of asthma in offspring of obese mothers. My data show these offspring have increased insulin and corresponding sensory nerve hyperinnervation as well as increased substance P expression. All together, these results suggest that preventing hyperinsulinemia can reduce airway hyperreactivity. Specifically targeting neuronal insulin receptors may lead to potential treatment options for individuals with obesity-related asthma. Continuing to investigate the mechanisms behind severe and poorly controlled obesity-related asthma will greatly impact this currently unmet clinical need.

References

1. Cao, D.-S., et al., Expression of transient receptor potential ankyrin 1 (TRPA1) and its role in insulin release from rat pancreatic beta cells. *PloS one*, 2012. 7(5): p. e38005-e38005.
2. Aun, M.V., et al., Animal models of asthma: utility and limitations. *J Asthma Allergy*, 2017. 10: p. 293-301.
3. Collaborators, G.D.a.I., Global burden of 369 diseases and injuries in 204 countries and territories, 1990-2019: a systematic analysis for the Global Burden of Disease Study 2019. *Lancet*, 2020. 396(10258): p. 1204-1222.
4. Wenzel, S.E., Asthma phenotypes: the evolution from clinical to molecular approaches. *Nature Medicine*, 2012. 18: p. 716.
5. Ilmarinen, P., et al., Cluster Analysis on Longitudinal Data of Patients with Adult-Onset Asthma. *The Journal of Allergy and Clinical Immunology: In Practice*, 2017. 5(4): p. 967-978.e3.
6. Szczeklik, A. and D.D. Stevenson, Aspirin-induced asthma: Advances in pathogenesis, diagnosis, and management. *Journal of Allergy and Clinical Immunology*, 2003. 111(5): p. 913-921.
7. Johnson, D. and L.M. Osborn, Cough Variant Asthma: A Review of the Clinical Literature. *Journal of Asthma*, 1991. 28(2): p. 85-90.
8. Tang, Q., et al., Evaluation of efficiency and safety of combined montelukast sodium and budesonide in children with cough variant asthma: A protocol for systematic review and meta-analysis. *Medicine (Baltimore)*, 2021. 100(25): p. e26416.

9. Holguin, F., et al., Obesity and asthma: an association modified by age of asthma onset. *J Allergy Clin Immunol*, 2011. 127(6): p. 1486-93.e2.
10. Anderson, G.P., Endotyping asthma: new insights into key pathogenic mechanisms in a complex, heterogeneous disease. *The Lancet*, 2008. 372(9643): p. 1107-1119.
11. Dixon, A.E. and M.E. Poynter, Mechanisms of Asthma in Obesity. Pleiotropic Aspects of Obesity Produce Distinct Asthma Phenotypes. *American Journal of Respiratory Cell and Molecular Biology*, 2016. 54(5): p. 601-608.
12. Agache, I., et al., Untangling asthma phenotypes and endotypes. *Allergy*, 2012. 67(7): p. 835-846.
13. Pillai, P., C.J. Corrigan, and S. Ying, Airway epithelium in atopic and nonatopic asthma: similarities and differences. *ISRN allergy*, 2011. 2011: p. 195846-195846.
14. O'Byrne, P.M. and M.D. Inman, Airway hyperresponsiveness. *Chest*, 2003. 123(3 Suppl): p. 411s-6s.
15. Hargreave, F.E., et al., The origin of airway hyperresponsiveness. *J Allergy Clin Immunol*, 1986. 78(5 Pt 1): p. 825-32.
16. Scott, G.D., *Sensory neuroplasticity in asthma*. 2012: Scholar Archive.
17. Bergeron, C., W. Al-Ramli, and Q. Hamid, Remodeling in Asthma. *Proceedings of the American Thoracic Society*, 2009. 6(3): p. 301-305.
18. National Heart, L., and Blood Institute (US), *National Asthma Education and Prevention Program, Third Expert Panel on the Diagnosis and Management of Asthma. Expert Panel Report 3: Guidelines for the Diagnosis and Management of Asthma.* 2007 Aug, Bethesda (MD).

19. Cloutier, M.M., et al., 2020 Focused Updates to the Asthma Management Guidelines: A Report from the National Asthma Education and Prevention Program Coordinating Committee Expert Panel Working Group. *Journal of Allergy and Clinical Immunology*, 2020. 146(6): p. 1217-1270.
20. Spaziano, G., et al., Exposure to Allergen Causes Changes in NTS Neural Activities after Intratracheal Capsaicin Application, in Endocannabinoid Levels and in the Glia Morphology of NTS. *BioMed Research International*, 2015. 2015: p. 980983.
21. Cloutier, M.M., et al., Managing Asthma in Adolescents and Adults: 2020 Asthma Guideline Update From the National Asthma Education and Prevention Program. *JAMA*, 2020. 324(22): p. 2301-2317.
22. Brusselle, G.G. and G.H. Koppelman, Biologic Therapies for Severe Asthma. *New England Journal of Medicine*, 2022. 386(2): p. 157-171.
23. Fahy, J.V., Type 2 inflammation in asthma — present in most, absent in many. *Nature Reviews Immunology*, 2015. 15(1): p. 57-65.
24. Ball M., H.M., Padalia D. *Anatomy, Airway*. 2021 Jan-; Available from: https://www.ncbi.nlm.nih.gov/books/NBK459258/.
25. Widdicombe, J.H. and J.J. Wine, Airway Gland Structure and Function. *Physiological Reviews*, 2015. 95(4): p. 1241-1319.
26. Sahin-Yilmaz, A. and R.M. Naclerio, Anatomy and Physiology of the Upper Airway. *Proceedings of the American Thoracic Society*, 2011. 8(1): p. 31-39.
27. Widdicombe, J.H., Early studies on the surface epithelium of mammalian airways. *Am J Physiol Lung Cell Mol Physiol*, 2019. 317(4): p. L486-l495.

28. Vieira Braga, F.A., et al., A cellular census of human lungs identifies novel cell states in health and in asthma. *Nat Med*, 2019. 25(7): p. 1153-1163.
29. Kuo, Christin S. and Mark A. Krasnow, Formation of a Neurosensory Organ by Epithelial Cell Slithering. *Cell*, 2015. 163(2): p. 394-405.
30. Brouns, I., et al., Neurochemical pattern of the complex innervation of neuroepithelial bodies in mouse lungs. *Histochem Cell Biol*, 2009. 131(1): p. 55-74.
31. Cutz, E., et al., Recent advances and contraversies on the role of pulmonary neuroepithelial bodies as airway sensors. *Seminars in Cell & Developmental Biology*, 2013. 24(1): p. 40-50.
32. Barkauskas, C.E., et al., Type 2 alveolar cells are stem cells in adult lung. *The Journal of Clinical Investigation*, 2013. 123(7): p. 3025-3036.
33. Wiebe, B.M. and H. Laursen, Human lung volume, alveolar surface area, and capillary length. *Microsc Res Tech*, 1995. 32(3): p. 255-62.
34. Butler, J.P. and A. Tsuda, Transport of gases between the environment and alveoli--theoretical foundations. *Comprehensive Physiology*, 2011. 1(3): p. 1301-1316.
35. Knudsen, L. and M. Ochs, The micromechanics of lung alveoli: structure and function of surfactant and tissue components. *Histochemistry and cell biology*, 2018. 150(6): p. 661-676.
36. Suresh, K. and L.A. Shimoda, Lung Circulation. *Comprehensive Physiology*, 2016. 6(2): p. 897-943.

37. Pan, H., et al., Comprehensive anatomic ontologies for lung development: A comparison of alveolar formation and maturation within mouse and human lung. *Journal of Biomedical Semantics*, 2019. 10(1): p. 18.
38. Irvin, C.G. and J.H. Bates, Measuring the lung function in the mouse: the challenge of size. *Respir Res*, 2003. 4(1): p. 4.
39. Gomes, R.F. and J.H. Bates, Geometric determinants of airway resistance in two isomorphic rodent species. *Respir Physiol Neurobiol*, 2002. 130(3): p. 317-25.
40. Canning, B.J., Reflex regulation of airway smooth muscle tone. *Journal of Applied Physiology*, 2006. 101(3): p. 971-985.
41. Canning, B.J. and D. Spina, Sensory nerves and airway irritability. *Handbook of experimental pharmacology*, 2009. 194(194): p. 139-183.
42. De Koninck, P., S. Carbonetto, and E. Cooper, NGF induces neonatal rat sensory neurons to extend dendrites in culture after removal of satellite cells. *J Neurosci*, 1993. 13(2): p. 577-85.
43. Kummer, W., et al., The sensory and sympathetic innervation of guinea-pig lung and trachea as studied by retrograde neuronal tracing and double-labelling immunohistochemistry. *Neuroscience*, 1992. 49(3): p. 715-37.
44. Mazzone, S.B. and B.J. Undem, Vagal Afferent Innervation of the Airways in Health and Disease. *Physiological reviews*, 2016. 96(3): p. 975-1024.
45. Coleridge, H.M. and J.C. Coleridge, Pulmonary reflexes: neural mechanisms of pulmonary defense. *Annu Rev Physiol*, 1994. 56: p. 69-91.
46. Mazzone, S.B. and B.J. Canning, Synergistic interactions between airway afferent nerve subtypes mediating reflex bronchospasm in guinea pigs. *American*

Journal of Physiology-Regulatory, Integrative and Comparative Physiology, 2002. 283(1): p. R86-R98.

47. Undem, B.J. and M.J. Carr, The role of nerves in asthma*. Current Allergy and Asthma Reports*, 2002. 2(2): p. 159.

48. Canning, B.J. and B.J. Undem, Evidence that distinct neural pathways mediate parasympathetic contractions and relaxations of guinea-pig trachealis*. J Physiol*, 1993. 471: p. 25-40.

49. Kummer, W., K.S. Lips, and U. Pfeil, The epithelial cholinergic system of the airways*. Histochemistry and cell biology*, 2008. 130(2): p. 219-234.

50. Nachmansohn, D. and A.L. Machado, THE FORMATION OF ACETYLCHOLINE. A NEW ENZYME: "CHOLINE ACETYLASE"*. Journal of Neurophysiology*, 1943. 6(5): p. 397-403.

51. Birks, R.I. and F.C. Macintosh, Acetylcholine metabolism at nerve-endings*. Br Med Bull*, 1957. 13(3): p. 157-61.

52. Barnard, E., The peripheral nervous system*. Plenum Press. New York*, 1974: p. 2001-224.

53. Colović, M.B., et al., Acetylcholinesterase inhibitors: pharmacology and toxicology*. Current neuropharmacology*, 2013. 11(3): p. 315-335.

54. Dey, R.D., et al., Origin and colocalization of CGRP- and SP-reactive nerves in cat airway epithelium*. J Appl Physiol (1985)*, 1990. 68(2): p. 770-8.

55. Hunter, D.D. and B.J. Undem, Identification and Substance P Content of Vagal Afferent Neurons Innervating the Epithelium of the Guinea Pig Trachea*. American Journal of Respiratory and Critical Care Medicine*, 1999. 159(6): p. 1943-1948.

56. Maghni, K., et al., Airway smooth muscle cells express functional neurokinin-1 receptors and the nerve-derived preprotachykinin-a gene: regulation by passive sensitization. *Am J Respir Cell Mol Biol*, 2003. 28(1): p. 103-10.

57. Wu, Z.X., B.E. Satterfield, and R.D. Dey, Substance P released from intrinsic airway neurons contributes to ozone-enhanced airway hyperresponsiveness in ferret trachea. *J Appl Physiol (1985)*, 2003. 95(2): p. 742-50.

58. Curran, D.R., M.T. Walsh, and R.W. Costello, Interactions between inflammatory cells and nerves. *Current Opinion in Pharmacology*, 2002. 2(3): p. 243-248.

59. Ramalho, R., et al., Tachykinin receptors antagonism for asthma: a systematic review. *BMC pulmonary medicine*, 2011. 11: p. 41-41.

60. Barnes, P.J., Neuropeptides and asthma. *Am Rev Respir Dis*, 1991. 143(3 Pt 2): p. S28-32.

61. Aoki-Nagase, T., et al., Attenuation of antigen-induced airway hyperresponsiveness in CGRP-deficient mice. *Am J Physiol Lung Cell Mol Physiol*, 2002. 283(5): p. L963-70.

62. Groneberg, D.A., J. Springer, and A. Fischer, Vasoactive intestinal polypeptide as mediator of asthma. *Pulm Pharmacol Ther*, 2001. 14(5): p. 391-401.

63. van der Velden, V.H. and A.R. Hulsmann, Autonomic innervation of human airways: structure, function, and pathophysiology in asthma. *Neuroimmunomodulation*, 1999. 6(3): p. 145-59.

64. Canning, B.J. and A. Fischer, Neural regulation of airway smooth muscle tone. *Respiration Physiology*, 2001. 125(1): p. 113-127.

65. Lammers, J.W., P.J. Barnes, and K.F. Chung, Nonadrenergic, noncholinergic airway inhibitory nerves. *Eur Respir J*, 1992. 5(2): p. 239-46.

66. Balentova, S., S. Conwell, and A.C. Myers, Neurotransmitters in parasympathetic ganglionic neurons and nerves in mouse lower airway smooth muscle. *Respir Physiol Neurobiol*, 2013. 189(1): p. 195-202.

67. Hadziefendic, S. and M.A. Haxhiu, CNS innervation of vagal preganglionic neurons controlling peripheral airways: a transneuronal labeling study using pseudorabies virus. *Journal of the Autonomic Nervous System*, 1999. 76(2): p. 135-145.

68. Haxhiu, M.A., et al., CNS innervation of airway-related parasympathetic preganglionic neurons: a transneuronal labeling study using pseudorabies virus. *Brain Research*, 1993. 618(1): p. 115-134.

69. Jordan, D., Central nervous pathways and control of the airways. *Respiration Physiology*, 2001. 125(1): p. 67-81.

70. Pérez Fontán, J.J. and C.R. Velloff, Labeling of vagal motoneurons and central afferents after injection of cholera toxin B into the airway lumen. *Am J Physiol Lung Cell Mol Physiol*, 2001. 280(1): p. L152-64.

71. Mazzone, S.B. and B.J. Canning, Central nervous system control of the airways: pharmacological implications. *Current Opinion in Pharmacology*, 2002. 2(3): p. 220-228.

72. Bonham, A.C., et al., Plasticity in the nucleus tractus solitarius and its influence on lung and airway reflexes. *Journal of Applied Physiology*, 2006. 101(1): p. 322-327.

73. Fernandes, L.B., A.D. Fryer, and C.A. Hirshman, M2 muscarinic receptors inhibit isoproterenol-induced relaxation of canine airway smooth muscle. *J Pharmacol Exp Ther*, 1992. 262(1): p. 119-26.

74. Ehlert, F.J., R.S. Ostrom, and G.W. Sawyer, Subtypes of the muscarinic receptor in smooth muscle. *Life Sci*, 1997. 61(18): p. 1729-40.

75. Dupont, L.J., et al., The effects of 5-HT on cholinergic contraction in human airways in vitro. *Eur Respir J*, 1999. 14(3): p. 642-9.

76. Gordan, R., J.K. Gwathmey, and L.H. Xie, Autonomic and endocrine control of cardiovascular function. *World J Cardiol*, 2015. 7(4): p. 204-14.

77. Brumpton, B.M., et al., Metabolic syndrome and incidence of asthma in adults: the HUNT study. *European Respiratory Journal*, 2013. 42(6): p. 1495.

78. Brumpton, B., et al., General and abdominal obesity and incident asthma in adults: the HUNT study. *Eur Respir J*, 2013. 41(2): p. 323-9.

79. Mosen, D.M., et al., The relationship between obesity and asthma severity and control in adults. *J Allergy Clin Immunol*, 2008. 122(3): p. 507-11.e6.

80. Miethe, S., et al., Obesity and asthma. *Journal of Allergy and Clinical Immunology*, 2020. 146(4): p. 685-693.

81. Shore, S.A., Obesity and asthma: lessons from animal models. *Journal of Applied Physiology*, 2007. 102(2): p. 516-528.

82. Peters, U., A.E. Dixon, and E. Forno, Obesity and asthma. *J Allergy Clin Immunol*, 2018. 141(4): p. 1169-1179.

83. Beuther, D.A. and E.R. Sutherland, Overweight, obesity, and incident asthma: a meta-analysis of prospective epidemiologic studies. *Am J Respir Crit Care Med*, 2007. 175(7): p. 661-6.

84. Chang, C., et al., Costs Attributable to Overweight and Obesity in Working Asthma Patients in the United States. *Yonsei Med J*, 2017. 58(1): p. 187-194.

85. Sutherland, E.R., et al., Body mass index and phenotype in subjects with mild-to-moderate persistent asthma. *J Allergy Clin Immunol*, 2009. 123(6): p. 1328-34.e1.

86. Leiria, L.O., M.A. Martins, and M.J. Saad, Obesity and asthma: beyond T(H)2 inflammation. *Metabolism*, 2015. 64(2): p. 172-81.

87. Sutherland, T.J., et al., The association between obesity and asthma: interactions between systemic and airway inflammation. *Am J Respir Crit Care Med*, 2008. 178(5): p. 469-75.

88. Farah, C.S., et al., Obesity is a determinant of asthma control independent of inflammation and lung mechanics. *Chest*, 2011. 140(3): p. 659-666.

89. van Veen, I.H., et al., Airway inflammation in obese and nonobese patients with difficult-to-treat asthma. *Allergy*, 2008. 63(5): p. 570-4.

90. Jensen, M.E., et al., Airway and systemic inflammation in obese children with asthma. *Eur Respir J*, 2013. 42(4): p. 1012-9.

91. Johnston, R.A., et al., Diet-induced obesity causes innate airway hyperresponsiveness to methacholine and enhances ozone-induced pulmonary inflammation. *Journal of Applied Physiology*, 2008. 104(6): p. 1727-1735.

92. Peters-Golden, M., et al., Influence of body mass index on the response to asthma controller agents. *Eur Respir J*, 2006. 27(3): p. 495-503.

93. Camargo, C.A., Jr., et al., Body mass index and response to asthma therapy: fluticasone propionate/salmeterol versus montelukast. *J Asthma*, 2010. 47(1): p. 76-82.

94. Rivera-Sanchez, Y.M., et al., Differential effects of ozone on airway and tissue mechanics in obese mice. *Journal of Applied Physiology*, 2004. 96(6): p. 2200-2206.

95. Lu, F.L., et al., Increased pulmonary responses to acute ozone exposure in obese db/db mice. *American Journal of Physiology-Lung Cellular and Molecular Physiology*, 2006. 290(5): p. L856-L865.

96. Johnston, R.A., T.A. Theman, and S.A. Shore, Augmented responses to ozone in obese carboxypeptidase E-deficient mice. *American Journal of Physiology-Regulatory, Integrative and Comparative Physiology*, 2006. 290(1): p. R126-R133.

97. Friedman, J.M., Leptin and the regulation of body weigh. *Keio J Med*, 2011. 60(1): p. 1-9.

98. Leibel, R.L., W.K. Chung, and S.C. Chua, Jr., The molecular genetics of rodent single gene obesities. *J Biol Chem*, 1997. 272(51): p. 31937-40.

99. Shore, S.A., et al., Responses to ozone are increased in obese mice. *Journal of Applied Physiology*, 2003. 95(3): p. 938-945.

100. Chen, H., et al., Evidence that the diabetes gene encodes the leptin receptor: identification of a mutation in the leptin receptor gene in db/db mice. *Cell*, 1996. 84(3): p. 491-5.

101. Fricker, L.D., et al., Carboxypeptidase E activity is deficient in mice with the fat mutation. Effect on peptide processing. *J Biol Chem*, 1996. 271(48): p. 30619-24.

102. Wang, C.-Y. and J.K. Liao, A mouse model of diet-induced obesity and insulin resistance. *Methods in molecular biology (Clifton, N.J.)*, 2012. 821: p. 421-433.

103. Matias, A.M., et al., Differential Effects of High Sugar, High Lard or a Combination of Both on Nutritional, Hormonal and Cardiovascular Metabolic Profiles of Rodents. *Nutrients*, 2018. 10(8).
104. Sutherland, E.R., et al., Comparative effect of body mass index on response to asthma controller therapy. *Allergy Asthma Proc*, 2010. 31(1): p. 20-5.
105. Dixon, A.E., et al., Effects of obesity and bariatric surgery on airway hyperresponsiveness, asthma control, and inflammation. *The Journal of allergy and clinical immunology*, 2011. 128(3): p. 508-15.e152.
106. Boulet, L.P., et al., Effect of bariatric surgery on airway response and lung function in obese subjects with asthma. *Respir Med*, 2012. 106(5): p. 651-60.
107. Spivak, H., et al., Weight loss and improvement of obesity-related illness in 500 U.S. patients following laparoscopic adjustable gastric banding procedure. *Am J Surg*, 2005. 189(1): p. 27-32.
108. Scott, H.A., et al., Dietary restriction and exercise improve airway inflammation and clinical outcomes in overweight and obese asthma: a randomized trial. *Clin Exp Allergy*, 2013. 43(1): p. 36-49.
109. Fu, Z., E.R. Gilbert, and D. Liu, Regulation of insulin synthesis and secretion and pancreatic Beta-cell dysfunction in diabetes. *Current diabetes reviews*, 2013. 9(1): p. 25-53.
110. James, D.E., et al., Insulin-regulatable tissues express a unique insulin-sensitive glucose transport protein. *Nature*, 1988. 333(6169): p. 183-5.
111. De Meyts, P., *The Insulin Receptor and Its Signal Transduction Network*, in *Endotext*, K.R. Feingold, et al., Editors. 2000, MDText.com, Inc.

112. Mosthaf, L., et al., Functionally distinct insulin receptors generated by tissue-specific alternative splicing. *Embo j*, 1990. 9(8): p. 2409-13.

113. Kosaki, A. and N.J. Webster, Effect of dexamethasone on the alternative splicing of the insulin receptor mRNA and insulin action in HepG2 hepatoma cells. *J Biol Chem*, 1993. 268(29): p. 21990-6.

114. Escribano, O., et al., The Role of Insulin Receptor Isoforms in Diabetes and Its Metabolic and Vascular Complications. *J Diabetes Res*, 2017. 2017: p. 1403206.

115. Frasca, F., et al., Insulin receptor isoform A, a newly recognized, high-affinity insulin-like growth factor II receptor in fetal and cancer cells. *Mol Cell Biol*, 1999. 19(5): p. 3278-88.

116. Seino, S. and G.I. Bell, Alternative splicing of human insulin receptor messenger RNA. *Biochem Biophys Res Commun*, 1989. 159(1): p. 312-6.

117. Belfiore, A., et al., Insulin receptor isoforms and insulin receptor/insulin-like growth factor receptor hybrids in physiology and disease. *Endocr Rev*, 2009. 30(6): p. 586-623.

118. Olefsky, J.M., The Insulin Receptor: A Multifunctional Protein. *Diabetes*, 1990. 39(9): p. 1009-1016.

119. Lee, J. and P.F. Pilch, The insulin receptor: structure, function, and signaling. *Am J Physiol*, 1994. 266(2 Pt 1): p. C319-34.

120. Jacobs, S. and P. Cuatrecasas, Insulin receptor: structure and function. *Endocr Rev*, 1981. 2(3): p. 251-63.

121. Belfiore, A., et al., Insulin Receptor Isoforms in Physiology and Disease: An Updated View. *Endocr Rev*, 2017. 38(5): p. 379-431.

122. Recio-Pinto, E., M.M. Rechler, and D.N. Ishii, Effects of insulin, insulin-like growth factor-II, and nerve growth factor on neurite formation and survival in cultured sympathetic and sensory neurons. *The Journal of Neuroscience*, 1986. 6(5): p. 1211.

123. Xu, Q.G., et al., Insulin as an in vivo growth factor. *Exp Neurol*, 2004. 188(1): p. 43-51.

124. Denley, A., et al., Structural Determinants for High-Affinity Binding of Insulin-Like Growth Factor II to Insulin Receptor (IR)-A, the Exon 11 Minus Isoform of the IR. *Molecular Endocrinology*, 2004. 18(10): p. 2502-2512.

125. Sugimoto, K., Y. Murakawa, and A.A.F. Sima, Expression and localization of insulin receptor in rat dorsal root ganglion and spinal cord. *Journal of the Peripheral Nervous System*, 2002. 7(1): p. 44-53.

126. Waldbillig, R.J. and D. LeRoith, Insulin receptors in the peripheral nervous system: a structural and functional analysis. *Brain Research*, 1987. 409(2): p. 215-220.

127. Derakhshan, F. and C. Toth, Insulin and the brain. *Curr Diabetes Rev*, 2013. 9(2): p. 102-16.

128. Frebel, K. and S. Wiese, Signalling molecules essential for neuronal survival and differentiation. *Biochemical Society Transactions*, 2006. 34(6): p. 1287-1290.

129. Shiflett, M.W. and B.W. Balleine, Contributions of ERK signaling in the striatum to instrumental learning and performance. *Behavioural Brain Research*, 2011. 218(1): p. 240-247.

130. Thomas, G.M. and R.L. Huganir, MAPK cascade signalling and synaptic plasticity. *Nat Rev Neurosci*, 2004. 5(3): p. 173-83.

131. Smith, U. and B.B. Kahn, Adipose tissue regulates insulin sensitivity: role of adipogenesis, de novo lipogenesis and novel lipids. *Journal of internal medicine*, 2016. 280(5): p. 465-475.
132. Sesti, G., Pathophysiology of insulin resistance. *Best Pract Res Clin Endocrinol Metab*, 2006. 20(4): p. 665-79.
133. Belfiore, A. and R. Malaguarnera, Insulin receptor and cancer. *Endocrine-Related Cancer*, 2011. 18(4): p. R125-R147.
134. Heidenreich, K.A., et al., Structural differences between insulin receptors in the brain and peripheral target tissues. *J Biol Chem*, 1983. 258(14): p. 8527-30.
135. Cardet, J.C., et al., Insulin resistance modifies the association between obesity and current asthma in adults. *European Respiratory Journal*, 2016. 48(2): p. 403.
136. Thuesen, B.H., et al., Insulin resistance as a predictor of incident asthma-like symptoms in adults. *Clin Exp Allergy*, 2009. 39(5): p. 700-7.
137. Carr, T.F., et al., High Insulin in Early Childhood Is Associated with Subsequent Asthma Risk Independent of Body Mass Index. *J Allergy Clin Immunol Pract*, 2021.
138. Nie, Z., D.B. Jacoby, and A.D. Fryer, Hyperinsulinemia potentiates airway responsiveness to parasympathetic nerve stimulation in obese rats. *Am J Respir Cell Mol Biol*, 2014. 51(2): p. 251-61.
139. Dekkers, B.G., et al., Insulin-induced laminin expression promotes a hypercontractile airway smooth muscle phenotype. *Am J Respir Cell Mol Biol*, 2009. 41(4): p. 494-504.

140. Park, Y.H., et al., Insulin resistance mediates high-fat diet-induced pulmonary fibrosis and airway hyperresponsiveness through the TGF-β1 pathway. *Experimental & Molecular Medicine*, 2019. 51(5): p. 59.

141. Wentworth, B.M., et al., Characterization of the two nonallelic genes encoding mouse preproinsulin. *J Mol Evol*, 1986. 23(4): p. 305-12.

142. Shiao, M.-S., et al., Adaptive evolution of the insulin two-gene system in mouse. *Genetics*, 2008. 178(3): p. 1683-1691.

143. Kolb, H., et al., Insulin translates unfavourable lifestyle into obesity. *BMC Medicine*, 2018. 16(1): p. 232.

144. Mehran, A.E., et al., Hyperinsulinemia drives diet-induced obesity independently of brain insulin production. *Cell Metab*, 2012. 16(6): p. 723-37.

145. Duvillié, B., et al., Phenotypic alterations in insulin-deficient mutant mice. *Proceedings of the National Academy of Sciences*, 1997. 94(10): p. 5137.

146. Louvi, A., D. Accili, and A. Efstratiadis, Growth-promoting interaction of IGF-II with the insulin receptor during mouse embryonic development. *Dev Biol*, 1997. 189(1): p. 33-48.

147. Kitamura, T., C.R. Kahn, and D. Accili, Insulin receptor knockout mice. *Annu Rev Physiol*, 2003. 65: p. 313-32.

148. Kim, H., et al., Mouse Cre-LoxP system: general principles to determine tissue-specific roles of target genes. *Laboratory animal research*, 2018. 34(4): p. 147-159.

149. Brüning, J.C., et al., A muscle-specific insulin receptor knockout exhibits features of the metabolic syndrome of NIDDM without altering glucose tolerance. *Mol Cell*, 1998. 2(5): p. 559-69.

150. Blüher, M., et al., Adipose tissue selective insulin receptor knockout protects against obesity and obesity-related glucose intolerance. *Dev Cell*, 2002. 3(1): p. 25-38.

151. Michael, M.D., et al., Loss of insulin signaling in hepatocytes leads to severe insulin resistance and progressive hepatic dysfunction. *Mol Cell*, 2000. 6(1): p. 87-97.

152. Kulkarni, R.N., et al., Tissue-specific knockout of the insulin receptor in pancreatic beta cells creates an insulin secretory defect similar to that in type 2 diabetes. *Cell*, 1999. 96(3): p. 329-39.

153. Grote, C.W., et al., Deletion of the insulin receptor in sensory neurons increases pancreatic insulin levels. *Experimental neurology*, 2018. 305: p. 97-107.

154. Lim, R.H., L. Kobzik, and M. Dahl, Risk for asthma in offspring of asthmatic mothers versus fathers: a meta-analysis. *PLoS One*, 2010. 5(4): p. e10134.

155. Morten, M., et al., Managing Asthma in Pregnancy (MAP) trial: FENO levels and childhood asthma. *J Allergy Clin Immunol*, 2018. 142(6): p. 1765-1772 e4.

156. Lebold, K.M., et al., IL-5 Exposure In Utero Increases Lung Nerve Density and Airway Reactivity in Adult Offspring. *Am J Respir Cell Mol Biol*, 2020. 62(4): p. 493-502.

157. Stothard, K.J., et al., Maternal overweight and obesity and the risk of congenital anomalies: a systematic review and meta-analysis. *Jama*, 2009. 301(6): p. 636-50.

158. Velten, M., et al., Perinatal inflammation induces sex-related differences in cardiovascular morbidities in mice. *Am J Physiol Heart Circ Physiol*, 2018. 314(3): p. H573-h579.

159. MacDonald, K.D., et al., Maternal body mass index before pregnancy is associated with increased bronchodilator dispensing in early childhood: A cross-sectional study. *Pediatr Pulmonol*, 2016. 51(8): p. 803-11.

160. Lock, M., et al., Regulation of fetal lung development in response to maternal overnutrition. *Clin Exp Pharmacol Physiol*, 2013. 40(11): p. 803-16.

161. Eising, J.B., C.S. Uiterwaal, and C.K. van der Ent, Maternal body mass index, neonatal lung function and respiratory symptoms in childhood. *Eur Respir J*, 2015. 46(5): p. 1342-9.

162. MacDonald, K.D., et al., Maternal high-fat diet in mice leads to innate airway hyperresponsiveness in the adult offspring. *Physiol Rep*, 2017. 5(5).

163. Hargreave, F.E., et al., The origin of airway hyperresponsiveness. *Journal of Allergy and Clinical Immunology*, 1986. 78(5, Part 1): p. 825-832.

164. O'Byrne, P.M. and M.D. Inman, Airway Hyperresponsiveness. *Chest*, 2003. 123(3, Supplement): p. 411S-416S.

165. Costello, R.W., et al., Localization of eosinophils to airway nerves and effect on neuronal M2 muscarinic receptor function. *Am J Physiol*, 1997. 273(1 Pt 1): p. L93-103.

166. Fryer, A.D. and D.B. Jacoby, Parainfluenza virus infection damages inhibitory M2 muscarinic receptors on pulmonary parasympathetic nerves in the guinea-pig. *Br J Pharmacol*, 1991. 102(1): p. 267-71.

167. Schultheis, A.H., D.J. Bassett, and A.D. Fryer, Ozone-induced airway hyperresponsiveness and loss of neuronal M2 muscarinic receptor function. *J Appl Physiol*, 1994. 76(3): p. 1088-97.

168. Proskocil, B.J., et al., Organophosphorus pesticides decrease M2 muscarinic receptor function in guinea pig airway nerves via indirect mechanisms. *PLoS One*, 2010. 5(5): p. e10562.

169. Scott, G.D., A.D. Fryer, and D.B. Jacoby, Quantifying nerve architecture in murine and human airways using three-dimensional computational mapping. *Am J Respir Cell Mol Biol*, 2013. 48(1): p. 10-6.

170. Drake, M.G., et al., Eosinophils increase airway sensory nerve density in mice and in human asthma. *Sci Transl Med*, 2018. 10(457).

171. Cheung, D., et al., Effects of inhaled substance P on airway responsiveness to methacholine in asthmatic subjects in vivo. *J Appl Physiol (1985)*, 1994. 77(3): p. 1325-32.

172. Chu, H.W., et al., Substance P and its receptor neurokinin 1 expression in asthmatic airways. *J Allergy Clin Immunol*, 2000. 106(4): p. 713-22.

173. Nieber, K., et al., Effect of azelastine on substance P content in bronchoalveolar and nasal lavage fluids of patients with allergic asthma. *Clin Exp Allergy*, 1993. 23(1): p. 69-71.

174. Joos, G.F., et al., The effect of inhaled FK224, a tachykinin NK-1 and NK-2 receptor antagonist, on neurokinin A-induced bronchoconstriction in asthmatics. *Am J Respir Crit Care Med*, 1996. 153(6 Pt 1): p. 1781-4.

175. Kraan, J., H. Vink-Klooster, and D.S. Postma, The NK-2 receptor antagonist SR 48968C does not improve adenosine hyperresponsiveness and airway obstruction in allergic asthma. *Clin Exp Allergy*, 2001. 31(2): p. 274-8.

176. Boot, J.D., et al., Effect of an NK1/NK2 receptor antagonist on airway responses and inflammation to allergen in asthma. *Am J Respir Crit Care Med*, 2007. 175(5): p. 450-7.

177. Scholzen, T.E., et al., Neutral Endopeptidase Terminates Substance P-Induced Inflammation in Allergic Contact Dermatitis. *The Journal of Immunology*, 2001. 166(2): p. 1285.

178. Samarasinghe, A.E., S.A. Hoselton, and J.M. Schuh, Spatio-temporal localization of vasoactive intestinal peptide and neutral endopeptidase in allergic murine lungs. *Regul Pept*, 2010. 164(2-3): p. 151-7.

179. Jacoby, D.B., et al., Influenza infection causes airway hyperresponsiveness by decreasing enkephalinase. *J Appl Physiol (1985)*, 1988. 64(6): p. 2653-8.

180. Dusser, D.J., et al., Virus induces airway hyperresponsiveness to tachykinins: role of neutral endopeptidase. *J Appl Physiol (1985)*, 1989. 67(4): p. 1504-11.

181. Dusser, D.J., et al., Cigarette smoke induces bronchoconstrictor hyperresponsiveness to substance P and inactivates airway neutral endopeptidase in the guinea pig. Possible role of free radicals. *J Clin Invest*, 1989. 84(3): p. 900-6.

182. Sont, J.K., et al., Enhanced expression of neutral endopeptidase (NEP) in airway epithelium in biopsies from steroid- versus nonsteroid-treated patients with atopic asthma. *Am J Respir Cell Mol Biol*, 1997. 16(5): p. 549-56.

183. Karagiannides, I., et al., Substance P as a Novel Anti-obesity Target. *Gastroenterology*, 2008. 134(3): p. 747-755.e1.

184. Ramalho, R., et al., Substance P antagonist improves both obesity and asthma in a mouse model. *Allergy*, 2013. 68(1): p. 48-54.

185. Chen, C.-Y., et al., Extended allergen exposure in asthmatic monkeys induces neuroplasticity in nucleus tractus solitarius. *Journal of Allergy and Clinical Immunology*, 2001. 108(4): p. 557-562.

186. Roffel, A.F., C.R. Elzinga, and J. Zaagsma, Muscarinic M3 receptors mediate contraction of human central and peripheral airway smooth muscle. *Pulm Pharmacol*, 1990. 3(1): p. 47-51.

187. Fryer, A.D. and J. Maclagan, Muscarinic inhibitory receptors in pulmonary parasympathetic nerves in the guinea-pig. *British Journal of Pharmacology*, 1984. 83(4): p. 973-978.

188. Minette, P.A., et al., A muscarinic agonist inhibits reflex bronchoconstriction in normal but not in asthmatic subjects. *J Appl Physiol (1985)*, 1989. 67(6): p. 2461-5.

189. Ayala, L.E. and T. Ahmed, Is there loss of protective muscarinic receptor mechanism in asthma? *Chest*, 1989. 96(6): p. 1285-91.

190. Nie, Z., D.B. Jacoby, and A.D. Fryer, Hyperinsulinemia potentiates airway responsiveness to parasympathetic nerve stimulation in obese rats. *Am J Respir Cell Mol Biol*, 2014.

191. Dürk, T., et al., Production of serotonin by tryptophan hydroxylase 1 and release via platelets contribute to allergic airway inflammation. *Am J Respir Crit Care Med*, 2013. 187(5): p. 476-85.

192. Kushnir-Sukhov, N.M., et al., Human mast cells are capable of serotonin synthesis and release. *J Allergy Clin Immunol*, 2007. 119(2): p. 498-9.

193. Potenzieri, C., S. Meeker, and B.J. Undem, Activation of mouse bronchopulmonary C-fibres by serotonin and allergen-ovalbumin challenge. *The Journal of Physiology*, 2012. 590(21): p. 5449-5459.

194. Woolcock, A.J., et al., Effect of vagal stimulation on central and peripheral airways in dogs. *J Appl Physiol*, 1969. 26(6): p. 806-13.

195. Karczewski, W. and J.G. Widdicombe, The role of the vagus nerves in the respiratory and circulatory reactions to anaphylaxis in rabbits. *J Physiol*, 1969. 201(2): p. 293-304.

196. Nandiwada, P.A., A.L. Hyman, and P.J. Kadowitz, Pulmonary vasodilator responses to vagal stimulation and acetylcholine in the cat. *Circ Res*, 1983. 53(1): p. 86-95.

197. Fryer, A.D. and M. Wills-Karp, Dysfunction of M2-muscarinic receptors in pulmonary parasympathetic nerves after antigen challenge. *Journal of Applied Physiology*, 1991. 71(6): p. 2255-2261.

198. Moffatt, J.D., T.M. Cocks, and C.P. Page, Role of the epithelium and acetylcholine in mediating the contraction to 5-hydroxytryptamine in the mouse isolated trachea. *Br J Pharmacol*, 2004. 141(7): p. 1159-66.

199. Ellis, J.L. and B.J. Undem, Non-adrenergic, non-cholinergic contractions in the electrically field stimulated guinea-pig trachea. *Br J Pharmacol*, 1990. 101(4): p. 875-80.

200. Myers, A.C. and B.J. Undem, Functional interactions between capsaicin-sensitive and cholinergic nerves in the guinea pig bronchus. *J Pharmacol Exp Ther*, 1991. 259(1): p. 104-9.

201. Undem, B.J., G.K. Adams, 3rd, and C.K. Buckner, Influence of electrical field stimulation on antigen-induced contraction and mediator release in the guinea pig isolated superfused trachea and bronchus. *J Pharmacol Exp Ther*, 1989. 249(1): p. 23-30.

202. Hsia, C.C., et al., An official research policy statement of the American Thoracic Society/European Respiratory Society: standards for quantitative assessment of lung structure. *Am J Respir Crit Care Med*, 2010. 181(4): p. 394-418.

203. Veres, T.Z., et al., Spatial interactions between dendritic cells and sensory nerves in allergic airway inflammation. *Am J Respir Cell Mol Biol*, 2007. 37(5): p. 553-61.

204. Scott, G.D., et al., Tissue optical clearing, three-dimensional imaging, and co mputer morphometry in whole mouse lungs and human airways. *Am J Respir Cell Mol Biol*, 2014. 51(1): p. 43-55.

205. Li, W., R.N. Germain, and M.Y. Gerner, Multiplex, quantitative cellular analysis in large tissue volumes with clearing-enhanced 3D microscopy (C(e)3D). *Proc Natl Acad Sci U S A*, 2017. 114(35): p. E7321-e7330.

206. Conchello, J.-A. and J.W. Lichtman, Optical sectioning microscopy. *Nature Methods*, 2005. 2(12): p. 920-931.

207. Dourmashkin, J.T., et al., Model for predicting and phenotyping at normal weight the long-term propensity for obesity in Sprague–Dawley rats. *Physiology & Behavior*, 2006. 87(4): p. 666-678.

208. Gallou-Kabani, C., et al., C57BL/6J and A/J Mice Fed a High-Fat Diet Delineate Components of Metabolic Syndrome. *Obesity*, 2007. 15(8): p. 1996-2005.

209. Huang, T.-J., A. Verkhratsky, and P. Fernyhough, Insulin enhances mitochondrial inner membrane potential and increases ATP levels through phosphoinositide 3-kinase in adult sensory neurons. *Molecular and Cellular Neuroscience*, 2005. 28(1): p. 42-54.

210. Ayala, J.E., et al., Standard operating procedures for describing and performing metabolic tests of glucose homeostasis in mice. *Disease models & mechanisms*, 2010. 3(9-10): p. 525-534.

211. Organization, W.H. *Obesity and Overweight*. 2018 [cited 2019 Dec 22].

212. Caulfield, M.P. and N.J.M. Birdsall, International Union of Pharmacology. XVII. Classification of Muscarinic Acetylcholine Receptors. *Pharmacological Reviews*, 1998. 50(2): p. 279-290.

213. Al-Shawwa, B.A., et al., Asthma and Insulin Resistance in Morbidly Obese Children and Adolescents. *Journal of Asthma*, 2007. 44(6): p. 469-473.

214. Li, C.Y., S.R. Erickson, and C.H. Wu, Metformin use and asthma outcomes among patients with concurrent asthma and diabetes. *Respirology*, 2016. 21(7): p. 1210-8.

215. Fuentes, N. and P. Silveyra, Endocrine regulation of lung disease and inflammation. *Experimental Biology and Medicine*, 2018. 243(17-18): p. 1313-1322.

216. Abramson, M., et al., Risk factors for asthma among young adults in Melbourne, Australia. *Respirology*, 1996. 1(4): p. 291-297.

217. Dodge, R.R. and B. Burrows, The prevalence and incidence of asthma and asthma-like symptoms in a general population sample. *Am Rev Respir Dis*, 1980. 122(4): p. 567-75.

218. Skobeloff, E.M., et al., The influence of age and sex on asthma admissions. *Jama*, 1992. 268(24): p. 3437-40.

219. Fisher, J.T., et al., Loss of vagally mediated bradycardia and bronchoconstriction in mice lacking M2 or M3 muscarinic acetylcholine receptors. *Faseb j*, 2004. 18(6): p. 711-3.

220. Haddad, E., Y. Landry, and J.-P. Gies, Muscarinic receptor subtypes in guinea pig airways. *American Journal of Physiology-Lung Cellular and Molecular Physiology*, 1991. 261(4): p. L327-L333.

221. Struckmann, N., et al., Role of muscarinic receptor subtypes in the constriction of peripheral airways: studies on receptor-deficient mice. *Mol Pharmacol*, 2003. 64(6): p. 1444-51.

222. Harvey, R.D. and A.E. Belevych, Muscarinic regulation of cardiac ion channels. *Br J Pharmacol*, 2003. 139(6): p. 1074-84.

223. Stengel, P.W., et al., M(2) and M(4) receptor knockout mice: muscarinic receptor function in cardiac and smooth muscle in vitro. *J Pharmacol Exp Ther*, 2000. 292(3): p. 877-85.

224. Henagan, T.M., et al., Sodium butyrate epigenetically modulates high-fat diet-induced skeletal muscle mitochondrial adaptation, obesity and insulin resistance through nucleosome positioning. *Br J Pharmacol*, 2015. 172(11): p. 2782-98.

225. Brozmanova, M., et al., Preferential activation of the vagal nodose nociceptive subtype by TRPA1 agonists in the guinea pig esophagus. *Neurogastroenterol Motil*, 2011. 23(10): p. e437-45.

226. Chatonnet, A. and O. Lockridge, Comparison of butyrylcholinesterase and acetylcholinesterase. *Biochemical Journal*, 1989. 260(3): p. 625-634.

227. Centers for Disease Control and Prevention. *Asthma and Obesity*. 2013 [cited 2019 Aug]; Available from: https://www.cdc.gov/asthma/asthma_stats/asthma_obesity.htm.

228. Keshavarz, M., et al., Caveolin-1: Functional Insights into Its Role in Muscarine- and Serotonin-Induced Smooth Muscle Constriction in Murine Airways*. Frontiers in Physiology*, 2017. 8.

229. Beckett, W.S., et al., Asthma is associated with weight gain in females but not males, independent of physical activity*. Am J Respir Crit Care Med*, 2001. 164(11): p. 2045-50.

230. Chen, Y., et al., Sex Specificity of Asthma Associated With Objectively Measured Body Mass Index and Waist Circumference: The Humboldt Study*. Chest*, 2005. 128(4): p. 3048-3054.

231. Wang, L., et al., Sex difference in the association between obesity and asthma in U.S. adults: Findings from a national study*. Respir Med*, 2015. 109(8): p. 955-62.

232. Appleton, S.L., et al., Sex differences in asthma morbidity associated with obesity in a representative population sample*. Journal of Allergy and Clinical Immunology*, 2008. 121(5): p. 1285-1287.e1.

233. Huovinen, E., J. Kaprio, and M. Koskenvuo, Factors associated to lifestyle and risk of adult onset asthma*. Respir Med*, 2003. 97(3): p. 273-80.

234. Sood, A., Sex differences: implications for the obesity-asthma association*. Exercise and sport sciences reviews*, 2011. 39(1): p. 48-56.

235. Forno, E., et al., Insulin resistance, metabolic syndrome, and lung function in US adolescents with and without asthma*. Journal of Allergy and Clinical Immunology*, 2015. 136(2): p. 304-311.e8.

236. Greenhill, C., Sex differences in insulin resistance. *Nature Reviews Endocrinology*, 2018. 14(2): p. 65-65.

237. Qiu, J., et al., Estradiol Protects Proopiomelanocortin Neurons Against Insulin Resistance. *Endocrinology*, 2018. 159(2): p. 647-664.

238. Baker, D.G., H.F. Don, and J.K. Brown, Direct measurement of acetylcholine release in guinea pig trachea. *Am J Physiol*, 1992. 263(1 Pt 1): p. L142-7.

239. Levin, B.E., et al., Selective breeding for diet-induced obesity and resistance in Sprague-Dawley rats. *Am J Physiol*, 1997. 273(2 Pt 2): p. R725-30.

240. Salinero, A.E., B.M. Anderson, and K.L. Zuloaga, Sex differences in the metabolic effects of diet-induced obesity vary by age of onset. *Int J Obes (Lond)*, 2018. 42(5): p. 1088-1091.

241. Sengupta, P., The Laboratory Rat: Relating Its Age With Human's. *Int J Prev Med*, 2013. 4(6): p. 624-30.

242. *Charles River Laboratories International I*. 2010.

243. Cohen, D.H. and D. LeRoith, Obesity, type 2 diabetes, and cancer: the insulin and IGF connection. *Endocr Relat Cancer*, 2012. 19(5): p. F27-45.

244. Cohen, P., et al., Leukotriene D4 facilitates airway smooth muscle cell proliferation via modulation of the IGF axis. *Am J Physiol*, 1995. 269(2 Pt 1): p. L151-7.

245. Noveral, J.P., et al., Insulin-like growth factor axis in airway smooth muscle cells. *Am J Physiol*, 1994. 267(6 Pt 1): p. L761-5.

246. Singh, S., et al., Insulin and the Lung: Connecting Asthma and Metabolic Syndrome. *Journal of Allergy*, 2013. 2013: p. 8.

247. Gosens, R., et al., Muscarinic receptor signaling in the pathophysiology of asthma and COPD. *Respiratory Research*, 2006. 7(1): p. 73.

248. Proskocil, B.J., et al., Pioglitazone prevents obesity-related airway hyperreactivity and neuronal M(2) receptor dysfunction. *Am J Physiol Lung Cell Mol Physiol*, 2021. 321(1): p. L236-l247.

249. Simonsson, B.G., F.M. Jacobs, and J.A. Nadel, Role of autonomic nervous system and the cough reflex in the increased responsiveness of airways in patients with obstructive airway disease. *J Clin Invest*, 1967. 46(11): p. 1812-8.

250. Hayes, D., Jr., et al., Bronchoconstriction triggered by breathing hot humid air in patients with asthma: role of cholinergic reflex. *Am J Respir Crit Care Med*, 2012. 185(11): p. 1190-6.

251. Rotheneichner, P., et al., Tamoxifen Activation of Cre-Recombinase Has No Persisting Effects on Adult Neurogenesis or Learning and Anxiety. *Frontiers in neuroscience*, 2017. 11: p. 27-27.

252. Nie, Z., et al., Lung eosinophils increase vagus nerve-mediated airway reflex bronchoconstriction in mice. *Am J Physiol Lung Cell Mol Physiol*, 2020. 318(2): p. L242-l251.

253. McAlexander, M.A., et al., Vagotomy reverses established allergen-induced airway hyperreactivity to methacholine in the mouse. *Respir Physiol Neurobiol*, 2015. 212-214: p. 20-4.

254. Wagner, E.M. and D.B. Jacoby, Methacholine causes reflex bronchoconstriction. *J Appl Physiol (1985)*, 1999. 86(1): p. 294-7.

255. Bookout, A.L., et al., High-throughput real-time quantitative reverse transcription PCR. *Curr Protoc Mol Biol*, 2006. Chapter 15: p. Unit 15.8.

256. Shinagawa, K. and M. Kojima, Mouse Model of Airway Remodeling*. American Journal of Respiratory and Critical Care Medicine*, 2003. 168(8): p. 959-967.

257. Fernyhough, P., et al., Stabilization of tubulin mRNAs by insulin and insulin-like growth factor I during neurite formation*. Brain Res Mol Brain Res*, 1989. 6(2-3): p. 109-20.

258. Fernyhough, P., et al., Insulin and insulin-like growth factor I enhance regeneration in cultured adult rat sensory neurones*. Brain Research*, 1993. 607(1): p. 117-124.

259. Kim, B. and E.L. Feldman, Insulin resistance in the nervous system*. Trends in endocrinology and metabolism: TEM*, 2012. 23(3): p. 133-141.

260. Brussee, V., F.A. Cunningham, and D.W. Zochodne, Direct insulin signaling of neurons reverses diabetic neuropathy*. Diabetes*, 2004. 53(7): p. 1824-30.

261. Hunter, D.V., et al., Advillin Is Expressed in All Adult Neural Crest-Derived Neurons*. eNeuro*, 2018. 5(5).

262. Pincus, A.B., *Assessing sensory and parasympathetic contributions to airway hyperreactivity using optogenetic activation and multicolor labeling of airway neurons*, in *Neuroscience Department*. 2021, Oregon Health & Science University School of Medicine: Portland, OR.

263. Calco, G.N., et al., Metformin prevents airway hyperreactivity in rats with dietary obesity*. American Journal of Physiology-Lung Cellular and Molecular Physiology*. 0(0): p. null.

264. Sahbaie, P., et al., Role of substance P signaling in enhanced nociceptive sensitization and local cytokine production after incision*. Pain*, 2009. 145(3): p. 341-349.

265. Abbadie, C., et al., Inflammation increases the distribution of dorsal horn neurons that internalize the neurokinin-1 receptor in response to noxious and non-noxious stimulation. *J Neurosci*, 1997. 17(20): p. 8049-60.

266. Lázár, B.A., et al., Insulin Confers Differing Effects on Neurite Outgrowth in Separate Populations of Cultured Dorsal Root Ganglion Neurons: The Role of the Insulin Receptor. *Frontiers in Neuroscience*, 2018. 12: p. 732.

267. Lazar, B.A., et al., The Insulin Receptor Is Colocalized With the TRPV1 Nociceptive Ion Channel and Neuropeptides in Pancreatic Spinal and Vagal Primary Sensory Neurons. *Pancreas*, 2018. 47(1): p. 110-115.

268. Kleemann, R., et al., Time-resolved and tissue-specific systems analysis of the pathogenesis of insulin resistance. *PLoS One*, 2010. 5(1): p. e8817.

269. Adam, C.L., et al., In vivo changes in central and peripheral insulin sensitivity in a large animal model of obesity. *Endocrinology*, 2012. 153(7): p. 3147-57.

270. Saltiel, A.R. and C.R. Kahn, Insulin signalling and the regulation of glucose and lipid metabolism. *Nature*, 2001. 414(6865): p. 799-806.

271. Cusi, K., et al., Insulin resistance differentially affects the PI 3-kinase- and MAP kinase-mediated signaling in human muscle. *The Journal of clinical investigation*, 2000. 105(3): p. 311-320.

272. Yu, X., et al., Egr-1 decreases adipocyte insulin sensitivity by tilting PI3K/Akt and MAPK signal balance in mice. *The EMBO journal*, 2011. 30(18): p. 3754-3765.

273. Boulton, T.G., et al., ERKs: a family of protein-serine/threonine kinases that are activated and tyrosine phosphorylated in response to insulin and NGF. *Cell*, 1991. 65(4): p. 663-75.

274. Winder, D.G., et al., ERK plays a regulatory role in induction of LTP by theta frequency stimulation and its modulation by beta-adrenergic receptors. *Neuron*, 1999. 24(3): p. 715-26.

275. Kim, S.Y., et al., Activation of p38 MAP kinase in the rat dorsal root ganglia and spinal cord following peripheral inflammation and nerve injury. *Neuroreport*, 2002. 13(18): p. 2483-6.

276. Ji, R.-R., et al., p38 MAPK Activation by NGF in Primary Sensory Neurons after Inflammation Increases TRPV1 Levels and Maintains Heat Hyperalgesia. *Neuron*, 2002. 36(1): p. 57-68.

277. Zhen, X., et al., The p38 mitogen-activated protein kinase is involved in associative learning in rabbits. *J Neurosci*, 2001. 21(15): p. 5513-9.

278. Zhu, J.J., et al., Ras and Rap control AMPA receptor trafficking during synaptic plasticity. *Cell*, 2002. 110(4): p. 443-55.

279. Butler, M.P., J.J. O'Connor, and P.N. Moynagh, Dissection of tumor-necrosis factor-α inhibition of long-term potentiation (LTP) reveals a p38 mitogen-activated protein kinase-dependent mechanism which maps to early—but not late—phase LTP. *Neuroscience*, 2004. 124(2): p. 319-326.

280. Carlson, C.J., et al., Enhanced basal activation of mitogen-activated protein kinases in adipocytes from type 2 diabetes: potential role of p38 in the downregulation of GLUT4 expression. *Diabetes*, 2003. 52(3): p. 634-41.

281. CDC, Obesity and overweight. 2021.

282. Chen, C., X. Xu, and Y. Yan, Estimated global overweight and obesity burden in pregnant women based on panel data model. *PLoS One*, 2018. 13(8): p. e0202183.

283. Fryer, A.D. and J. Maclagan, Muscarinic inhibitory receptors in pulmonary parasympathetic nerves in the guinea-pig. *Br J Pharmacol*, 1984. 83(4): p. 973-8.

284. Boushey, H.A., et al., Bronchial hyperreactivity. *Am Rev Respir Dis*, 1980. 121(2): p. 389-413.

285. Sheppard, D., et al., Dose-dependent inhibition of cold air-induced bronchoconstriction by atropine. *J Appl Physiol Respir Environ Exerc Physiol*, 1982. 53(1): p. 169-74.

286. Simonsson, B.G., B.E. Skoogh, and B. Ekstrom-Jodal, Exercise-induced airways constriction. *Thorax*, 1972. 27(2): p. 169-80.

287. Gold, W.M., Vagally-mediated reflex bronchoconstriction in allergic asthma. *Chest*, 1973. 63: p. Suppl:11S.

288. Makker, H.K. and S.T. Holgate, The contribution of neurogenic reflexes to hypertonic saline-induced bronchoconstriction in asthma. *J Allergy Clin Immunol*, 1993. 92(1 Pt 1): p. 82-8.

289. Crimi, N., et al., Protective effects of inhaled ipratropium bromide on bronchoconstriction induced by adenosine and methacholine in asthma. *Eur Respir J*, 1992. 5(5): p. 560-5.

290. Papi, A., et al., Inhaled long-acting muscarinic antagonists in asthma - A narrative review. *Eur J Intern Med*, 2021. 85: p. 14-22.

291. Ghasemi, R., et al., Insulin in the brain: sources, localization and functions. *Mol Neurobiol*, 2013. 47(1): p. 145-71.

292. Raizada, M.K., J.W. Yang, and R.E. Fellows, Binding of [125I]insulin to specific receptors and stimulation of nucleotide incorporation in cells cultured from rat brain. *Brain Res*, 1980. 200(2): p. 389-400.

293. Heni, M., et al., Insulin promotes glycogen storage and cell proliferation in primary human astrocytes. *PLoS One*, 2011. 6(6): p. e21594.

294. Mingrone, G., et al., Influence of maternal obesity on insulin sensitivity and secretion in offspring. *Diabetes Care*, 2008. 31(9): p. 1872-6.

295. Volpato, A.M., et al., Maternal high-fat diet programs for metabolic disturbances in offspring despite leptin sensitivity. *Neuroendocrinology*, 2012. 96(4): p. 272-84.

296. Scott, G.D., et al., Tissue Optical Clearing, 3D Imaging, and Computer Morphometry in Whole Mouse Lungs and Human Airways. *Am J Respir Cell Mol Biol*, 2014.

297. Calco, G.N., et al., Metformin prevents airway hyperreactivity in rats with dietary obesity. *Am J Physiol Lung Cell Mol Physiol*, 2021.

298. Bucher, M., et al., Dyslipidemia, insulin resistance, and impairment of placental metabolism in the offspring of obese mothers. *J Dev Orig Health Dis*, 2021. 12(5): p. 738-747.

299. Hoyle, G.W., et al., Hyperinnervation of the airways in transgenic mice overexpressing nerve growth factor. *Am J Respir Cell Mol Biol*, 1998. 18(2): p. 149-57.

300. Kajekar, R., et al., Early postnatal exposure to allergen and ozone leads to hyperinnervation of the pulmonary epithelium. *Respir Physiol Neurobiol*, 2007. 155(1): p. 55-63.

301. McDonald, D.M., et al., Neurogenic inflammation. A model for studying efferent actions of sensory nerves. *Adv Exp Med Biol*, 1996. 410: p. 453-62.

302. Ji, R.-R., et al., Neuroinflammation and Central Sensitization in Chronic and Widespread Pain. *Anesthesiology*, 2018. 129(2): p. 343-366.

303. Park, H.J., et al., Empagliflozin and Dulaglutide are Effective against Obesity-induced Airway Hyperresponsiveness and Fibrosis in A Murine Model. *Sci Rep*, 2019. 9(1): p. 15601.

304. Nyenhuis, S.M., A.E. Dixon, and J. Ma, Impact of Lifestyle Interventions Targeting Healthy Diet, Physical Activity, and Weight Loss on Asthma in Adults: What Is the Evidence? *J Allergy Clin Immunol Pract*, 2018. 6(3): p. 751-763.

305. Forno, E., et al., The impact of bariatric surgery on asthma control differs among obese individuals with reported prior or current asthma, with or without metabolic syndrome. *PLOS ONE*, 2019. 14(4): p. e0214730.

306. Forno, E., et al., Maternal obesity in pregnancy, gestational weight gain, and risk of childhood asthma. *Pediatrics*, 2014. 134(2): p. e535-46.

307. Liu, S., et al., Pre-pregnancy Maternal Weight and Gestational Weight Gain Increase the Risk for Childhood Asthma and Wheeze: An Updated Meta-Analysis. *Front Pediatr*, 2020. 8: p. 134.

308. Denley, A., et al., The insulin receptor isoform exon 11- (IR-A) in cancer and other diseases: a review. *Horm Metab Res*, 2003. 35(11-12): p. 778-85.